# On the Return of HP West: The Revival and Restoration of a Hewlett-Packard 5950A Photoelectron Spectrometer

MARSHALL JOHN STYCZINSKI

Charles Fadley, Advisor

SENIOR THESIS

Submitted in partial satisfaction of the requirements for the degree of

BACHELOR OF SCIENCE WITH HIGHEST HONORS

in

Physics

in the

College of Letters and Science

of the

UNIVERSITY OF CALIFORNIA

DAVIS

June 2010

For my father, who has given me an intense curiosity
about the physical world,
and for Nichole, who has taught me
how to enjoy it.

# Table of Contents

## Abstract

A photoelectron spectrometer and its associated equipment, which had deteriorated somewhat over many years of use and a recent period of disuse, were assessed component by component and restored to operating condition. Some parts of the machine were disassembled, cleaned, and reassembled, including the aluminum X-ray anode, sample probe, and differential seals. A new X-ray monochromator angle adjustment knob and feed-through were designed and installed into the spectrometer. The photoelectron detector attached to the spectrometer's hemispherical analyzer was reconfigured; spectrometer performance improved in terms of spectral line widths, peak intensities, and difference in energy from apparent binding energy to expected binding energy, but future work is necessary to determine why rearranging detector components contributed to this result.

A thorough discussion of spectrometer functional theory and the functional theory of various individual components has also been included due to its relevance to the repair work. The past uses, present condition, and future directions of the specific spectrometer covered by this exposition are discussed as well. In addition, detailed accounts of all of the problems encountered during restoration and the solutions applied are outlined.

The spectrometer was also employed in three simple experiments:

1. An examination of consistency of measurement over the first two hours of "cold" operation to look for changes in spectra over the 2-hour warm-up period recommended by the HP 5950A operation manual; intensities of spectra sampled immediately after power-on were found to be about 50% of the maximum when all power supplies were cold, about 60% of the maximum when only the HP supplies were cold, and about 75% of the maximum when only the X-ray power supply was cold.

2. A comparison of the differences in Au sample spectra (Au 4f and $-10$ to 1000 eV wide scans) for a dirty sample, a sample with a 200 nm layer of Au sputtered onto it by Peter Greene, and a sample prepared by *in situ* Au evaporation: large differences in peak intensities, some small binding energy shifts, and an iodine contaminant were observed when comparing the clean (*in situ* prepared) sample to the others.

3. A determination of the native oxide layer thickness of a 40-period multilayer made of 4 nm Si/Mo bilayers with a thickness ratio of 0.6 Si / 0.4 Mo on a $SiO_2$ substrate via ARXPS; the native oxide layer thickness was determined from standard equations to be 14Å, which matched closely to the 15Å thickness derived from a more accurate determination based on calculations using the SESSA computer program.

Several recommendations for future HP West operation based on the results of the first two experiments are discussed. Several more instrumental examinations must still be undertaken so that a complete status report of the revived machine may be outlined based on comparison to monochromator variation tests, X-ray power tests, and HP West response function $R(\theta)$ determinations performed in the past.

# 1 Introduction

The photoelectric effect was one of the most important discoveries in the study of electromagnetic waves. It was first observed by Heinrich Hertz in 1887 [1], but its explanation by Albert Einstein in 1905 [2] introduced the concept of the quantization of light and connected particle properties to its well-known wave-like properties.

There are many ways to exploit the photoelectric effect. Photoelectron spectroscopy (aka Photoemission spectroscopy, or electron spectroscopy for chemical analysis – ESCA) is one such important method: photons of a specific energy are focused onto a solid sample and the kinetic energy of the emitted electrons is analyzed to determine the binding energy of the orbitals of the sample. The characteristic energy conservation equation [3] describing this behavior is given by

$$h\nu = E_{binding}^{vacuum} + E'_{kinetic} = E_{binding}^{Fermi} + \varphi_{spectrometer} + E_{kinetic}, \tag{1}$$

where $E_{binding}^{vacuum}$ is the apparent binding energy of the electrons; $E'_{kinetic}$ is the kinetic energy the electrons have just as they are ejected from the sample surface; $E_{binding}^{Fermi}$ is the energy difference between the electron binding energy and the Fermi Energy of the bound electrons; $\varphi_{spectrometer}$ is the work function of the spectrometer; and $E_{kinetic}$ is the final kinetic energy of the electrons as detected in the spectrometer. Though there will also be some small recoil energy absorbed by the target atoms due to conservation of momentum, this energy is typically small with soft X-rays ($h\nu$ from $10^2$ eV to $10^3$ eV), especially with heavy atoms.

Eq. (1) demonstrates some of the utility of this method of exploiting the photoelectric effect: every element has its own unique values of $E_{binding}$ for its electrons. If one knows the values of $h\nu$ and $\varphi_{spectrometer}$, then by measuring the kinetic energy of the emitted electrons, the binding energies of the electrons in the target sample may be determined. Because the photons used in the photoemission process are X-rays for these experiments, the practice is also known as *X-ray* Photoemission Spectroscopy (XPS).

XPS is of particular importance because of the much higher resolution it can provide [4] over other methods for measuring binding energy, such as X-ray absorption spectroscopy. XPS also enables the operator to analyze far more than electron binding energies [5], especially through Angle-Resolved X-ray Photoemission Spectroscopy (ARXPS). Angular distribution measurements expose myriad lattice and chemical properties of surfaces by measuring the differences in emitted electron intensity (the X-ray beam intensity is known and may be fixed) as a function of the varying surface angle.

In order to examine such surface effects, careful sample handling and an ultra-high vacuum (UHV, ambient pressures in the $10^{-9}$ Torr range or better) environment are necessary. Special equipment must therefore be constructed that can:

- accommodate the large pressure differential from atmosphere to UHV while still allowing samples to be removed and replaced without venting the experimental chamber
- permit rotation of the sample in the X-ray beam about an axis lying in the surface of the sample
- minimize outgassing, even at UHV levels, by selecting materials with very low vapor pressures
- maximize resolution of energy spectrum measurements.

It is necessary to establish UHV conditions inside the machine so that the sample does not become contaminated by adsorbed gas molecules during operation. The mean free path $\lambda_{mfp}$ of the gases in the chamber is given by [17]

$$\lambda_{mfp} = \frac{k_B T}{\sqrt{2}\pi d^2 P}, \tag{2}$$

where $k_B$ is Boltzmann's constant, T is the temperature in K, d is the molecular diameter, and P is the pressure. When the $\lambda_{mfp}$ of the gases in the chamber greatly exceeds the dimensions of the chamber, the ratio of the rate of interaction with other molecules versus the rate of interaction with chamber surfaces is very low, so the gas behavior is largely determined by the surface interactions of the molecules. Over time, a sample in the chamber will become coated with adsorbed molecules and this will change the spectrum observed by XPS experimentation. In molecular flow conditions, when $\lambda_{mfp}$ greatly exceeds the chamber dimensions, the impingement rate $\Phi$ of the residual gas in the experimental chamber may be shown to be [11]

$$\Phi \approx \frac{n v_{avg}}{4} \sim 3.8 \times 10^{20} \cdot P \tag{3}$$

for air at 300K, $\Phi$ in units of 1/(cm$^2$-sec), and $P$ in units of Torr; $n$ and $v_{avg}$ are the number density of and average velocity of the air molecules, respectively. For air, the time taken to coat the sample with one monolayer of solid adsorbed contaminants will be about 3 seconds at $10^{-6}$ Torr; at $10^{-9}$ Torr, however, the time to form one monolayer is increased to about 1000 seconds. In order to prevent a contaminant overlayer from obscuring the underlying sample, a very low vacuum is therefore necessary. Though the residual gas in the chamber will not have molecular constituents identical to air at atmospheric pressure, the above rough order-of-magnitude estimate demonstrates the importance of maintaining a low residual gas pressure.

This discourse will explore the theory behind the operation and engineering of a machine designed around the above criteria and follow its return from disuse to a functioning scientific apparatus during my thesis research. There will also be a discussion of the past, present, and future of the machine in question: what it has been used for, including my experiments *on* and *with* the machine, how I have attempted to return it to operating condition and improved various functions, and what still needs to be done to achieve optimal operation.

Most of the research and repair detailed below was conducted in the Fadley Group Laboratory, 236 Physics at UC Davis. Some work, mostly learning ARXPS theory and experiment, was also undertaken with Fadley Group Researchers at the Advanced Light Source at Lawrence Berkeley National Laboratory. In the Davis Fadley Group Lab there are two HP (Hewlett-Packard) spectrometers, designated HP East and HP West based on their relative physical orientations. HP West is the focus of my study; HP East provided a convenient source of replacement parts as HP West was returned to service.

## 2 XPS Theory

*Much of the material in this section was originally presented by R. J. Baird and C. S. Fadley, in which the properties of the HP 5950A spectrometer were analyzed in detail [5].*

In order to make any quantitative statements about a sample being probed by XPS measurements, a detailed, quantitative understanding of the spectrometer geometry must be known. Figure 1 shows a schematic representation of a general spectrometer geometry and Table 2 the carefully measured geometrical values for the HP 5950A spectrometer. It is beneficial to also define a coordinate system as in Table 1 which will be consistent with Figure 1. The functions $I'_x(\gamma, y)$, $I_x(\theta, x, y)$, and $R'(\theta, \Delta E)$ presented by R.J. Baird and C.S. Fadley in [5] correspond to $I_x$, the X-ray intensity

| | |
|---|---|
| $x$ | distance along the sample surface parallel to plane of Figure 1 |
| $y$ | distance along the sample surface normal to plane of Figure 1 |
| $z$ | distance normal to the plane of the sample surface |
| $\gamma$ | distance perpendicular to the direction of X-ray propagation |
| $\theta$ | angle between x-axis and spectrometer imaging/retarding lens central axis |
| $\alpha$ | angle between X-ray propagation direction and lens central axis |
| $\phi$ | azimuthal angle orthogonal to lens axis (rotation not equipped) |
| $\phi_x$ | angle between X-ray propagation direction and horizontal (lens axis set to vertical) |
| $\Omega_0$ | solid angle subtended by electron lens acceptance aperture |
| $\psi$ | angle between sample translation handle and horizontal (for alignment purposes) |
| $\Delta\theta$ | manipulator angle setting (adjusts $\theta$) |
| $\varphi$ | monochromator angle setting (for alignment – see Section 5.2.2) |

Table 1: Definitions of the various coordinates typical to XPS and spectrometer geometries. The bottom three are specific to HP West and were introduced by the author.

distribution as a function of two sets of coordinates ($\gamma$ and $y$ versus $\theta$, $x$, and $y$) and $R'$, the adjusted spectrometer response, a function of both $\theta$ and $\Delta E$. The "adjusted" part stems from inclusion of non-ideal aspects of the spectrometer in the normalized spectral broadening function, $B(\Delta E, \theta, x, y)$, as introduced below.

Once a photoelectron has been emitted following photon absorption it will, in the simplest picture, travel in a straight line until it interacts with an atom, gas molecule, or another electron. In a UHV environment, the probability of interacting with gas molecules is small; the spectrometer geometry is also very large and the effective electron current very low, so the scale for inter-electronic distances is very large and these interactions may be ignored. The main source of interactions, then, is the atoms of the solid sample. An electron traveling through the sample will have a probability of interacting with various excitations in the solid (electronic, plasmonic, and vibrational), thereby either altering its path or changing its kinetic energy; the probability of escaping the sample with no inelastic scattering $P(l)$ will be given by [6]

$$P(l) = \exp\{-l/\Lambda_e(E_{kin})\}, \tag{4}$$

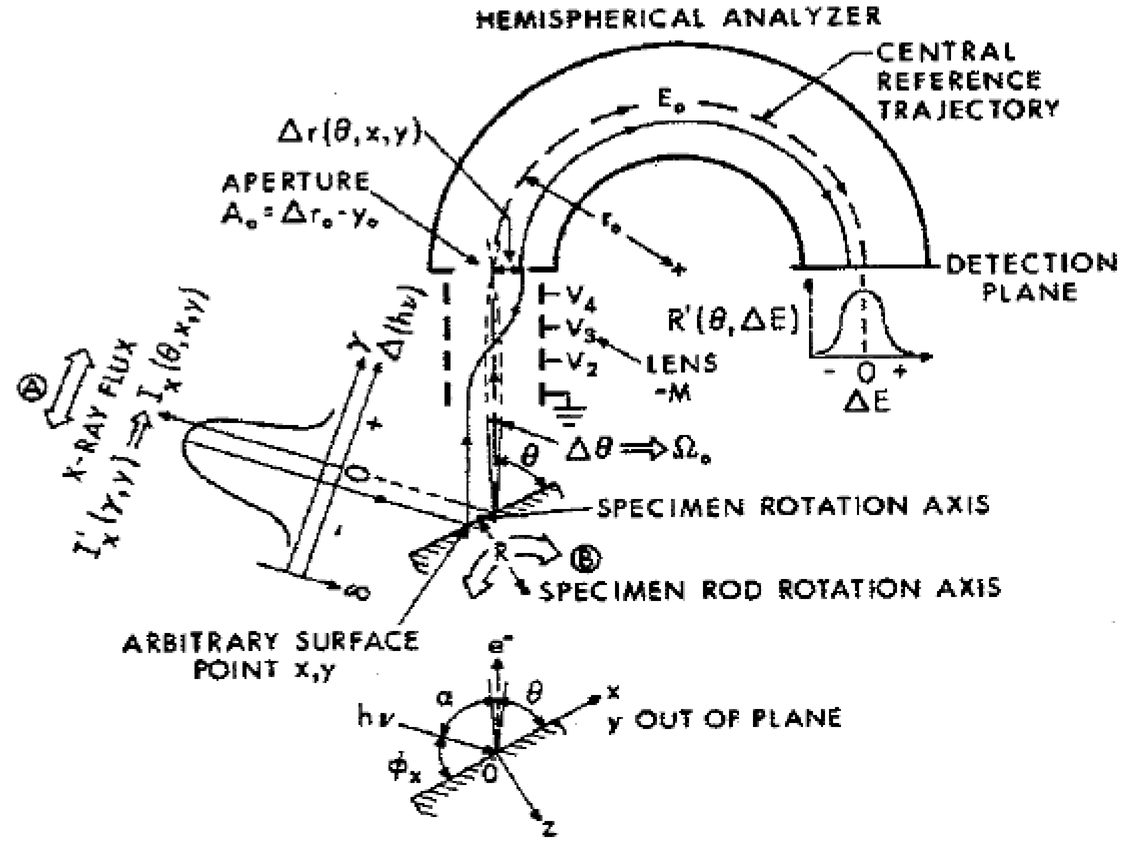

Figure 1: General spectrometer geometry. Reproduced from [5].

where $l$ is the distance traveled through the sample, and $\Lambda_e(E_{kin})$ is known as the electron attenuation length or inelastic mean free path, as it denotes the distance at which the percentage of electrons with energy $E_{kin}$ which have not interacted has dropped to $\frac{1}{e}$. $\Lambda_e$ is of interest because the electrons entering the spectrometer lens aperture with the appropriate kinetic energy will have been emitted from atoms along an average depth $\Lambda_e$ parallel to the lens axis. As demonstrated schematically by Figure 2, for a perfectly smooth, atomically clean sample, varying the electron take-off angle $\theta$ will vary the average emission depth $t$ along the $z$-axis according to [6]

$$t = \Lambda_e(E_{kin}) \sin\theta. \tag{5}$$

Table 2: Values of many physical parameters characterizing Hewlett-Packard 5950A spectrometers. Reproduced from [5].

---

*Crystal monochromator*
Bragg angle $= \theta_B = 78.5°$
Rowland circle diameter = 27.94cm (11.00 in)
Dispersion $= d(h\nu)/d\gamma = 11.03$ eV $\mathrm{cm}^{-1}$
Flux distribution $= I'_x(\gamma, y) \approx$ Gaussian of 0.64 eV FWHM along $\gamma$
*Electrostatic lens*
Magnification $= M = -5.0 or - 2.3$ (two modes)
Acceptance solid angle $= \Omega_0 = \begin{cases} \text{cone of } 3.5° \text{ half-angle } (M = -5.0) \\ \text{cone of } 2.8° \text{ half-angle } (M = -2.3) \end{cases}$
Angle between X-ray incidence and lens axis $= \alpha = 72°$
*Hemispherical analyzer*
Radius of central trajectory $= r_0 = 15.56$ cm (6.13 in)
Energy of analysis $= E_0 = 115$ eV
Dispersion $= dE/dr = 3.71$ eV $\mathrm{cm}^{-1}$
Entrance aperture width $= \Delta r_0 = 0.60$ cm
Entrance aperture height $= y_0 = 2.5$ cm
*Specimen probe*
Radius of rotation of specimen axis $= R = 0.714$ cm (0.281 in)
Horizontal offset of specimen rod rotation axis from lens axis = 0.559 cm (0.220 in)

---

This is an exciting behavior because for an optimally aligned monochromator [5], decreasing $\theta$ allows the experimenter to emphasize the surface layer(s) and deemphasize the bulk crystal. This surface enhancement is the fundamental principle exploited by ARXPS to study the surfaces of samples [6]; I will later make use of this result to determine the thickness of a $SiO_2$ overlayer on a Si/Mo multilayer mirror.

Grazing-incidence X-rays may also be used to highlight the surface of a sample. The X-ray penetration depth $d$ follows a similar behavior to $\Lambda_e$ [21], but X-rays tend to experience far less attenuation than electrons, so the electron attenuation is the limiting factor [6] except for very shallow incidence angles $\phi_x$. Figure 3 shows the X-ray attenuation length (depth of penetration at which *photon* intensity has dropped to $\frac{1}{e}$ of the maximum) as a function of the incidence angle $\phi_x$ at the specific energy of 1486.6 eV Al-K$\alpha$ radiation used in the HP 5950A spectrometer. At low $\phi_x$, the X-ray

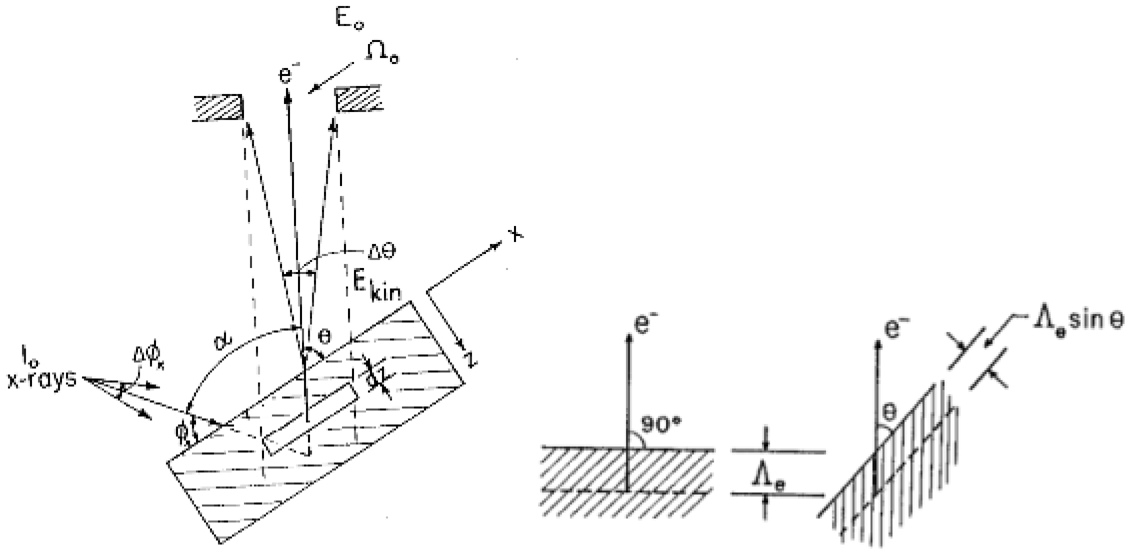

(a) General sample orientation.

(b) Angular dependence of $t$ resulting in surface enhancement.

Figure 2: Schematic representations of samples. Reproduced from [6].

attenuation becomes the limiting factor and the surface spectra become enhanced. For the incidence angles used in this thesis, the X-rays may be assumed to penetrate much more deeply than the depth from which no-loss photoelectrons can escape.

It is now important to consider a quantitative representation of the photoelectric cross section that may be used in intensity calculations. The electronic transition selection rules for a transition from an electronic state $\Psi$ characterized by the quantum numbers $n$, $l$, $m$, and $m_s$ to a state $\Psi^f$ characterized by the quantum numbers $n^f$, $l^f$, $m^f$, and $m_s^f$ are known to be [6]

$$\begin{aligned} \Delta l &= l^f - l = \pm 1 \\ \Delta m &= m^f - m = 0, \pm 1 \\ \Delta m_s &= m_s^f - m_s = 0 \end{aligned} \tag{6}$$

where in the case of photoemission, $\Psi^f$ is the continuum photoelectron wavefunction.

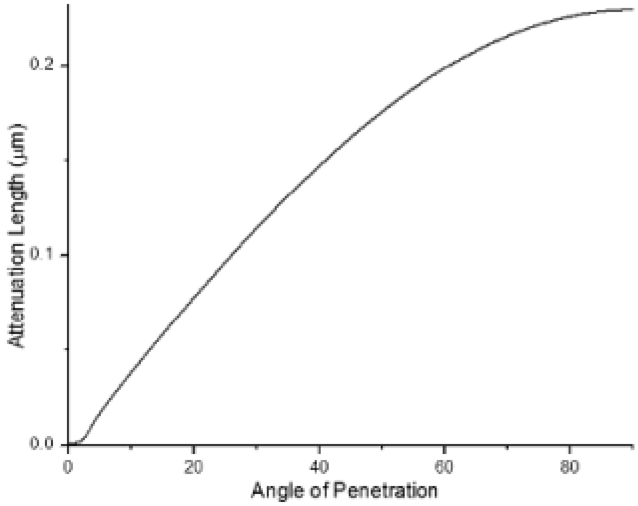

Figure 3: Skin depth of Al-K$\alpha$ X-rays of 1486.6 eV into a gold sample.

These limit the angular momentum components in the photoelectron wave to those satisfying the condition $l^f = l \pm 1$. Incorporating the selection rules into the angular and radial matrix elements, summing over initial states and averaging over final states for emission from a given subshell, and squaring them as required by Fermi's Golden Rule [6] then yields

$$\frac{d\sigma_{nl}}{d\Omega}(E^f) = \frac{\sigma_{nl}}{4\pi}[1 + \frac{1}{2}\beta_{nl}(E^f)(\frac{3}{2}\sin^2\alpha - 1)] \tag{7}$$

where $\sigma_{nl}$ is the total subshell cross section and $\beta_{nl}$ is the asymmetry parameter. $\beta_{nl}$ may have a value $-1 \leq \beta_{nl} \leq 2$; negative values for $\beta_{nl}$ correspond to photoemission preferentially parallel or antiparallel to the X-ray propagation direction, 0 gives an isotropic distribution, and for positive values photoelectrons are preferentially emitted normal to the direction of X-ray incidence, or equivalently, along the electric field vector of the radiation. In general [6], $\sigma_{nl}$ is given by

$$\sigma_{nl}(E^f) = \frac{4\pi\alpha_0 a_0}{3}(h\nu)[lR^2_{l-1}(E^f) + (l+1)R^2_{l+1}(E^f)] \tag{8}$$

with $\alpha_0$ the fine structure constant, $a_0$ the Bohr radius, and $R_{l\pm1}$ the radial matrix elements associated with the two photoelectron components.

Only electrons ejected from the sample within the spectrometer acceptance solid angle $\Omega_0$ may be detected; at the sample, $\Omega$ occurs as a function of $\theta$, $x$, and $y$. $R'(\theta, \Delta E)$, as presented in [5], is the spectral intensity response as a purely instrumental response function dependent only on the electron take-off angle, $\theta$, and energy dispersion width, $\Delta E$. $R'(\theta, \Delta E)$ is defined to be [5]

$$R'(\theta, \Delta E) \equiv \sin\theta \iint\limits_A I(\theta, x, y)\Omega(\theta, x, y)B(\Delta E, \theta, x, y)dxdy \tag{9}$$

where $A$ is the total planar surface area of the sample, and $B(\Delta E, \theta, x, y)$, as mentioned earlier, is the normalized spectral broadening function; this term includes imperfections in spectrometer geometry, crystalline aberrations, imperfect component alignment, spatial dispersion of the X-ray beam, imperfect focusing of electrons by the lens, non-uniformity of the hemispherical analyzer electric field, and cross-channel blurring in the multichannel detector. The $\sin\theta$ term derives from the implied integral over $z$, which accounts for the average depth of photoemission producing no-loss electrons, $\Lambda_e(E_{kin})\sin\theta$ (see Figure 2). $R'(\theta, \Delta E)$ permits absolute intensity comparisons for electrons emitted from the $k^{th}$ energy level of perfectly clean, ideal samples when included into

$$N(\theta) = D_0 \cdot F\left(\frac{E_0}{E}\right) \cdot \rho \cdot \left[\frac{d\sigma_k}{d\Omega}\right] \cdot \Lambda_e(E) \cdot R'(\theta, \Delta E); \tag{10}$$

$D_0$ is the detection efficiency of the spectrometer, $F\left(\frac{E_0}{E}\right)$ is a term which accounts for any intensity loss as an consequence of retardation to the analysis energy $E_0$ (related to the Liouville Theorem in classical mechanics), $E_0$ is the central reference energy, $\rho$ is the number density of the atoms emitting electrons from the $k^{th}$ level, and $\frac{d\sigma_k}{d\Omega}$ is the differential photoelectric cross section for the $k^{th}$ level. Eq. (10) further allows comparison of spectral intensity as a means of measuring the thickness $t$ of an overlayer on substrate by taking the ratio of the two intensities:

$$\frac{N_l(\theta)}{N_k(\theta)} = \frac{\Omega_0(E_l)A_0(E_l)D_0(E_l)\rho'\left(\frac{d\sigma_l}{d\Omega}\right)\Lambda'(E_l)}{\Omega_0(E_k)A_0(E_k)D_0(E_k)\rho\left(\frac{d\sigma_k}{d\Omega}\right)\Lambda(E_k)} \cdot \tag{11}$$
$$\cdot\, exp\{t/(\Lambda_e'(E_k)\sin\theta)\}\cdot[1-exp\{-t/(\Lambda_e'(E_l)\sin\theta)\}],$$

where $A_0$ is the aperture area and $\rho'$, $\Lambda_e'$, and the subscript $l$ denote the same quantities as above, but as relevant to the surface overlayer and its $l^{th}$ level. Quantitative calculations involving the ratio $\frac{N_l(\theta)}{N_k(\theta)}$ must involve peak *areas*, rather than the peak intensity value, so as to account for the natural peak width and energy dispersion by the X-ray beam and spectrometer. Eq. (11) may also be used to compare the relative intensities of two samples at the same $\theta$ for many purposes – see Figure 4.

In practice, it is often helpful to reduce Eq. (11) by modeling the sample as having a semi-infinite, atomically clean substrate with a semi-infinite, uniform overlayer. Incorporating these assumptions transforms Eq. (10) to

$$N_k(\theta) = N_k^\infty \cdot R''(\theta), \tag{12}$$

where $N_k^\infty$ is the intensity response of a semi-infinite sample (infinite in $\pm x$, $\pm y$, and $+z$ directions) and $R''(\theta)$ is either $[1-\exp\{-t/(\Lambda_e'(E_k)\sin\theta)\}]$ (for the overlayer) or $\exp\{-t/(\Lambda_e'(E_k)\sin\theta)\}$ (for the substrate). This equation fails to account for any surface contaminants, but such contaminants will attenuate the electrons from the substrate and the overlayer of interest roughly equally, so taking the ratio $\frac{N_l(\theta)}{N_k(\theta)}$, as in Eq. (11), will still allow for overlayer thickness calculation. Inserting both $R''(\theta)$

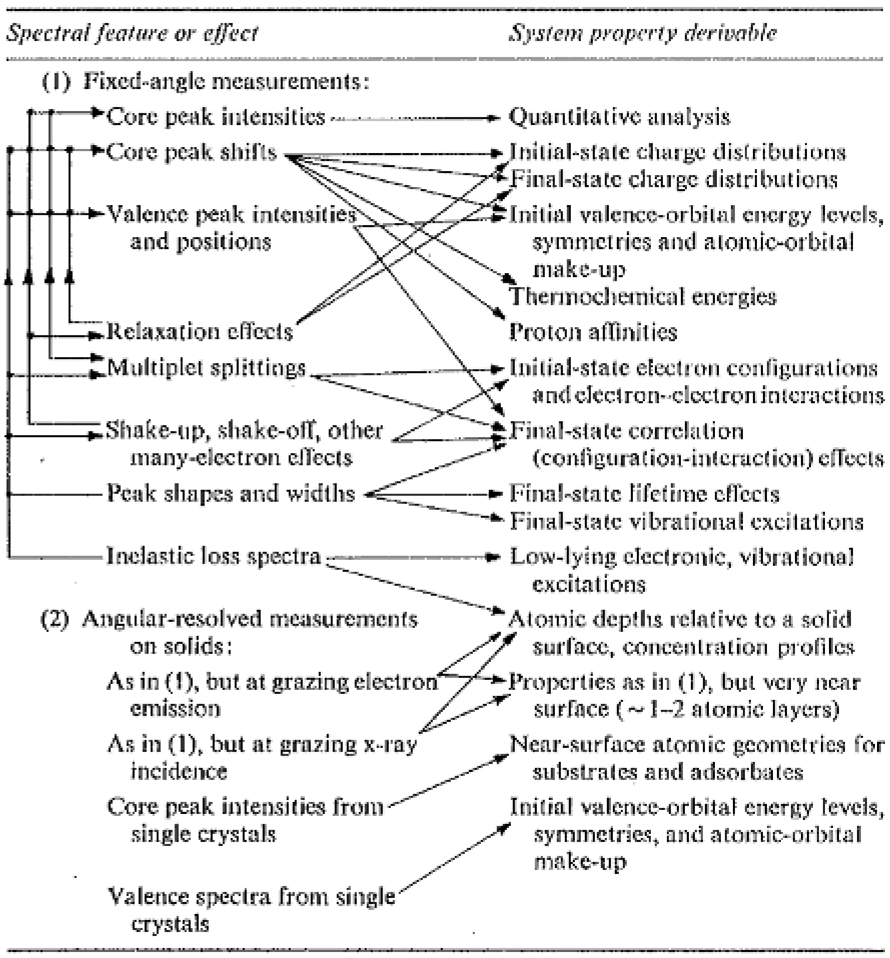

Figure 4: The versatility of XPS techniques in solid state physics.

into Eq. (12) and taking the mentioned ratio gives [18]

$$\frac{N_l(\theta)}{N_k(\theta)} = \frac{N_l^\infty}{N_k^\infty} \cdot \frac{[1-\exp\{-t/(\Lambda_e'(E_l)\sin\theta)\}]}{\exp\{-t/(\Lambda_e'(E_k)\sin\theta)\}} \tag{13}$$

Eq. (13) may be solved for $t$ provided $\Lambda_e'(E_l) \approx \Lambda_e'(E_k)$, as will be the case for an overlayer which contains the same element as the substrate, but which exhibits a chemical binding energy shift from the substrate's binding energy (as with the $SiO_2$ on Si examined later). In this case, both $\Lambda_e'$ will be very similar because the electron kinetic energies $E_l$ and $E_k$ will be large compared to the difference in binding energy (and therefore kinetic energy).

The natural width of spectral peaks, and hence the maximum achievable spectrometer spectral resolution, results from both the uncertainty principle as it relates to the lifetime of the electron hole state and what are known as the inelastic tails [19] of spectral lines. Inelastic tails are so termed because they occur as spectral broadening due to inelastic collisions of electrons before analysis; photoelectrons emitted by the sample undergoing an energy loss of $\Delta E'_{kin}$ will be detected at an energy of

$$E_{binding}^{apparent} = E_{binding}^{vacuum} + \Delta E'_{kin} \tag{14}$$

according to the notation used in Eq. (1), where $\Delta E'_{kin}$ is a positive quantity. The + in Eq. (14) appears due to the binding energy being calculated by subtracting the electron kinetic energy from the incident photon energy.

Beyond these intrinsic contributions to peak widths and shapes, we must also consider the overall contributions of the X-ray source and spectrometer: the instrumental line width. In order to examine the natural spectral broadening, then, the instrumental width must be minimized. This minimization is somewhat complex for the HP 5950A due to its simultaneous use of spatial dispersion of both the incident X-ray beam and hemispherical analyzer. Nonetheless, with an inverting lens, the spatial dispersion from these two sources can be made to closely cancel [5] – this effect is known as dispersion-compensation. Dispersion-compensation occurs only if the sample is positioned directly under the lens aperture and only for a specific, well-defined angle $\theta_0$ (see Figure 5). Dispersion-compensation can also only occur if the monochromator is optimally aligned – the center of the X-ray beam must reach the sample at the point where the X-ray propagation vector intersects the lens central axis in order for its dispersion to equal that of the spectrometer. For the case of an optimally aligned monochromator and sample probe angle (shifts sample position under lens), the dispersion-compensation angle $\theta_0$ may be be derived [5] from

$$\frac{\cos(\theta_0 + \alpha - \frac{\pi}{2})}{\sin\theta_0} = \frac{ME_0}{2r_0 \cdot \frac{d(h\nu)}{d\gamma}}, \tag{15}$$

where $M$ is the magnitude of the magnification of the electron imaging lens ($|-2.3|$ or $|-5.0|$ for the spectrometer in question), $E_0$ is the central reference energy, $r_0$ is the radius of curvature of the central reference trajectory in the hemispherical analyzer, and $\frac{d(h\nu)}{d\gamma}$ is the spatial dispersion of the X-ray beam. Experimentally determined values for the HP 5950A spectrometer used in many Fadley Group studies may be found in Table 2, as originally presented in [5]. For the two values of magnification available to HP 5950A, $-5.0$ and $-2.3$, $\theta_0$ may be analytically calculated to be $\sim 35^\circ$ and $\sim 64^\circ$, respectively. These calculations yield values that are within the experimental error of those measured in [5]: $\theta_0 = 31^\circ$ and $61^\circ$.

# 3 HP West

As stated in Section 1, HP West is the name of one of a pair of HP ESCA 5950A spectrometers in the Davis Fadley Group Lab. HP West was specially modified to allow for independent adjustment of several parameters (see Figure 1):

- sample angle $\theta$ for ARXPS measurements
- monochromator angle $\varphi$, which adjusts X-ray incidence angle $\phi_x$ and shifts the beam position on the sample surface
- sample translation rod (sample probe) angle $\psi$

Both $\varphi$ and $\psi$ are angles that were preset to the optimum angles by HP on manufacture of 5950A machines, but devices were installed [5] to allow easy external adjustment. The effects of differences in all three angles ($\theta$, $\varphi$, and $\psi$) on spectra were studied by Baird and Fadley with HP East [5], a spectrometer identical to HP West.

## 3.1 How It Works

HP West shares most of its design with other HP ESCA 5950A spectrometers. Samples are moved from atmosphere into a chamber under UHV conditions by a long probe through a series of differentially-pumped seals. A monochromatic beam of X-rays impinges on the sample and electrons are excited into vacuum by the photoelectric effect. The electron source at the sample surface is magnified by a lens and deflected by a hemispherical analyzer, which measures the original kinetic energy of the electrons, thereby measuring their initial binding energy by Eq. (1).

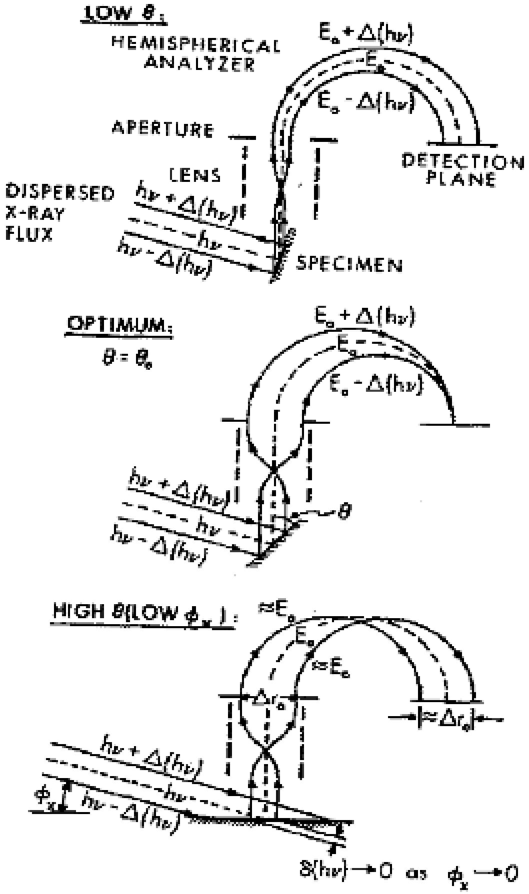

Figure 5: Model of the spread in detector energies at the detector as it depends on $\theta$. Adapted from [5].

Samples of dimensions 12.7 mm × 10.7 mm × 1.4 mm are fixed to a sample tray and held in place by a pair of rails and a small bent piece of stainless steel

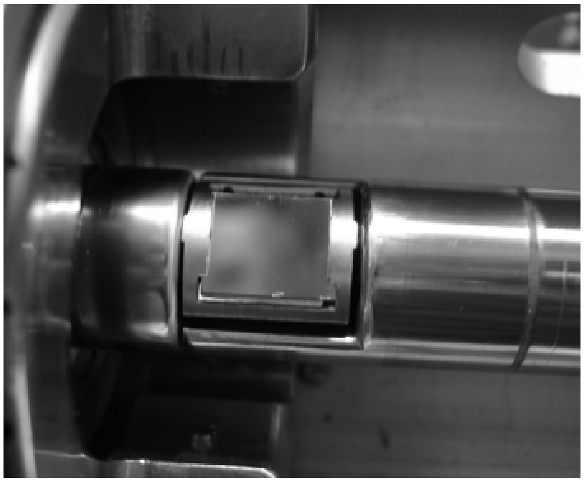

Figure 6: A highly reflective sample positioned in the sample tray of the manipulator.

acting as a spring. An image of the sample tray with a reflective sample inserted is displayed in Figure 6. The sample holder tray is mounted near the inboard end of a long, polished steel rod. A handle attaches to the outboard end of the rod to allow for translation of the sample into and out of the chamber while at low pressure. A trio of differential seals prevents air from leaking into the chamber while still allowing for lateral movement of the sample. The seals and rod must be machined to excellent precision in order to preserve UHV conditions inside the experiment chamber.

### 3.1.1 Basic Operation

While in operation, the first stage of vacuum occurs between the first and second seal, where a mechanical pump achieves a minimum pressure (base pressure) of about 75 mTorr ($7.5 \times 10^{-2}$ Torr). When inserting a sample into the experiment chamber, the operator must wait for the pressure at this stage to approach the base pressure before proceeding to the next stage so as to avoid overloading the low-pressure ion pump(s) that pump the second stage and the interior chambers of the spectrometer. The second stage of vacuum occurs between the second and third seal, where a small

(20L) ion pump achieves a base pressure of about $6 \times 10^{-6}$ Torr before the sample is ready to continue into the sample staging (or preparation) chamber.

Once the sample has cleared the three differential seals, it enters the staging chamber. The staging chamber is equipped with several ports for attaching various probes for sample treatments in a low-pressure environment; this allows the operator to prevent or control contamination of the sample between sample treatment and XPS measurements. Angle-resolved measurements may then examine the surface effects and chemical shift effects that these treatments have on the sample (see Section 2, [3]). The staging chamber is attached to both an ion pump (60L) and an ion gauge (hot cathode) for measuring the pressure. When a sample has been inserted into the main chamber, the ion gauge will read the pressure of both chambers because they are open to each other. The base pressure of the system is affected by many factors (see Section 4.1).

The sample finally comes to rest in the main chamber, immediately adjacent to the staging chamber. Attached to the main chamber is a large (220L) ion pump capable of reducing the ambient pressure to about $4 \times 10^{-9}$ Torr without system bakeout. A beryllium "window" separates the main chamber from the monochromator chamber, which has its own 110L ion pump. Beryllium absorbs X-rays weakly [8] so it allows the beam directed by the monochromator to pass, but stops other unwanted photons and electrons from entering the main chamber.

### 3.1.2 X-ray Illumination

In order to generate X-rays, a potential difference of about 15kV is applied between a heated tungsten filament (cathode) and an aluminum anode. The tungsten releases electrons, which are accelerated through the potential difference toward the aluminum. Upon striking the aluminum, bound electrons are released, creating vacancies in the electronic structure. The potential difference is chosen such that the incident electrons have enough energy to kick out K-shell electrons at a high rate; these K-shell vacancies are then filled by electrons at lower binding energies making transitions to these higher binding energy (lower potential energy) orbitals. The most intense X-rays come from the so-called K$\alpha_{1,2}$ transitions of aluminum, from the L$_{III}$ shell (a $2p_{\frac{3}{2}}$ orbital) and the L$_{II}$ shell (a 2p$_{\frac{1}{2}}$ orbital) to the K shell (a $1s_{\frac{1}{2}}$ orbital), which emit close-lying photons of energy $h\nu = 1486.6$ eV. Because we are speaking of the electronic K$\alpha$ transition for aluminum it is known as Al-K$\alpha$ radiation. This emission of Al-K$\alpha$ radiation is often referred to as X-ray Fluorescence (XRF).

Bombardment of the aluminum with electrons, as is required for XRF, also results in the deposit of many kinds of electron and phonon excitation energy to the aluminum; this heats the aluminum, so a heat exchanger pumps distilled water coolant through channels underneath the aluminum anode to carry away the generated heat. Under sustained operation, the temperature of the coolant water comes to equilibrium with the anode at about 35°C. The heat exchanger is attached to the X-ray power supply control unit through a series of interlocks for the safety of the X-ray anode; these shut off the X-ray power supply if either the water flow rate is too low or the water temperature rises too high (discussed further in Section 5.2.1).

The X-rays from the aluminum anode are emitted toward monochromator crystals which Bragg reflect them back toward the sample in a focused beam [9]. The angle of reflection depends on the crystal structure of the monochromator and the wavelength of the photons, according to Bragg's Law in first order: $\lambda_x = 2d\sin(\theta_B)$, with $\lambda_x$ the X-ray wavelength, $d$ the spacing between diffracting planes, and $\theta_B$ the Bragg angle. For this case, for Al-K$\alpha$ photons and with the quartz monochromator crystals installed, the Bragg angle (measured with respect to the crystal surface) is $\theta_B = 78.5°$. The monochromator consists of three individual, spherically bent, (001)-oriented, quartz crystals [5]; together, they focus X-rays from the aluminum anode onto the sample. Because there will be a spread in the energies of the X-rays incident on the monochromator, the Bragg angle will vary across the range of energies centered around $h\nu = 1486.6$ eV $\rightarrow \theta_B = 78.5°$. This results in some spatial dispersion of the X-ray flux incident on the sample, approximately a Gaussian distribution of 0.64 eV FWHM along the $\gamma$ direction of Figure 1 [5].

The photoelectrons ejected from the sample are retarded and their source image is magnified and inverted by specific potential differences in the lens. The electrons are then selected for the appropriate kinetic energy by the hemispherical analyzer. The hemispherical analyzer selects the electrons exiting the lens for one specific value of kinetic energy by applying an electric field between two large concentric hemispherical plates. Electrons moving too slow will be deflected too much to continue through the gap between plates to reach the detector; thus, they will strike the inner (positively charged) plate. Electrons moving too fast will not be deflected enough and will strike the outer (negatively charged) plate. The hemispherical analyzer has a central analyzed energy $E_0$ of 115 eV, but because there is a finite gap between the charged plates, there will be a non-zero spread in energies of the detected electrons as seen finally by the detector. The calculated dispersion in the detector plane is $\frac{dE}{dr} = 3.71 \frac{eV}{cm}$ [5].

HP 5950A spectrometers are designed around the principle of dispersion- compensation. This is a specific arrangement of the sample and monochromator alignment that causes the hemispherical analyzer dispersion to cancel the X-ray flux dispersion, thereby maximizing the overall resolution of the spectrometer (see Section 2, Figure 5). That is, the width of the Bragg-reflected flux can, in principle, be dispersion-compensated into a single peak in kinetic energy.

## 3.2 Why It Is Special

What makes HP West special is that instead of being equipped with the HP standard sample translation probe, it has a custom-designed sample manipulator [5] that is capable of being rotated smoothly through an angle of 80° through an axis connected to the sample from outside the chamber. This allows the operator to adjust the angle of the sample with respect to the X-ray beam without translating the sample, thereby yielding angle-resolved measurements that include far more information than single-angle energy spectrum data alone (see Section 2).

HP West has also been equipped with a stepping motor for rotating the sample probe and an adjustment knob for movement of the monochromator crystals from outside the chamber. The combination of monochromator movement and sample probe movement was built into the machine specifically to examine the effects that adjusting these parameters has on the spectra produced, especially regarding the optimum case of achieving dispersion-compensation. The stepping motor is no longer attached because it is no longer operational, but was once capable of 0.9° steps, giving the operator excellent control over sample positioning. All rotations in this thesis were made manually.

## 3.3 Studies With HP West

HP West was very active with the Fadley Group from when it was donated to UC Davis by a former student of Prof. Fadley's working at IBM until July 2003, when various known and unknown problems were determined to affect proper functioning and a lack of interested Fadley Group graduate students from Davis restricted the potential for restoration. HP West was originally purchased by IBM San Jose and was used for characterization of magnetic materials for applications in magnetic reading and recording devices; the specialized sample probe designed for ARXPS was purchased from another vendor and installed for this purpose.

Throughout much of HP West's operation, it has been used for analysis of sample surfaces, especially layer thickness characterization and chemical shift analysis for other research teams. To this end, it has been an excellent apparatus for young graduate students with which to gain laboratory experience and learn about applications of solid state physics, while also providing other researchers on campus with valuable information about their samples.

HP West has also been used by graduate students in a comparative mode with data gathered in studies done with HP East, such as analyzing purely instrumental effects of the monochromator, sample probe, and sample angle orientations on spectra. HP West has thus proven to be an excellent educational and informational tool, and the several problems it has recently experienced present an opportunity to gain experience solving challenging real-world problems in an experimental physics laboratory for graduate students (and undergraduates, such as myself). Details of my experiments may be found in Section 6.

HP West is currently controlled by a dedicated, though rather old, PC running Windows 3.1. The software for the interface was written specifically for HP West and its custom-designed interface unit by Alex Kay, a former graduate student in the Fadley Group. The interface unit was designed by Britt Holbrook and built by Georgi Rumiansev, of the UC Davis Physics Electronics Shop. Several initial problems were encountered with the interface unit and software, and these are commented on at the end of this thesis.

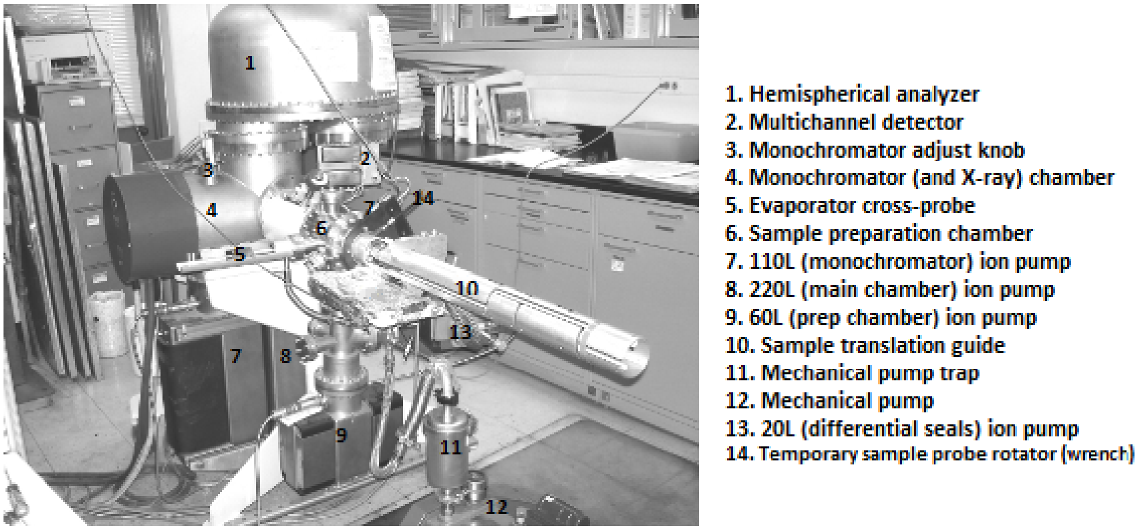

Figure 7: HP West, with various components labeled.

# 4 Initial Operation

When the restoration project for HP West was suggested by Prof. Fadley, the machine had been idle since July 2003, before which its use had been sporadic due to lack of interested local students, as well as numerous malfunctions and difficulty in fixing the associated problems. In the time between July 2003 and July 2009, when the restoration project was begun, HP West had been allowed to come to equilibrium with the air in the laboratory (its chambers were at atmospheric pressure). The first step to restoration was to achieve a vacuum inside the machine so that its operating status could be determined.

## 4.1 Achieving a Vacuum

HP West utilizes a total of seven pumps to attain and maintain low pressure conditions in the main chamber and monochromator chamber; one mechanical pump (aka roughing pump) lowers the pressure just inside the first differential seal to about $\frac{1}{1{,}000}$ of atmospheric pressure; two cryogenic sorption pumps (aka cryosorption or cryopumps) connect to the first pair of differential seals and also directly to the main chamber, efficiently and cleanly lowering the pressure into the low $10^{-3}$ Torr range for rough pumping the system from atmosphere; four ion pumps operational only below a certain level (elaborated below – see Section 4.1.2) ionize gas molecules and accelerate them into reactive titanium, thereby lowering the pressure in the second pair of differential seals, the staging chamber, the main chamber, and monochromator chamber, where they are directly attached.

Many flanges are welded into the structure of the main chamber and sample chamber to provide interfaces with the interior components while under UHV. To provide a very tight seal, tight enough to withstand a pressure differential of up to about one atmosphere (760 Torr), copper gaskets are placed between all flange connections. The flange connections all have a sharp knife-edge surface which presses into and deforms the soft copper gasket, forming an extremely tight seal.

The instantaneous pumping speed of any pump is given by

$$S = \frac{Q}{P}, \tag{16}$$

where $S$ = pumping speed in Liters/sec, $Q$ = mass flow rate in Torr-Liters/sec, and $P$ = the pressure in Torr. The pumping speed is dependent on the type of pump used; for the mechanical pump and the cryopumps, the pumping speed will be approximately constant over the range of operation because each of these pumps move whole air without any kind of treatment (unlike the ion pumps). Because of the way the ion pumps operate (see Section 4.1.2), the pumping speed will be dependent on the pressure, but the instantaneous pumping speed S at any given time will still obey Eq. (16). Eq. (16) gives a simple equation for P which reveals that at a constant pumping speed S, P decreases asymptotically with time (and approaches

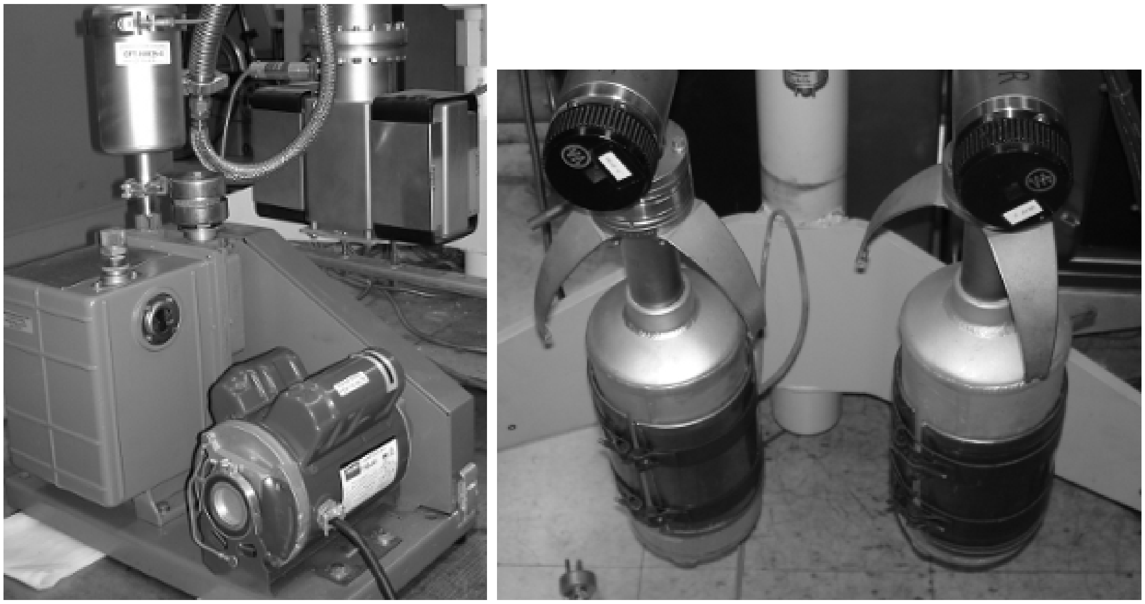

(a) The mechanical pump and 60L ion pump.

(b) HP West's VacSorb cryopumps.

Figure 8: Various pumps used to obtain and maintain UHV conditions inside HP West.

a value specific to the system and pump). The mechanical and cryopumps reflect this behavior in their operational range (from atmospheric pressure to their mTorr lower limits, where their pumping speeds drop abruptly), but the ion pumps have a pumping speed that varies with pressure and so the pressure behavior for them is more complex.

### 4.1.1 Mechanical Pump and Cryosorption Pumps

Both the mechanical pump and the cryopumps are attached to plumbing that runs along the side of the main chamber (see Figure 9) and connects to the outer pair of differential seals and also directly to the main chamber. Valves attached to the mechanical pump, the differential seals, each of the two cryopumps, the main chamber, and between the main chamber and monochromator chamber allow for selective pumping on each chamber or all chambers with whichever pump is appropriate.

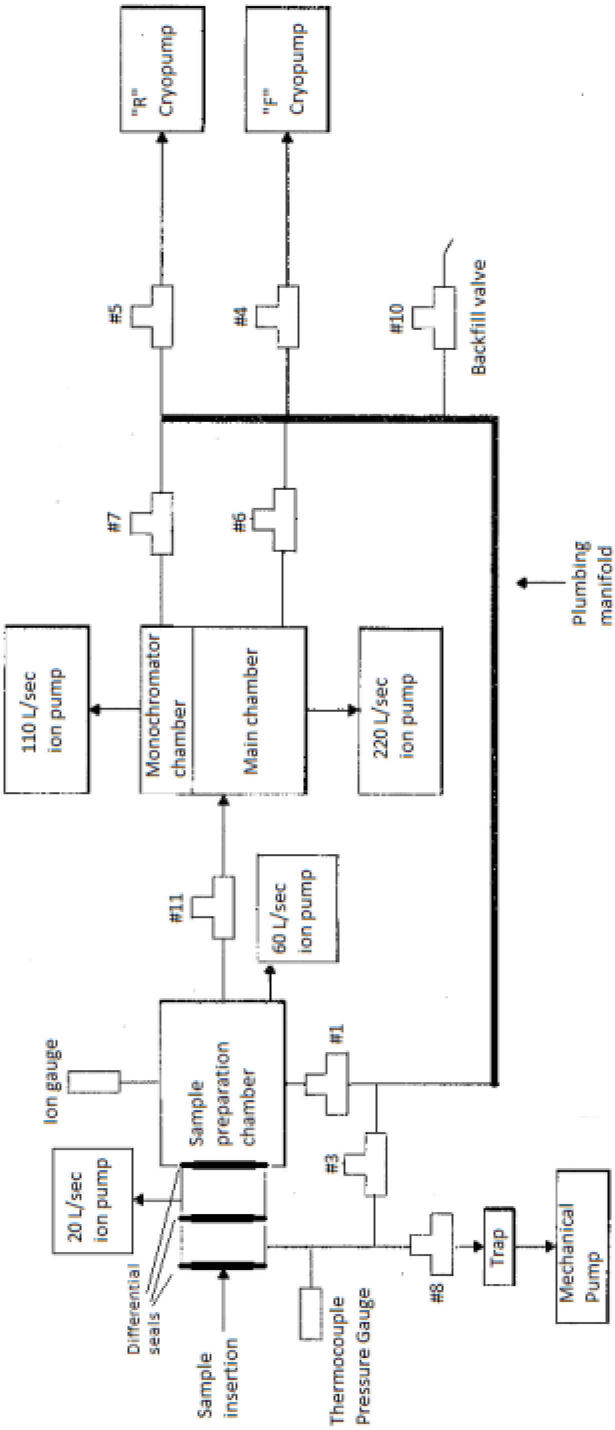

Figure 9: A schematic diagram of the outer plumbing and the attached pumps and gauges of HP West. Adapted from [16].

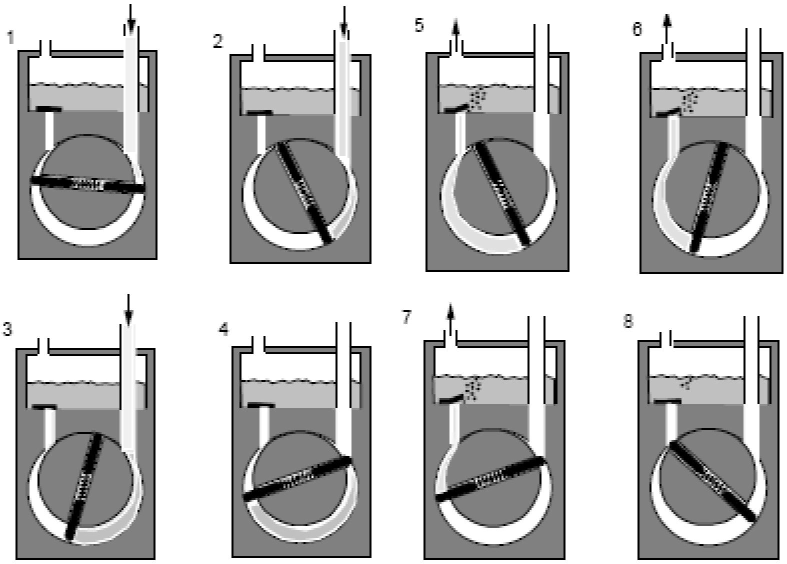

Figure 10: The operating procedure of an oil-sealed rotary mechanical pump. Reproduced from [11].

The mechanical pump is an oil-lubricated rotary pump which decreases the pressure on the inlet side by expanding air from the lower pressure region and pushing it to the exhaust port while compressing it so that it is released when vented to atmosphere (see Figure 12). An offset cylinder rotates within the pump chamber and a sliding wall spanning the chamber separates the inlet tube from the higher-pressure part of the movement cycle. This continually moves air *from* the inlet *to* the exhaust port.

Because the cryopumps are capable of achieving a significantly lower pressure than the mechanical pump, the cryopumps are used as second-stage pumps, after the mechanical pump. Due to the significantly lower base pressure achieved, the mechanical pump must be valved off from the chambers before engaging the cryopumps in order to prevent drawing oil from the reservoir of the mechanical pump into the chamber. Drawing oil into the chamber would be detrimental because of its low vapor pressure and high viscosity – oil would contaminate chamber surfaces and all other pumps and

UHV ambient pressures would be nearly impossible to obtain again. These properties for heavy hydrocarbons are said to give these molecules "relative immobility" in vacuum. The relative immobility of these molecules can be reduced by baking the chamber surfaces at high temperatures ($250° - 400°C$); the high temperatures raise the vapor pressure of these molecules and also, to some degree, cause the molecules to break apart into smaller molecules because it is energetically favorable to do so. Higher temperatures can cause vibration of components that have molecular binding energies comparable to $k_BT$, the ambient thermal kinetic energy, so the molecules break apart into smaller molecules with lower molecular binding energies to the surfaces inside vacuum.

Baking out the chamber also has the added benefit of vaporizing adsorbed water vapor molecules; both large hydrocarbons and water vapor have high sticking coefficients (the probability of adsorbing to a surface in the event of a collision). Raising the temperature drastically reduces the sticking coefficients of these molecules, which will make their entry into an ion pump far more probable and result in their eventual removal from the system. Unfortunately, with HP West, the teflon differential seals allowing easy movement of samples into and out of UHV are delicate and are easily damaged by high temperatures so baking the machine must be done with great care so as to prevent overheating and damaging these seals.

The cryopumps consist of a metallic case surrounding a synthetic zeolite molecular sieve adsorbent material [12]. This material is extremely porous and molecules traveling into the pump are adsorbed onto its very large surface area. A quick glance at the ideal gas law,

$$PV = Nk_BT, \tag{17}$$

shows that decreasing the number of particles in the air will decrease the pressure, all other factors remaining constant. Though adsorption to the molecular sieve surfaces *will* occur at room temperature, molecules in the air will bind much more readily to the zeolite surfaces at lower temperatures because the kinetic energy of the molecule will be transferred to the lattice. At higher temperatures, the porous lattice holds more thermodynamic energy in the form of phonons. The phonons make it energetically favorable to release the adsorbed molecules; this phenomenon is also exploited to "recharge" the zeolite molecular sieve when the pump has become saturated by adsorbing the effective maximum number of molecules.

In the recharge process, the pump is valved off from the plumbing and heated using a resistive heating jacket to about 200°C (500K). The pump must bake for long enough that the entirety of the zeolite has reached the baking temperature; at the end of the bake, the pump is vented to atmosphere through a one-way elastomeric valve to release the excess molecules extracted from the chamber. The pump is then allowed to cool to room temperature, where it will achieve a pressure below 1 atm again (see Eq. (17)). In order to maximize the pumping capabilities of the cryopumps, each is cooled by an attached thermally insulated bucket filled with liquid nitrogen at 77K.

To maximize the efficiency of and lower the base pressures of the mechanical pump and cryopumps, the mechanical pump is first used to "rough" the chamber and differential seals to about 75 mTorr. The mechanical pump is then valved off to prevent oil backstream and only one of the two cryopumps is valved open to the chamber and differential seals.

The first cryopump is allowed to pump for about 15 minutes – shorter than the time needed to reach saturation – so that there is still some air flowing into the pump at the time it is valved off. This is done because inert gas molecules do not readily adsorb to the molecular sieve so they are "dragged" into the pump with the initial stream of whole air from the chamber [13]. As long as *some* air is flowing into the pump (before the pressures in the pump and chamber equilibrate), these inert gases will be trapped via collisions with the incoming air. If the pressures are allowed to equilibrate, some of the inert gases in the pump will escape back into the chamber, where they will cause the air to have a much higher percentage of these gases than in natural air, meaning a far lower percentage of the remaining air will be able to be pumped by the second cryopump. When the first cryopump is valved off at the opportune time to maximize dragging of inert gases, a distribution of gases with a low percentage of inert gases is maintained, so the second cryopump will achieve a much lower base pressure after being allowed to equilibrate.

Altogether, the three pumps are capable of reaching pressures in the low $10^{-3}$ Torr range. The second cryopump typically does not reach saturation by the time the ion pumps are activated; the base pressure for the cryopumps depends on the type of molecules adsorbed, the initial pressure, and the use of "dragging" to limit the inert gas percentage of the air pumped by the second cryopump. Provided that the liquid nitrogen cooling has been fully achieved, as verified by a constant low boil-off rate of the liquid, it is not necessary to wait longer than about 20 minutes for the second pump to achieve base pressure.

In order to minimize the time needed to reach the lower pressure limits, when returning the chamber to atmospheric pressure for repairs or during a long period of disuse, nitrogen gas is slowly backstreamed into the chamber because its relatively low adsorption binding energy (on metallic and glass chamber surfaces) ensures that it will pump out of the chamber easily compared to water vapor and inert gases, which bind more strongly to these surfaces and will slow the pumpdown rate.

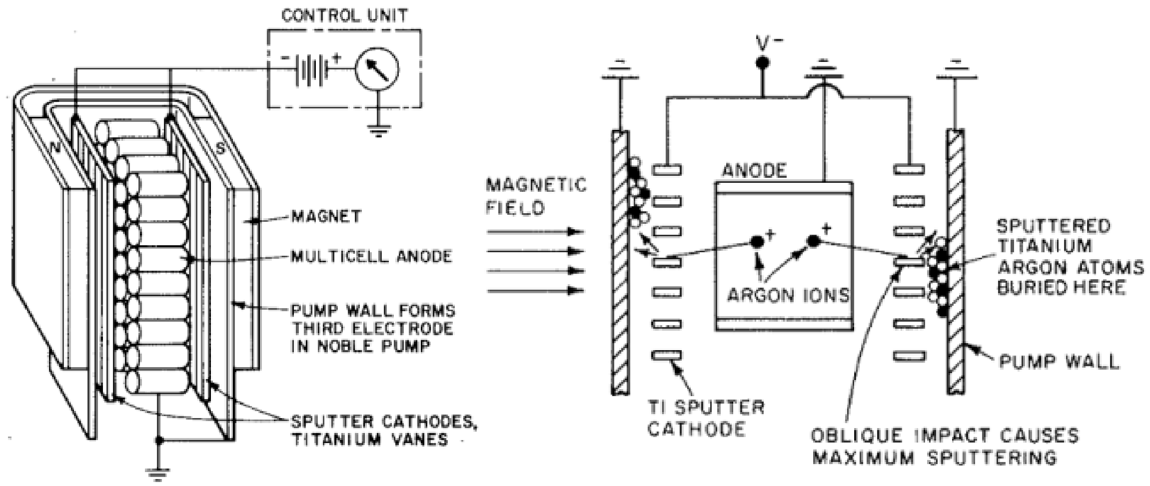

(a) A perspective-drawn schematic of an ion pump.

(b) Cutaway cross-section of a triode ion pump.

Figure 11: Diagrams of noble (triode) ion pumps, of the type attached to HP West. Reproduced from [14].

### 4.1.2 Ion Pumps

Ion pumps operate and behave very differently from mechanical and cryopumps. Ion pumps remove gases from the chamber by ionizing the air molecules that enter the pump chamber and attracting them to the charged walls of the pump body.

A triode consisting of a high-voltage stainless steel anode and a pair of titanium cathodes accelerates electrons into the pump body, where a permanent magnetic field traps the electrons within the body. Gas molecules from the vacuum vessel enter the pump body, where the trapped electrons collide with the neutral gas atoms, positively ionizing them, and these ions are then strongly attracted to one of the cathodes [14]. Upon reaching the cathode, the ions have a large amount of kinetic energy and become buried in the highly reactive Ti cathode wall and/or sputter titanium atoms into the chamber, which react with other molecules to remove them from the gas phase (a process known as chemisorption) [11].

The lower the pressure in an ion pump, the lower the rate of ionization, net current flow, and sputtering and so the higher the voltage across the triode electrodes will be. The lower sputtering rate also means a lower current draw to maintain triode voltages, and this current may be measured to give a direct measure of the pressure in the chamber. All of HP West's ion pumps have built-in pressure gauges; a knob allows the selection of the displayed scale. One of the selections of the scale-select knob reads a current measurement converted to an absolute pressure reading.

Ion pumps, like all vacuum pumps, exhibit an exponential decrease in mass flow rate as a function of pressure (once they have reached their maximum pumping speed) as per Eq. (16). The pumping speed of an ion pump will vary over the range of operating pressures because at the higher end of the pressure range, relatively high densities of gas molecules in the body of the pump will make several key differences [14]:

- neutral gas molecules will screen triode potential differences by electric polarization
- high sputtering rates decrease the triode potential difference and increase current load
- entrapped electrons are accelerated less before colliding with gas atoms and may not ionize them
- ionized gas particles are more likely to collide with other atoms before reaching cathode walls, decreasing burying events (but increasing sputtering events)

As the gas concentration in the pump body decreases, the pumping rate increases to its maximum value, which is specified by the rated pumping speed (the 20L, 60L, 110L, and 220L pumps of HP West all refer to maximum per-second pumping volumes). The pumping speed of any ion pump will also depend on the species of gas

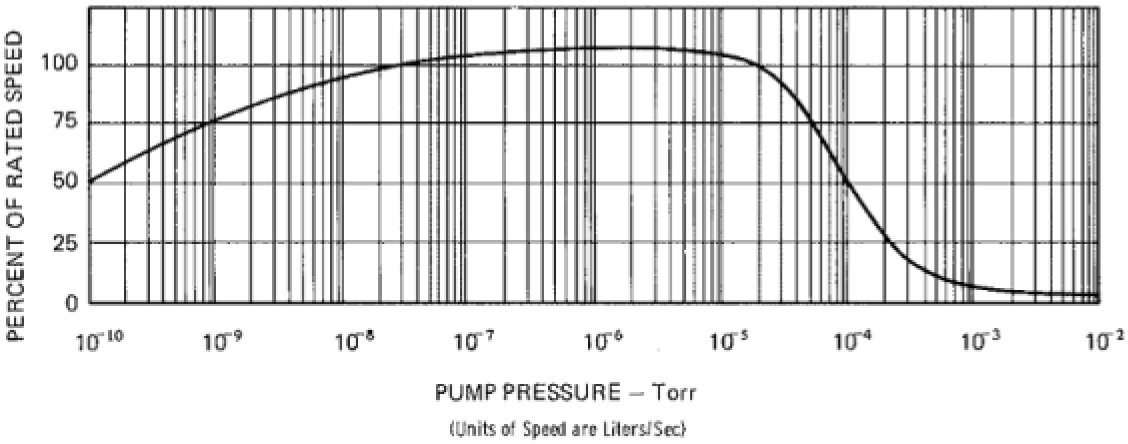

Figure 12: Approximate pumping speed of an ion pump over its range of operation. Reproduced from [14].

being pumped. Lighter, more reactive gases, such as oxygen and nitrogen, are pumped quickly and efficiently, whereas heavier gases and inert gases pump as low as 20% of the speed of whole air [11]. It is mostly due to the non-uniformity of pumping speeds across gas species that contributes to a slowing of the pumping speed of ion pumps at lower pressures (see Figure 12). A small amount of the slowing of pumping speed is also attributable to the lower probability of collisions with the ionizing trapped electrons in the pump body at the lower end of the pressure range.

Because ion pumps operate by reacting with and/or burying gas molecules into the walls of the pump and/or the titanium cathodes, and because the amount of titanium on the cathodes decreases over time and with usage, ion pumps have a limited service lifetime that is dependent on the pressure of operation. The total amount of gas molecules buried and chemisorbed is the true limiting factor that determines pump service lifetime. The rate at which molecules are buried and chemisorbed in the pump is dependent on the operating pressure; the relation is not linear, but ion pumps have *much* shorter lifetimes when operating in the $10^{-6}$ Torr range and above for extended periods of time. It is for this reason that the cryopumps are used to lower the pressure as much as possible *before* activating the ion pumps.

The ion pumps are all equipped with a switch toggling between "Start" mode and "Protect" mode. In "Protect" mode, if the pump current jumps suddenly or rises too high, or if the pump is running in some other unstable way, the power to the pump is cut off by a circuit breaker-type switch in order to protect the pump from damage. Being opened to atmosphere, even with the precaution of venting the chamber to dry nitrogen, can lead to some adsorption of molecules, including water vapor, onto cathode surfaces. In this case, outgassing will occur when the pump is started, resulting in a high operating current. If the pump must be started at a high pressure or after being open to atmosphere, the pump must be placed in "Start" mode and carefully monitored, because in "Start" mode the threshold cutoff current is much higher, and so requires careful attention and good judgment on behalf of the operator to prevent damage to the pump.

When an ion pump is operated continuously at a relatively high pressure for an extended period of time, or begins operation at a high pressure and takes a long time (hours) to lower the chamber pressure to a "comfortable" operating pressure (below $10^{-6}$ Torr), titanium "flakes" can appear. These flakes are spikes of deposited titanium and other chemisorbed elements that affix to a cathode or anode unevenly; when a spike begins to form, electric field effects around the tip of the spike [10] attract more ions, eventually reaching far enough from the surface to allow an arc from cathode to anode. This causes the pumping speed to drop to zero because there is no longer a mentionable potential difference to accelerate electrons into the pump body to ionize the neutral gases. To free the pump of flakes, a "shake," or a sharp kick with a soft object like a rubber mallet or shoe is needed. Once the pump has been shaken and the flakes dislodged, it will return to normal operation.

When an ion pump reaches the end of its service lifetime, it must be recharged.

This entails a dissection of the pump, including a cleaning of some surfaces (like the stainless steel anode) and a replacement of others (like the cathodes, whose titanium will be depleted). Ion pumps ready to be recharged exhibit characteristically low pumping speeds, and so settle to higher base pressures. HP West's ion pumps appear to be in good working condition, but a few shakes have been necessary to achieve the expected (for normal operation) current-voltage responses.

### 4.1.3 Measuring the Pressure

In order to monitor the pressure in the chamber, three gauge varieties are used. One has already been discussed, the conversion of the ion pump current measurement in order to determine the pressure of the gases in the pump body. Two other types of gauges are used, each of which has a different functional pressure range based on its operational principle – an ion gauge for the lowest pressures and a thermocouple gauge for the outer plumbing (and also used during pumpdown).

The ion gauge operates in a way similar to the pressure measurement of the ion pumps:

1. A filament is heated and held at a low positive potential so that it emits a regulated electron current
2. A helical wire is wrapped around a central wire at a measured radius and held at a high positive potential so that it attracts the electrons
3. Gas molecules are ionized by the electron current and attracted to the central collector wire held at a low negative potential
4. The rate of incidence of the ionized gas molecules will create a measurable current which will be indicative of the ambient pressure of the chamber

5. The measured current is converted to a pressure displayed on the electronic control unit.

The thermocouple gauge works in a much different way:

1. A constant DC current heats a thermocouple junction between two different metals which is sealed within the chamber
2. Collisions of gas molecules with the thermocouple transfer thermal energy to the gas
3. The rate of thermal energy transfer will be proportional to the rate of collisions (hence, the pressure, as per Eq.(3))
4. The thermocouple voltage is a direct measure of the temperature of the filament; thus, the voltage is converted to an electronic pressure reading by suitable manufacturer calibration.

The functional operating range for the thermocouple will be from about 1 Torr down to about 1 mTorr. The thermocouple gauge operating limits are determined by the thermal properties of the hot filament; above 1 Torr there is a higher rate of collisions than is necessary to remove all of the power thermally dissipated by the filament, which is held at a fixed current; below 1 mTorr there is too low a rate of collisions for the temperature of the filament to change an amount detectable by the thermocouple. The operating range for the ion gauge is from about 1 mTorr down to about $10^{-10}$ Torr [14]; above 1 mTorr, the mean free path of the gas molecules is shorter than the dimensions of the gauge, meaning the ions will often collide with other molecules many times before striking the collector wire, giving unstable current measurements which are not proportional to the pressure; below $10^{-10}$ Torr, X-rays generated by X-ray fluorescence of the materials in the helical electron attractor will create a noise signal in the collector filament that is comparable to the current of ionized gas molecules, so the gauge will read a fixed (base) pressure even if the pressure in the chamber drops lower.

## 4.2 Observing Component Status – What Needs Attention?

Once I had learned what was necessary to begin to operate and diagnose a UHV system, it was finally time to begin assessing the condition of HP West. The items observed in my initial assessment made with the aid of Prof. Fadley, Peter Klavins, and Georgi Rumiansev were as follows:

- There was no working means of measuring the pressure above the operational range of the ion pumps and ion gauge (1 mTorr and above)
- There was no mechanical pump attached for roughing purposes and maintaining the first of two differential seal pressure "barriers" between UHV and atmosphere
- Prof. Fadley recalled a history of issues with the ion gauge, one of the ion pumps, and the X-ray power supply preventing the use of each
- Prof. Fadley recalled problems with the heat exchanger cooling the X-ray anode.

Prof. Fadley advised cannibalizing any parts necessary from HP East, which had been further removed from use than HP West and was in worse condition, and so warranted less sympathy.

The first problem to be addressed was the need to measure roughing pump pressure. A pressure gauge mounted in the HP West control stack that was missing a cover was tested with a thermocouple gauge borrowed from the Liu group, down the hall from the Davis Fadley Group Lab. The pressure gauge was tested for pressure measurement by attachment to the (isolated) plumbing between cryopumps (see Figures 8, 9) and opening the valve of one pump to see if the gauge showed a response. Though a sound of rushing air was heard, the gauge registered no movement. The gauge was found to have three connections on the rear and a switch with a label matching each connection. The switch was cycled along with the connector to test for activity in each connection; one was found to cause the gauge to register a pressure reading, so a cover was salvaged from a non-operational gauge and the problem was eliminated.

Once the pressure gauge had been attached and deemed operational, the chamber and plumbing were checked high and low for open valves and flanges. The chamber was observed to be closed at first inspection and an overnight bakeout of the cryopumps was instituted. Each cryopump has a heat jacket installed which bakes the pumps at about 250°C. The pumps were given another 24 hours to cool to room temperature so as not to waste liquid nitrogen in cooling the pumps to cryogenic temperatures, and in order to give time for me to renew my knowledge of cryogen handling and safety and study vacuum operating conditions.

Once ready, insulating buckets were attached to the cryopumps and liquid nitrogen was poured into the buckets to cool the pumps to liquid nitrogen temperatures. Due to the low thermal conductivity of the zeolite adsorbent molecular sieve material inside the cryopumps, the wait time of 20 minutes suggested by the operating manual [12] was allowed after the pumps' skin reached 77K for each pump to fully cool before being valved open to the plumbing. During the pumpdown, all valves between the cryopump plumbing and the chamber were opened so that the cryopumps would pump on the entire chamber, including the differential seals. Both pumps were opened in an order corresponding to the procedure described in Section 4.1.1 and with the advice of Prof. Fadley and a base pressure of about 10 mTorr was established.

Once the cryopumps had reached their base pressure, each of the ion pumps was activated in "Start" mode, as detailed in Section 4.1.2. The chamber was valved off from the outer plumbing once the ion pumps had all begun steady operation to prevent drawing adsorbed molecules from the zeolite adsorbent (and the zeolite itself) into the chamber. The cryopumps were allowed to warm while continuing to pump on the outer plumbing.

The two smaller ion pumps have "overload" buttons and lights which display when "Protect" mode has shut off the pump and must be overridden, whereas the two larger pumps have breaker-type power switches. The 20L (smallest) pump, attached to the inner differential seals, exhibited the most trouble starting, and was finally started after the other three pumps had lowered the pressure at the 20L pump into the $10^{-5}$ Torr range. The power light on the 20L pump is also misleadingly burnt out. Care should be exercised in using all of the ion pumps, as some gauge and indicator light functions are not operational; repairing the non-functional ion pump controller components would be beneficial.

The monochromator ion pump of 110L pumping speed still has exhibited no issues in startup or operation, and consistently reads the lowest pressure of all the gauges attached to HP West – $1 \times 10^{-9}$ Torr or lower. The sample prep chamber (60L) pump also started up with no significant problems. The main chamber (220L) pump, however, initially required a kick from Prof. Fadley to begin pumping, presumably due to previous growth of Ti flakes. The pressure slowly dropped into the $10^{-5}$ Torr range before the needle began to dance and then the pump shut itself off. The pump control unit was then swapped with an identical control unit from HP East and although the readings were initially unstable with the new control unit, they eventually settled down and read a smooth drop in pressure down to a base pressure of $7 \times 10^{-8}$ Torr in the first 2 hours of operation (see Figure 13 for a similar pressure/time comparison).

The next problem tackled was the lack of a mechanical roughing pump. Unlike the cryosorption pumps, a mechanical pump may be run continuously because it only needs a source of electricity, whereas cryosorption pumps require a source of liquid nitrogen and have a limited (short-term) lifetime before they become saturated. An electrically powered mechanical pump near HP East, assumed to have been used with that machine, unfortunately had an inlet connection that could not be attached to HP West in any location. A suitable connector was welded by technicians at Lawrence Berkeley National Laboratory, but it did not arrive at the Davis Lab for about one week after the initial pumpdown, during which time the cryopumps were activated as much as possible to maintain a pressure "barrier" in the differential seals.

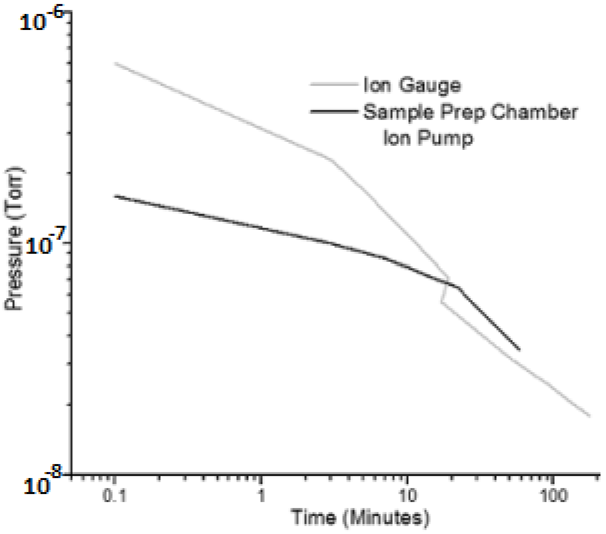

Figure 13: Pressures measured during sample changeover on a log-log scale.

Once the mechanical pump had been attached to the differential seals, the thermocouple gauge was reattached from the cryopump plumbing to immediately adjacent to the differential seals to monitor the pressure there. The mechanical pump was then activated and a base pressure of about 200 mTorr was observed. Even this sustained medium vacuum level provided enough of a pressure "barrier" to allow the ion pumps to lower the main chamber pressure down to $9 \times 10^{-9}$ Torr (as read on the ion pump pressure gauge) without baking out the machine. The base pressure achieved in the main chamber before the mechanical pump was attached and running was about $3 \times 10^{-8}$ Torr.

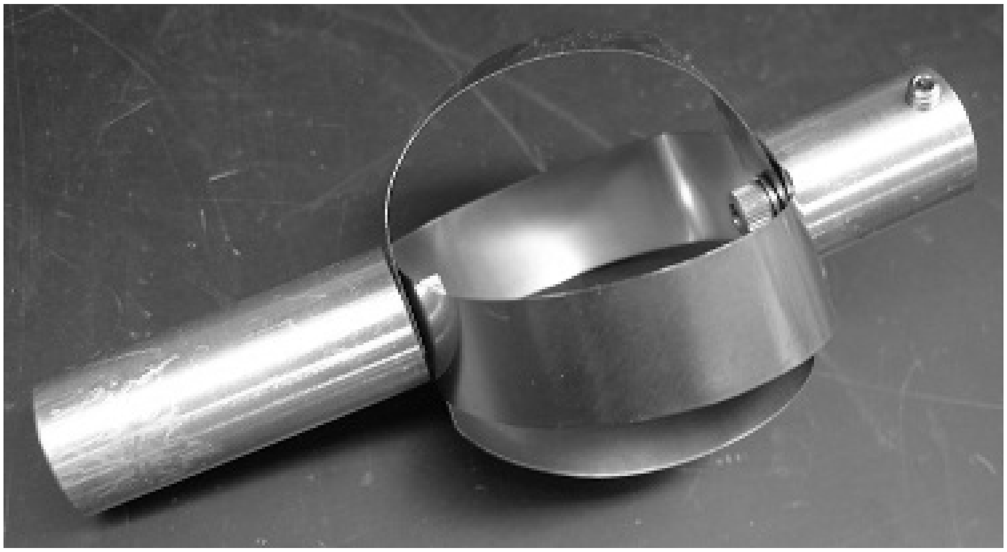

Figure 14: Previously installed connection between monochromator knob and adjusting screw. The spring-like material was likely chosen to allow for rotation through the horizontal offset.

As the machine had now been lowered into the UHV regime, the heat exchanger pump was activated and the X-ray power supply came to life. Several spectra were taken on a gold-on-copper calibration standard at several monochromator angles and were observed to have varying peak shapes and intensities. A nonfunctional ion gauge control unit was swapped with a control unit from HP East in order to assist in accurately monitoring the chamber pressure, and thus better observe the operation of the sensitive equipment running inside.

Over the next few days, many spectra were taken at several monochromator angles in order to observe the performance of the X-ray power supply, ion pumps, and ion gauge so that any outstanding issues needing attention would make themselves known. The monochromator adjust knob, which connected to the screw directly moving the monochromator by a set of four spring-like stainless steel ribbons (see Figure 14), was deemed to be too sloppy in motion, with too much backlash and in need of redesign. The ribbon attachment was observed to bend substantially with knob movement before the adjusting screw began to turn, and so the external monochromator angle scale was scarcely able to provide reproducible measurements; a lack of reproducibility is obviously a problem needing direct attention with a scientific apparatus such as HP West.

Three days after the first day of spectral measurements, the main chamber ion pump began tripping off overnight for unknown reasons. Two days later, the tungsten filament X-ray cathode was observed to gradually increase and decrease in intensity over the course of minutes. The filament's operation may be observed directly; in addition to the electrons emitted from the filament, optical wavelength photons are also generated due to the fact that the filament behaves as a blackbody. The bright filament may be viewed through a glass window mounted in a flange on the side of the monochromator chamber. The day after this further complication was observed, the X-ray power supply began tripping a circuit breaker attached to the high voltage transformer between the control unit and the anode during sustained operation. The events associated with the X-ray supply were assumed to be related.

# 5 Restoration

With some idea of the symptoms ailing HP West, but at first little information to consult for repair advice for this complex, aging system, I resorted to educated guess-and-check. I utilized thorough physical investigation (with the help of Peter Klavins) and inspection of system operating manuals and entries in a recent experimental logbook to decide, after consultation with Prof. Fadley, how to proceed on each issue.

To begin to deal with the X-ray supply problems, the X-ray control units were swapped between HP West and HP East in order to give a preliminary screening for

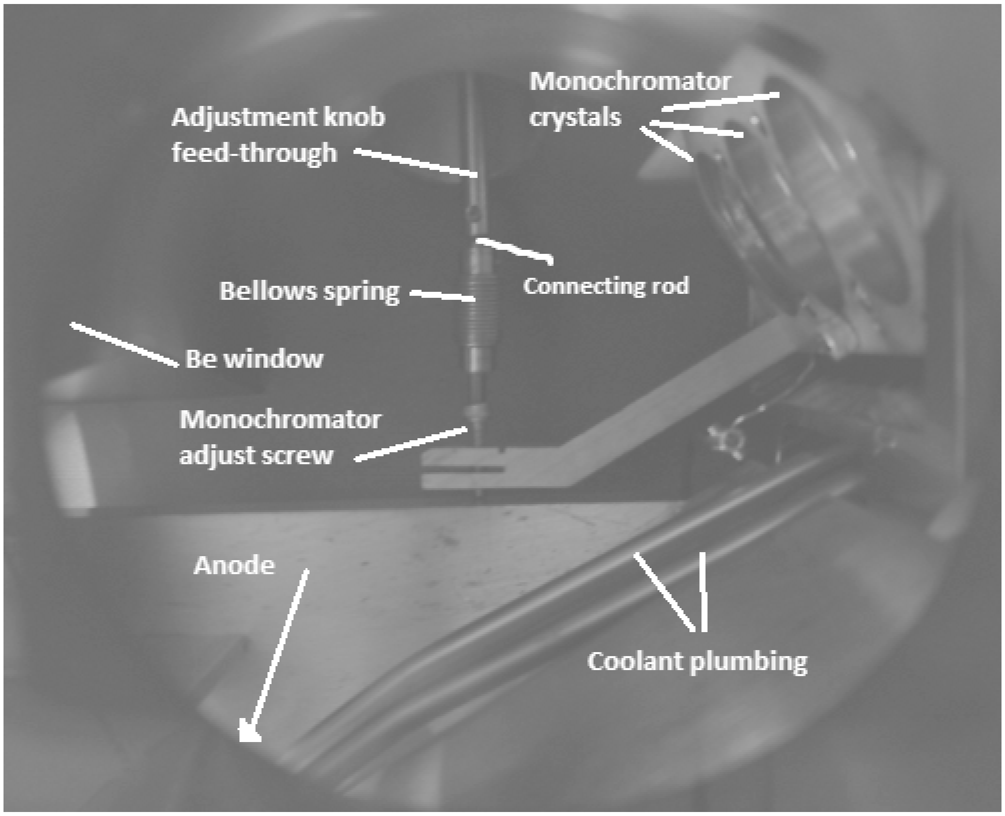

Figure 15: The monochromator chamber through the viewing window while in operation. The improved adjustment knob couple is shown.

faults in the in-use unit. The second unit worked fine, but the problems described in Section 4.2 were still observed and there were no apparent changes.

During a long sample scan, the main chamber ion pump tripped off, and this caused the X-ray power supply to shut off, and so the X-ray supply was discovered to be interlocked with the main chamber pump; I was later informed by Prof. Fadley that this is a natural factory setting to prevent having the X-ray high voltage and filament current on if the vacuum level is not low enough. The rear panel of the main chamber pump control unit was found to be hot to the touch and the small cooling fan mounted in the rear panel was found to have seized. The broken cooling fan was guessed to be the root of the problem – the fan itself was also hot to the touch, and so must have been dissipating power, adding to the problem. The cooling fan was swapped with that from one of HP East's identical ion pump control units and the problem never resurfaced.

Inspection of the sample probe angle stepping motor used to examine effects of machine misalignment (see Section 3.2) revealed that the motor was functional, but its use was neither desired nor necessary for the purposes of the HP West revival project. The day after this inspection, I entered the lab to discover a puddle of oil pooling around the mechanical pump; the pressure gauge attached to the differential seals read atmospheric pressure and the pump sounded as though it were straining. Also, upon examining the differential seals, it was discovered that, despite the computer and interface devices having been shut down the previous day, the stepping motor had mysteriously activated and rotated the sample transfer arm on its axis. The motor had rotated the axis as far as it could go; the translation handle was attached and blocked the axis from rotating further. Because the handle was pressing against the probe guide, the stepping motor placed a torque on the entire differential seal housing, creating a small leak due to the strain. Fortunately, no permanent damage had been done and the differential seal leak only allowed air past the first seal; the second and third seal maintained high vacuum conditions inside the chamber. The stepping motor was subsequently removed and an Allen Wrench was affixed in its place (see Figure 7) to give the operator a smooth, easy method of rotating the sample probe.

The spectrometer detector manual [15] gives calibration values for idealized relative component orientations for both gold on glass calibration standards and graphite calibration standards. Gold-on-copper, the available samples, were suggested to be satisfactory for calibration purposes. The monochromator angle was set to some rough approximation to an optimum value [5] with one of the available gold-on-copper samples. Because no graphite sample was available, a layer of Aquadag$^{\text{TM}}$, a commercially available pure graphite paste, was mixed with distilled water and painted onto the sample with a clean brush. The sample was heated using a hot plate to evaporate the water and the process was repeated until a relatively thick layer of graphite covered the surface of the sample. The makeshift carbon standard was inserted into the chamber and a calibration spectrum was sampled. The peak shape was distorted, and although some of the distortion was likely due to contaminants present on the substandard calibration sample, both Prof. Fadley and the detector manual suggested several possible actions which could positively influence the spectrum and the overall reliability of operation:

- Clean the X-ray anode
- Check the X-ray anode for leaks, as water from the heat exchanger may leak into the aluminum and affect anode function
- Examine monochromator angle
- Examine sample probe angle
- Calibrate both of these angle carefully, using methods derived previously by Baird and Fadley [5]

In order to reliably examine the monochromator angle, the adjustment knob needed to be replaced; in order to best determine the effect of sample probe angle on sample positioning, the measurable references on the outer portion of the shaft needed to be quantitatively related to the actual sample angle; in order to leak-check and clean the anode, it needed to be removed from the monochromator chamber; therefore, in order to accomplish any of the above items, HP West needed to be brought up to atmospheric pressure.

## 5.1 Cleaning, Upgrades, and Repair

Now armed with a list of appropriate measures to complete, I shut down all of the pumping equipment and vacuum gauges and waited several days for the (very) slow-leaking differential seals to allow air ingression and raise the pressure. Though a better method would have been to slowly backfill the chamber with nitrogen gas, a substantial amount of work needed to be done with and inside of openings to the chambers. Due to the law of partial pressures [17], which states that at equilibrium each species of gas exerts a pressure independent of other gases, the molecules of the non-nitrogen makeup of air would enter through the openings unless a slight positive pressure was sustained during the entire time the machine was not sealed. Because the work to be done would be spread out over a week or more, a sustained flow of nitrogen was not practical; furthermore, HP West had been opened to atmosphere while dormant – as such, nitrogen backfill would serve only to increase the pumpdown rate (not lower the base pressure) and so nitrogen backfill was omitted.

The first of the measures to be taken to restore operating conditions was to remove the sample probe (a long, highly polished rod used for translating the sample into and out of the chamber while under UHV) and inspect the differential seals. The spring-loaded teflon differential seals showed no signs of physical damage but had red, powdery deposits layered in, on, and around them; it appeared that some previous sample of a red powder had been insufficiently bound to its substrate, and this powder was deposited onto the seals on entry and exit from the chamber. To fix this problem, the seals themselves and the immediate surrounding surfaces were all thoroughly cleaned with isopropanol, KimWipes, and sterile cotton swabs. The sample probe was also thoroughly cleaned as the deposits on the differential seals were also found in red rings around the shaft surfaces which rest inside the seals during operation. The red deposits were suggested by Prof. Fadley to have been iron compounds from

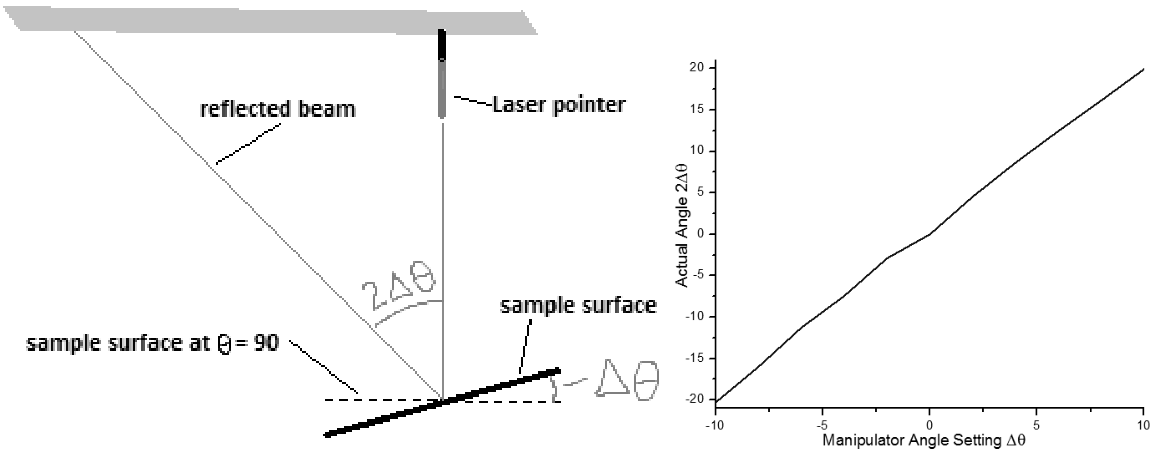

(a) Test geometry.

(b) Test results.

Figure 16: Manipulator linearity test geometry and results.

a previous study with apparent poor planning in sample preparation; the powder was apparently stripped by the rapidly changing pressures present while translating through the differential seals.

Before the sample probe was replaced within the chamber, the area immediately surrounding the sample loading area just outside the differential seals was thoroughly cleaned and the sample tray's orientation relative to the translation handle (the only easily measurable reference angle) was measured to be very close to 60°. The operation of the sample manipulator was also examined for smooth, reproducible movement by fixing a laser onto the target at normal incidence, varying the manipulator angle, and measuring the angular displacement of the reflected beam (see Figure 16). This information was used along with data from the experiments of [5] to adjust the sample probe angle such that the center of the sample rests directly under the center of the magnifying-retarding lens when fully engaged.

The final setting of the sample probe angle $\psi$ (see Figure 17) was $\psi = 21.5°$. When the manipulator is set to $\Delta\theta = 0°$ (as required for sample translation to prevent damage to differential seals), at the aforementioned setting of $\psi = 21.5°$, the

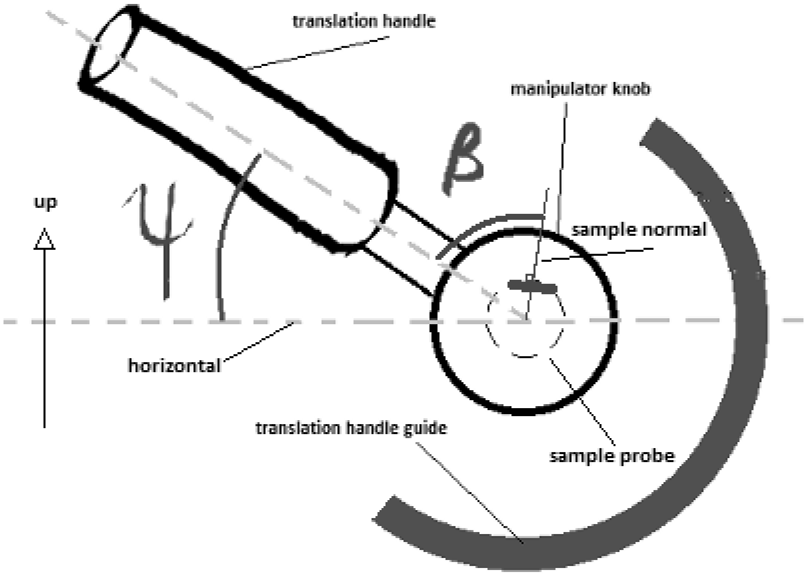

Figure 17: The sample probe angle $\psi$, as I have defined it for ease of reference. An end-on view of the sample probe is depicted.

sample surface angle $\theta$ is less than the dispersion-compensation angle [5] described in Sections 2 and 3.2. At $\psi = 21.5°$ and $\Delta\theta = 0$, the sample surface is oriented at $\theta = 51.5°$; therefore, the final manipulator angle should be +8.5° (8.5° clockwise) when the sample probe is fully engaged in order for dispersion-compensation to occur.

Next, the X-ray anode was carefully removed from the monochromator chamber and handed off to David Hemer in the Physics Department Machine Shop to be checked for high vacuum leaks. When the anode was returned and reported to have no leaks, the aluminum was inspected for defects. The aluminum matched the figure provided in the HP 5950A service manual [16] – Figure 18 – and clearly needed to be cleaned. A piece of fine sandpaper was used to gently scrub the anode free of all visible defects and a more gentle pink rubber pencil eraser (which always contain a small amount of abrasive material) followed the sandpaper at Prof. Fadley's recommen-

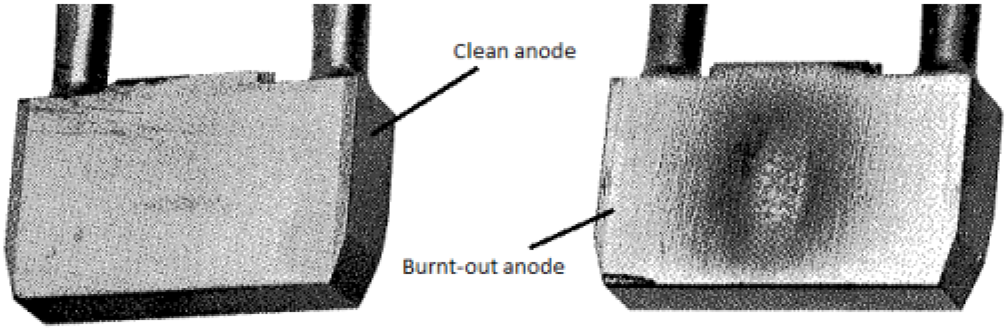

Figure 18: X-ray anodes. Adapted from [16].

dation. The anode was then cleaned using isopropanol and KimWipes and replaced within the monochromator chamber and reattached with a fresh copper gasket. The freshly cleaned anode is displayed in Figure 19.

Figure 19: HP West's X-ray anode after a fine sandpaper and rubber eraser scrub.

My brief study of the effects of monochromator adjustment on the resulting spectrum (hoping to optimize the positioning) while HP West was up and running had demonstrated the clear importance of upgrading the knob used to interface with the adjusting screw from outside the chamber. Because the adjusting screw is positioned near the wall of the chamber (see Figure 15), the flange directly above the screw, where the monochromator knob may be attached, is not centered over the screw. Whatever type of interface is installed must have the ability to turn the screw which is permanently located about $\frac{3}{4}$" from the center of the flange. This is the idea behind the stainless steel ribbon connection (Figure 14) between cylindrical feed-through shaft and adjusting screw.

Unfortunately, though the stainless steel ribbons did allow rotation of the screw from outside the chamber, the spring-like nature of the thin ribbons required the operator to turn past the desired angle when adjusting the monochromator setting; such a requirement adds difficulty to setting an angle and increases the uncertainty in the measurement of the monochromator position – a value that is not only difficult to quantify, but is typically insignificant in quantitative experiments. This is because the non-zero resolution in other experimental parameters (especially due to dispersion) typically render the relatively small uncertainty in such a measurement irrelevant.

The monochromator knob was removed and studied to gather ideas about how to create more directly correlated motion between the knob and the adjusting screw. The stainless steel ribbons were detached from the knob feed-through shaft and a bellows-spring type connection was used to attach the feed-through shaft to a $\frac{3}{16}$" rounded-end hex-wrench shaft; the bellows spring (see Figure 15) allows rotation through a bend in the shaft. The depth of the screw cap was determined to be 4.12" and the wrench shaft was cut slightly longer than was necessary to allow for flexibility in the depth of the monochromator feed-through shaft. The bellows connections were about $\frac{1}{8}$" at one end and $\frac{3}{16}$" at the other, so the wrench shaft was narrowed from $\frac{3}{16}$" to just under $\frac{1}{8}$" on a lathe and flat surfaces were added with a file to provide an area for set screws of the bellows to be fastened into the shaft. A short connecting rod was fashioned from stainless steel to attach the feed-through shaft to the bellows spring from above. Again with a file, the larger end ($\frac{3}{16}$") of the bellows was widened to fit the shaft connector (set screw flats were also filed into the connector). Altogether, the new adjust knob depth was set to the specified 4.12" with the wrench head engaged into the head of the adjusting screw. The wrench shaft was attached slightly short ($\frac{1}{16}$") so that when the adjustment knob flange was fastened back onto the chamber, the slight change in height due to depressing the new copper gasket required would be accounted for. The new monochromator knob was carefully cleaned with isopropanol and KimWipes and fastened onto the chamber with a new copper gasket.

Unfortunately, I did not have the foresight to thoroughly test the monochromator adjust knob until after the chamber had been returned to a high vacuum level. My first tests with the movement of the knob proved comfortingly smooth, though tight; I did not realize until a breakage occurred that the arrangement was *too* tight. Once all of the distended components were reassembled and all seals tightened, HP West was pumped down to high vacuum (high $10^{-8}$ Torr range). After turning the monochromator knob back and forth to get a feel for its new operation before beginning a new array of tests to find the optimum angle, the knob snapped just inside the chamber. Though the vacuum level was not affected, the monochromator adjust knob turned freely and the feed-through shaft did not respond.

The monochromator adjust knob from HP East was then extracted and adapted to attach to the existing bellows spring and wrench combination while HP West was slowly backfilled with dry, high purity nitrogen gas to increase the speed of pumpdown when returning to high vacuum conditions. HP East's monochromator knob attaches through a smaller flange, a $1\frac{3}{8}$" flange instead of the $2\frac{3}{4}$" flange in place. Fortunately, a $2\frac{3}{4}$" mounting flange had been employed to attach the adjust knob to HP East and so this mounting plate was also extracted. A slight positive pressure was maintained while the broken monochromator was quickly removed from the chamber and a clean piece of aluminum foil pressed tightly over the opening to discourage atmospheric gases from entering the chamber. The feed-through shaft on the knob from HP East easily attached to the connecting rod used with the previous knob.

The new assembly was cleaned with isopropanol and KimWipes and tested for the correct positioning and length when seated in the monochromator chamber. The mounting position for the smaller diameter flange to which the knob mounts is not in

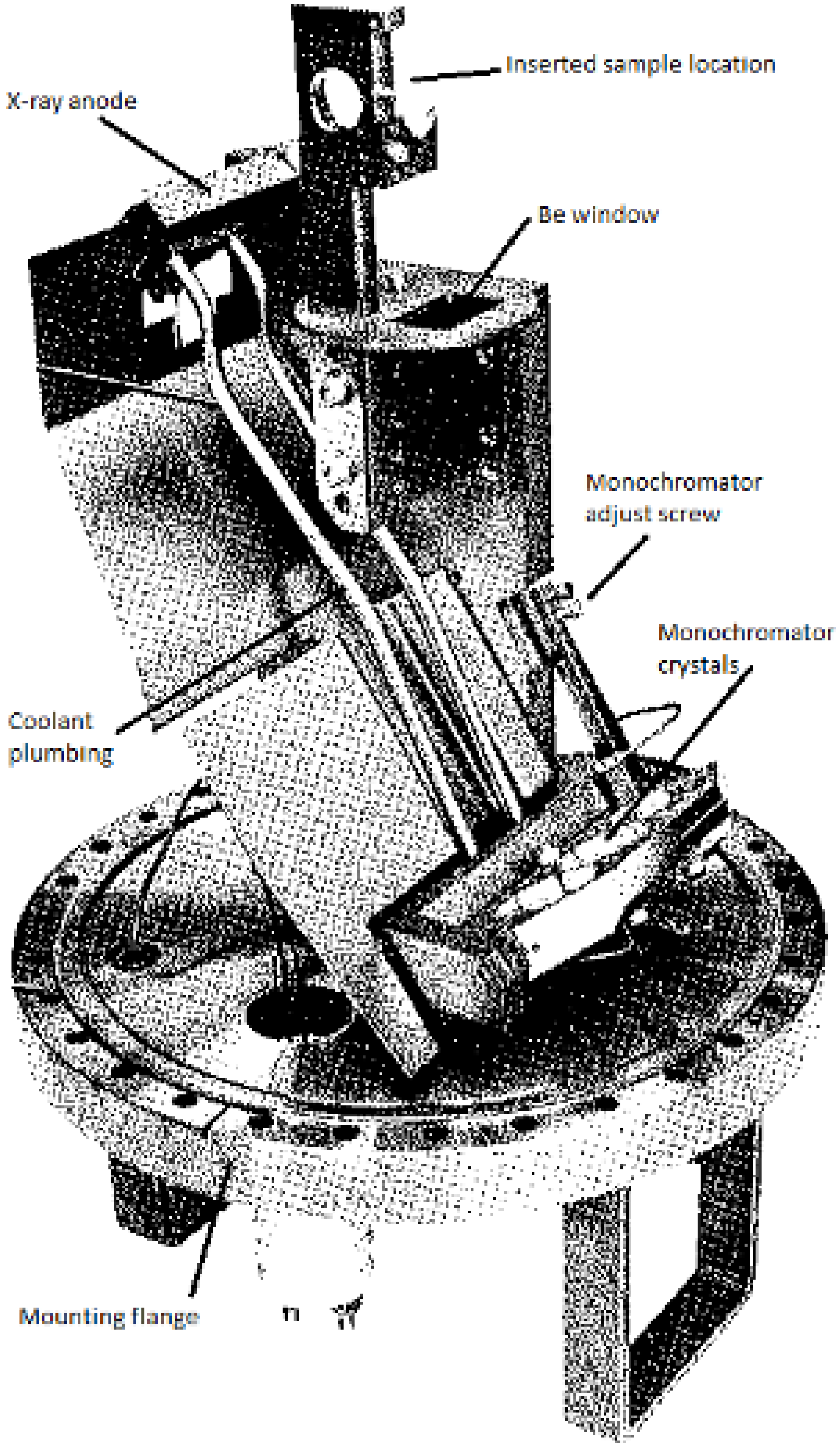

Figure 20: The interior of the monochromator chamber. Adapted from [16].

the center of the larger mounting flange; this offset was exploited to position the new monochromator adjustment knob feed-through shaft nearly directly over the adjusting screw (only about $\frac{1}{8}$" off-center). This gave the bellows spring a very slight bend angle, just enough that the feed-through shaft was held tightly in place but not so tightly that a large amount of stress would be placed on the shaft as before the repair. The 360° angle selector ring previously attached to the HP West monochromator had superior labeling and a larger radius (easier to select angles), so a platform was cut from a thin piece of stainless steel to attach the superior angle ring to the superior (functional) adjustment knob (Figure 21).

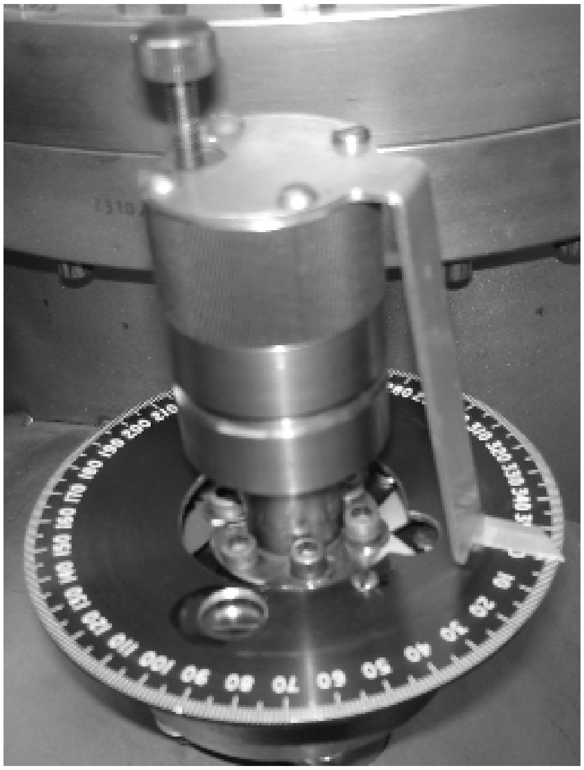

Figure 21: The monochromator adjust knob removed from HP East and adapted to HP West.

Once the newest monochromator knob was attached with fresh copper gaskets, the nitrogen supply was valved off and the cryopumps cooled while the mechanical pump began pulling a vacuum on HP West yet again. The pump-down procedure outlined in Section 4.1 was carefully followed and the pressures read by all gauges read significantly lower than they had ever reached since I had begun working with the machine – around $7 \times 10^{-9}$ Torr in the sample prep chamber and around $4 \times 10^{-9}$ Torr in the main chamber. About 2 weeks after the X-ray had returned to operation, the gauge on the monochromator read a pressure of $1 \times 10^{-9}$ Torr – the bottom of the scale. The lower monochromator chamber pressure may be attributed to its isolation from the main chamber by a valve and the beryllium window (translation of samples into and out of the main chamber from atmospheric pressure increases the amount of vacuum-immobile atmospheric gases allowed into the chamber). The difference in pressures between the monochromator and main chamber may also be attributed to the heating of the X-ray anode and hot tungsten filament – the heating provides a low-temperature bake of the inner chamber surfaces, so a larger amount of these gases are trapped by the ion pump than would be in the main chamber.

## 5.2 Troubleshooting, Optimization, and Examination

Now that HP West had been reassembled and returned to UHV conditions, the monochromator and sample angle position adjustment mechanisms had been upgraded, and the X-ray anode had a freshly groomed surface of aluminum, the investigation of problems with the X-ray power and the optimization of the orientation angles were set to continue.

The X-ray source had not been operated since filament power fluctuations and circuit breaker tripping had been observed, so several investigative maintenance precautions were taken while waiting for pumpdown in an attempt to eliminate those problems. The high voltage transformer connecting the X-ray control unit to the anode high voltage lines is immersed in a small tank of insulating oil; one problem encountered shortly prior to HP West's period of dormancy was a blown capacitor located in this very oil. Though the capacitor had been replaced and the X-ray returned to operation before HP West became dormant, the transformer fluid level was the next item to be reviewed.

The HP 5950A service manual [16] was consulted for recommended fluid levels; a vent hole on the filling cap plug was determined to set the appropriate fill level. A sterile cotton swab shaft was utilized as a dipstick to measure the fluid level. The level was slightly low, so a cleaned turkey baster was used to transfer some fluid from HP East's X-ray high voltage transformer to HP West's.

Despite exposing a fresh aluminum surface and topping up the high voltage transformer fluid, the X-ray power supply continued to trip the circuit breaker on power-up. Though the X-ray supply activated after resetting the breaker, it tripped the breaker each time it was powered on after about 4 minutes of operation. On the interface of the X-ray source control unit, there are a power button, power selection knob, and three indicator lights: "filament preheat," "high voltage ready," and "high voltage on;" upon activation, the "ready" light delays for about 10 seconds while the filament preheats and finally lights once the filament has been heated. The filament-preheating stand-by phase is mandated because it slowly heats the filament so that its operation is steady when the high voltage power is finally energized. I realized after pondering the breaker-tripping problem for a while that this steady activation may be important for the X-ray source, even after the control unit has declared the filament to be preheated.

I began implementing a slow power ramp each time the X-ray source was activated:

1. Activate heat exchanger
2. Activate X-ray power and wait for filament to preheat
3. When "ready" light activated, increase power from "standby" to 100W
4. Wait about 5 minutes before increasing power to next power setting (200W)
5. Continue increasing power level every 5 minutes until 800W is reached
6. Begin sampling at 800W

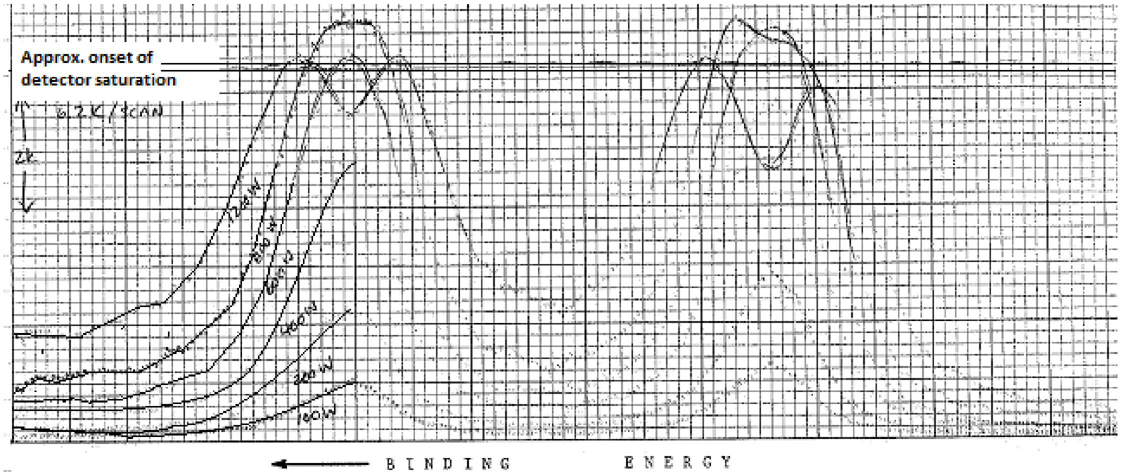

Figure 22: A test of the intensity response at each X-ray power supply setting from the Fadley Group record books: dated 02/06/1975, pg. 134 of "HP Log 1." The plots have been traced at the left edge for clarity. Note the misshapen appearance of the 1200W settings, during which scan the detector reached saturation at peak intensities.

The problem was instantly solved; the X-ray source still has not tripped the circuit breaker again. The power is stopped at 800W (there are two higher power settings) because above 800W, detector saturation occurs and the spectra become horribly misshapen at peak intensities; sampling of the effect of detector saturation have been recorded in the Fadley Group spectrometer log books (see Figure 22).

### 5.2.1 Heat Exchanger Restoration

As soon as I began my array of tests to determine the optimum monochromator angle with the new adjustment knob, the heat exchanger pump began to emit a high-pitched squeal. There were no visible problems, and the water pressure and fluid flow meters read nominal levels (about 100 psi and 2.5 gal/min respectively – nominal levels compared to readings recorded in the record book). I ignored the squealing until I returned to the lab after taking a short break to find that the heat exchanger had shut itself off, opening the interlock to the X-ray power supply and shutting that off as well.

A quick survey of the HP West stack fuse box, through which the heat exchanger is connected, revealed that a blown 20A fuse was the culprit. I asked around nearby labs for a fuse to replace the blown one and received a replacement from Britt Holbrook. I suspected the age of the fuse to have been the cause of failure; I removed the blown fuse and installed the new one and the heat exchanger ran for about 20 minutes with very low pressure and flow readings (no positive pressure and marginal, intermittent flow) before I heard a loud pop emanate from the fuse box. I opened the cover and attempted to extract the newly replaced fuse, but pulling up on it left the lower contact behind – the adhesive binding the fuse body and lower contact seemed to have melted and allowed the tightly held lower contact to remain in place while freeing the fuse body. The piece of fuse I extracted had an intact internal wire. Plugging the heat exchanger into the HP East power box caused the pump to run, but again with very low readings; because the flow and temperature readings utilized by the X-ray power supply interlocks are also fed through the power cable, connecting the heat exchanger to the HP East power box would not be able to solve this problem without extensive electrical modifications to bypass this critical safety equipment.

The suspicious circumstances surrounding the second fuse were ignored until another fuse was inserted and the heat exchanger refused to activate. Visibility into the fuse box was limited; the fuses are mounted at the top of a power relay bolted to the frame of the HP West control stack so there was no way to view the inside of the fuse connection below the cap without removing the power relay. I was not able to find a simple cause for the loss of power from outside the box, so I shut off all power supplies and removed the box from the stack. Upon opening the power relay box, I found that the lower connection to the fuse had detached from the upper connection; the insulation around the wire close to the connection had been melted and the exposed

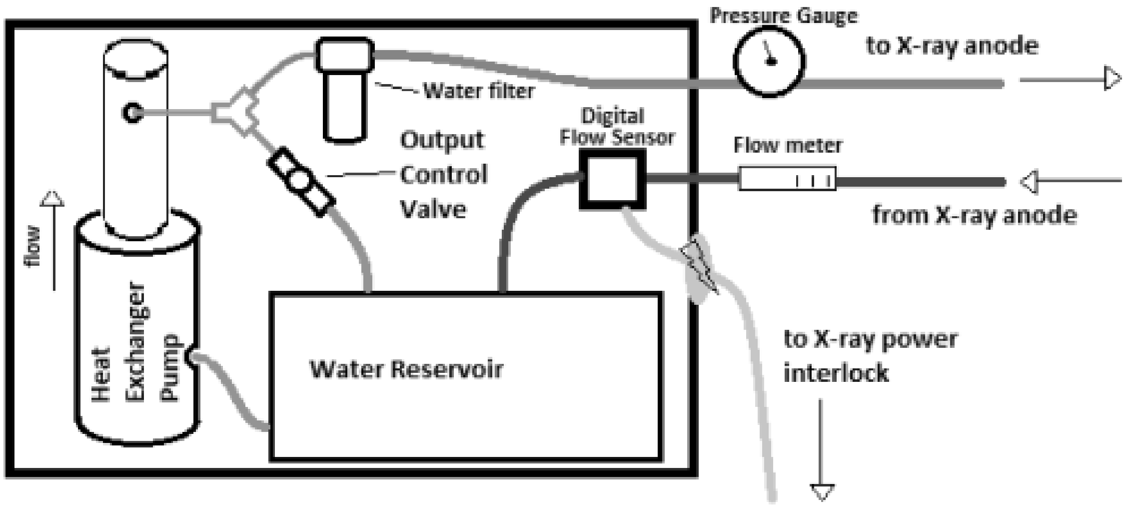

Figure 23: Heat exchanger plumbing diagram.

wire, lower fuse contact and lower connection of the fuse holder were all blackened and hung disconnected from the fuse box. The blackened wire was removed and a new fuse and fuse holder, obtained by Peter Klavins, were installed.

After the fuse box had been repaired, my attention was turned to the clear problem – the heat exchanger. The fuses would only have blown in the event the current passing through it exceeded 20A; therefore, the pump must have malfunctioned in a way that caused it to draw excess current. HP East had its own heat exchanger, so the faulty pump was swapped with the disused one. When activated, the pump seemed to struggle; the water filter was exchanged for a fresh one and the interior plumbing of the pump housing was inspected for any available adjustment. The water in the pump reservoir was drained and filled with fresh distilled water.

Inside the pump housing, a needle valve was located just downstream from a Y-shaped connection attached to the pump itself (see Figure 23); this valve was deduced to allow the operator to regulate the output pressure and flow rate by redirecting part of the flow directly back into the reservoir. I labeled the valve "Output Valve" so that its purpose will be elucidated for an uninitiated operator. Closing the valve completely will direct 100% of the pump's output to the X-ray anode; opening the valve completely directs nearly all of the pump's output back into the reservoir because the water filter acts as a low-conductance barrier, such that very little water will travel through it, in comparison to the high conductance path to the reservoir. Keeping the valve completely closed increases the pressure in the output lines to above the rated capacity of the water filter, so some slightly open flow setting is required.

The flow rate was observed for several settings of the output valve; the X-ray power supply was also energized so as to quantify the minimum flow rate necessary to allow X-ray operation. The X-ray interlock opened (cutting the power to the X-ray anode) when the flow rate dropped below 1.6 gal/min and an output pressure of 40 psi; the interlock closed (connecting the power to the X-ray anode) when the flow rate was raised to 2.0 gal/min and an output pressure of 60 psi. Though I set the valve open just far enough to yield a flow rate of 1.8 gal/min (54 psi), the output flow and pressure began to fluctuate gradually in a cyclic pattern between 1.4gal/min (35 psi) and 2.0 gal/min (60 psi), opening the X-ray interlock each time the flow rate dropped below the 1.6 gal/min interlock threshold. I set the output valve such that the minimum flow rate of the cycling output flow remained slightly above 2.2 gal/min (73 psi) and reached a maximum of 2.8 gal/min (103 psi). The flow cycle was observed to slow once the pump has reached operating temperatures along with an increase in the flow and pressure range – cycling between 2.8 gal/min (100 psi) and 3.0 gal/min (130 psi) at the same output valve setting.

Closing the output valve down to increase the output flow rate also forced the water pump to work harder to drive the cooling water through the filter, especially at the higher end of the flow rate cycle; this caused the pump to add its own heat to the cooling water and increase the equilibrium temperature during X-ray anode operation to 46°C, which caused the power to the X-ray to shut off. Previously recorded heat exchanger equilibrium temperatures reached about 35°C (before swapping heat exchangers). In order to maintain a lower cooling water temperature and thus avoid X-ray interlock opening or damage to pumping equipment, the end covers were removed from the pump housing and a pair of large, unused stack fans were used to blow air past the pump. The cooling water temperature now comes to equilibrium at about 35°C. This mounting is still somewhat crude and could easily be improved with help from the Physics Machine Shop personnel.

The day after the fluctuating heat exchanger flow was sorted out, the X-ray power supply began exhibiting strange behavior. When powered on, the "filament preheat" indicator would light but the "high voltage ready" light would not; this prevented the activation of the X-ray anode because the control unit cuts the power to the filament if the power selection knob is not set to "standby" during filament preheat. Ultimately, whether the filament was preheating or not, the control unit never registered the filament to have reached operating temperature and so the X-ray supply could not be powered on. The log book was examined for the reasoning behind swapping the power supplies when initially reviving HP West; no such reason was discovered, so the unused power supply was swapped with the apparently faulty one. At first, the swapped-in unit appeared to exhibit the same behavior as the faulty one; after a brief inspection, however, the high voltage "ready" and "on" indicators were discovered to shine very dimly so the translucent caps covering the indicator bulbs were removed. After a few test scans were run, the active unit seemed to function properly and there still has not been any problems with it.

### 5.2.2 Monochromator and Sample Probe Angle Optimization – Initial Investigations

The monochromator and sample probe orientations initially proved confusing to optimize. Many characteristics of the spectrometer geometry and lens function must be incorporated in determining the optimum angles; though the optimum arrangement has been well researched with HP East [5], which has a spectrometer geometry identical to HP West, I had not yet consulted any literature about the spectrometer component orientations.

First, the monochromator was optimized for a fixed sample probe angle $\psi$; I had set the handle position $\psi$ to 7° in an attempt to set sample angle $\theta$ to the dispersion-compensation angle discussed by [5], $\theta_0 = 30°$. Unfortunately, the value measured for the angle difference $\beta$ (see Figure 17) had been incorrectly measured to be 37°; I later re-measured the angle to be 30° after deciding to double-check my work. $\psi$ was next optimized while holding the monochromator angle fixed. There were unsettling characteristics about the spectra taken at these "optimized" angles, including low resolution (high FWHM) and low peak intensities. The dispersion-compensation angle is labeled as such because it is the angle at which the resolution is increased; I knew that both the monochromator ($\varphi$) and sample probe ($\psi$) angles must be optimized, but I did not realize until this point that I would need to optimize the angles all at the same time.

I next performed a 2-dimensional sweep of $\psi$ and $\varphi$ using 3° steps for $\psi$ and 15° steps for $\varphi$ (see Figure 24). The peak intensities and $\text{FWHM}^{-1}$ are plotted as functions of both angles to show the general trend in these quantities with respect to each angle. The sweep of angles did not provide a clear optimum collective orientation because dispersion-compensation was not observed at any combination of angles. Extensive study of [5] made the effects of shifting $\varphi$ and $\psi$ more clear and also presented

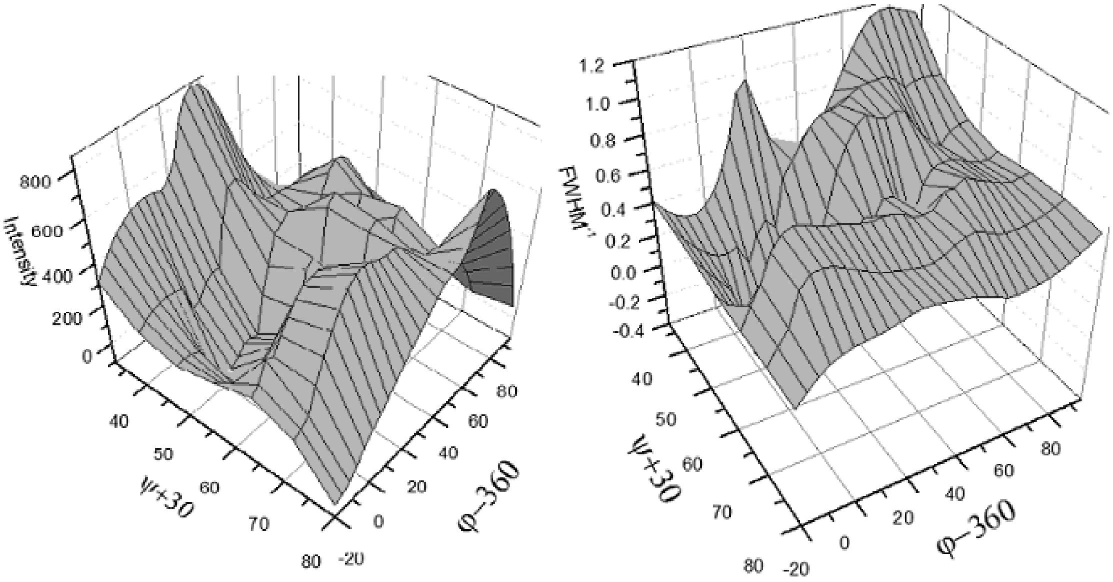

(a) Peak intensities versus both $\psi$ and $\varphi$.

(b) $\mathrm{FWHM}^{-1}$ versus both $\psi$ and $\varphi$.

Figure 24: Plots of the values extracted from raw spectral data over a sweep of many sample/X-ray orientations. The complex nature of the dependence on these angles derives from the simultaneous 2-dimensional movement of the sample surface with variation in $\psi$.

quantitative measurements of the relative orientation geometry for the spectrometer components. Geometrical data and knowledge from [5] combined to show that the optimum $\psi$ places the center of the sample directly under the spectrometer lens axis, at $\psi = 21.5°$. With the known optimum angle for the sample probe fixed, the special sample manipulator permitting one more angle of rotation was brought into the optimization study.

The detailed study presented by Baird and Fadley [5] also demonstrated the effects of monochromator misalignment on sample spectrum. A displacement $\gamma$ along the surface of the sample in a direction perpendicular to the X-ray propagation direction varies not only the intensity of electrons in the detector but also the energy of the electrons analyzed. Displacement along and spatial dispersion of photon energies along $\gamma$ will then cause a shift in the photon energy along the lens axis. Eqs. (1) and

(14) reveal an associated shift in the electron kinetic energy which will cause apparent binding energy shifts in the sampled spectrum.

Before finalizing the geometric alignment, I decided to look into whether any electronics problem might be influencing the resolution.

### 5.2.3 Electronics Troubleshooting

Because dispersion-compensation is characterized by a sharp increase in spectrometer resolution, service manuals [15] were consulted to locate various machine interface settings which may affect the final image analyzed by the detector. The first item potentially affecting the spectra HP West produces that was examined was the hemispherical analyzer plate voltages set by a potentiometer located within the HP 5956B power supply located in the HP West stack.

The recommended potential difference for the plates is 25V from the reference potential at the central trajectory (50V potential difference from inner hemisphere to outer hemisphere) [15]. The measured potential differences on the plates were found to be ±19.7V; adjusting the potentiometer inside the power supply increased the potential, but only to ±23.5V. My attention was then turned to the spare 5956B power supply located in the HP East stack, where I found the potentials initially to be ±22.0V. I adjusted the potentiometer inside this power supply as well, but this time the potentials were able to be increased to the recommended ±25V. The power "on" indicator light was found to be faulty; a glance at the detector window image revealed an intensity response very similar to that with the previous 5956B unit, so the new supply was operational.

Adjusting the 5956B voltages did not seem to affect the resolution of the response in the detector – the resolution was still very poor (with about 2.5 eV FWHM). Study of the records for the last 10 years of HP West's operation prior to its dormancy re-

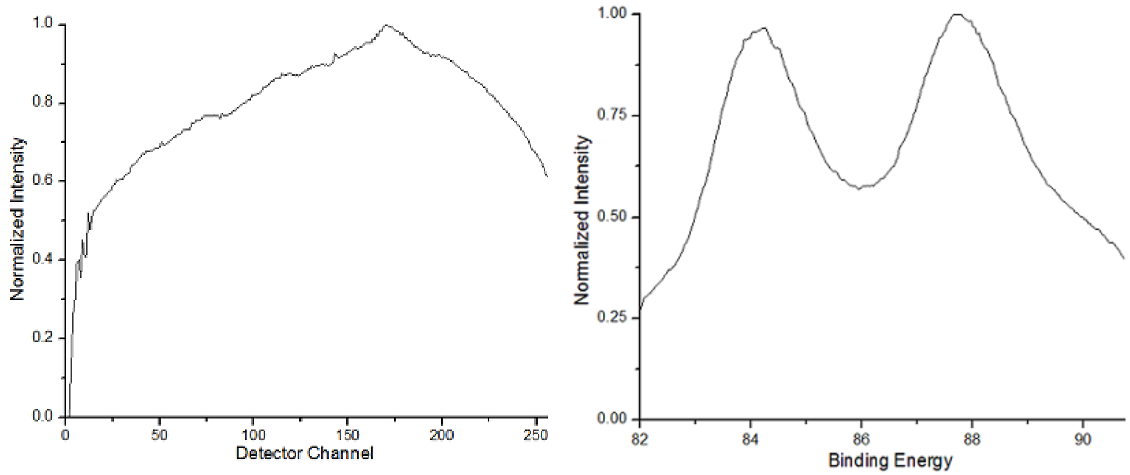

(a) Photoelectron detector signature before resetting 5956B.

(b) Approximate intensity response in detector window over Au 4f peaks before removing preamp D.

Figure 25: Detector contributions to spectral line shapes.

vealed a *strikingly* similar problem encountered; the solution employed was to "gently jiggle" the wires connecting the detector to the detector's signal processing preamps. That solution did not eliminate the problem this time, so I began experimenting with disconnecting various preamps attached to the outside of the detector circuitry. The detector manual [15] noted that the output signal sent to the computer interface circuitry had a voltage proportional to a combination of position signal voltages measured at the four corners of a resistive anode

$$V_{out} = \frac{A+D}{A+B+C+D}, \tag{18}$$

where A, B, C, and D are the output voltages from the four preamps and $V_{out}$ is the signal voltage sent to the interface box. The preamps convert pulses created by electrons from the detector to a pulse readable by the detector digital circuitry. The photoelectron detector attached to HP West has been converted from 2-dimensional photoelectron position detection (designed for spatially-resolved measurements) to 1-

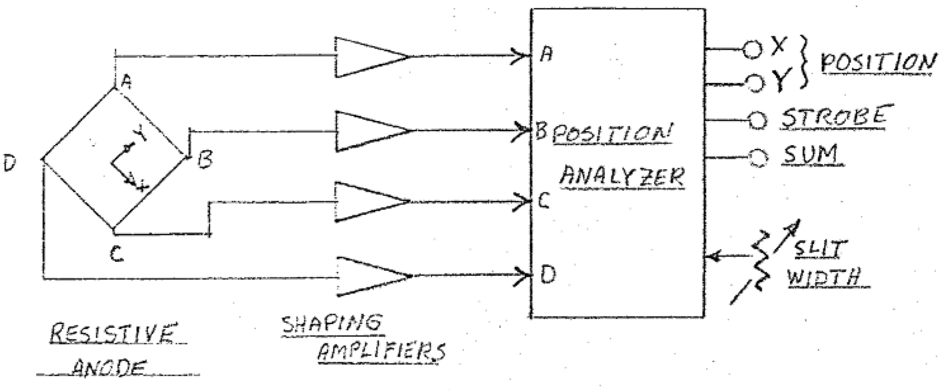

Figure 26: Block diagram of 2-dimensional HP SSL Model 239 ESCA Photoelectron Detector. Reproduced from [15]. In the case of 1-dimensional (energy spectrum) use, the detector y-axis becomes the energy axis.

dimensional energy spectrum resolution. A block diagram of detector preamp function is depicted in Figure 26. The detector manual [15] noted that the "y" axis (as in Figure 26) of the detector becomes the energy axis when the detector is configured for 1-dimensional use.

Based on the appearance of only A and D in the numerator of Eq. (26), the asymmetric, triangular appearance of the detector signature (Figure 25a), and the preamp function displayed in Figure 26, I supposed that either preamp A or preamp D was non-functional. This led me to guess that disconnecting only one of either A or D would have no effect on the spectrum read by the detector, and disconnecting only the other would cause the detector to read absolutely nothing. Disconnecting preamp D dropped the counts on the detector to zero and disconnecting preamp A had no effect on the detector reading, just as I had surmised such a combination would.

The detector was centered at 85.8 eV to immediately observe the effects of my tinkering on the Au 4f spectrum of the sample in the chamber. When I removed preamp A from the detector box, the signal in the detector changed from a poor signal (see Figure 25b) to a signal with relatively narrow peaks and low background counts between them, but shifted in energy by about -2.5 eV. I later discovered that removing preamp D from the detector box and disconnecting it while leaving preamp A attached and connected gave no counts; however, when a preamp from HP East was placed in the preamp A circuitry attachment slot and connected to the detector, a well-shaped signal was again obtained, but this time with the binding energies only about 1.25 eV lower than the appropriate energies.

A dithered scan of Au 4f was run, and the spectrum had FWHM of about 1.5 eV and peak intensities greater than that of spectra surveyed just hours before at the same component orientations – the only anomaly was the 1.25 eV shift in peak binding energies. I decided to assume that the problem with the preamps had introduced a binding energy shift of +1.25 eV and I raised the monochromator to raise the apparent binding energy (see plot (2.) of Figure 27). The peak intensity doubled with a 20° increase in $\varphi$, but after the apparent binding energy shifted to be -0.5 eV from the expected $83.93 \pm 0.07 eV$; increasing $\varphi$ further only decreased the intensity.

The upper limit of 83.5eV hinted that the sample was likely oriented at a less-than-optimal angle. In order to quickly locate a more optimal angle, I took the following steps:

1. Set $\varphi$ to 350°, a monochromator orientation known to yield typically well-shaped spectra with average intensities over a large range of sample orientations (see Figure 24)

2. Began a fixed Au 4f scan (holds the binding energies analyzed constant) so that the overall detector response may be viewed in real time

3. Held the manipulator adjustment knob steady while varying the translation axis angle (to hold $\theta$ constant while varying $\psi$)

4. Observed qualitative relationship between $\psi$ and detector response, including

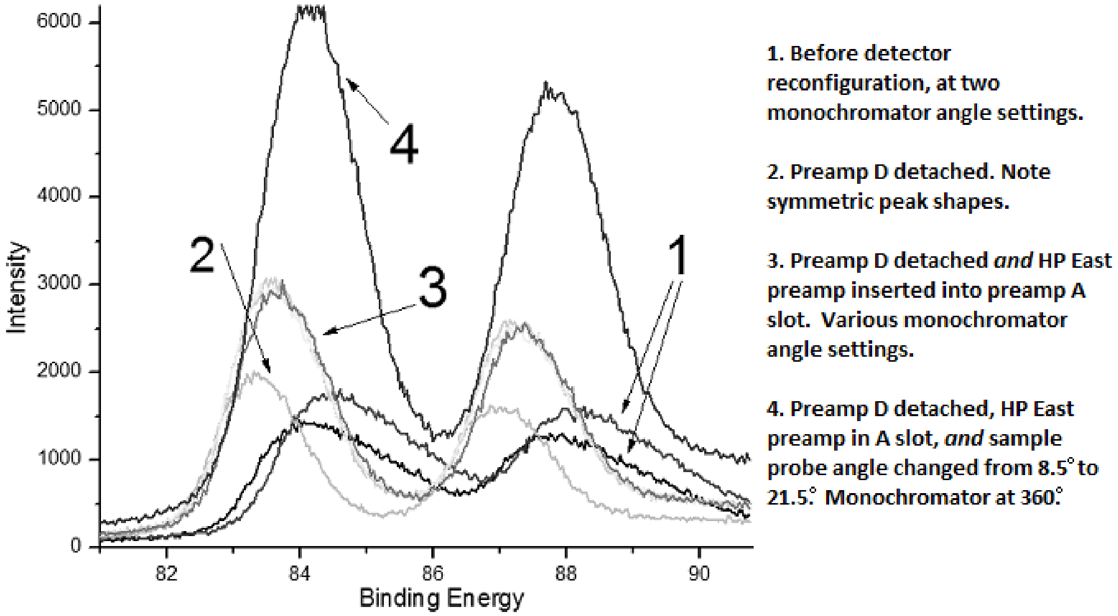

**1. Before detector reconfiguration, at two monochromator angle settings.**

**2. Preamp D detached. Note symmetric peak shapes.**

**3. Preamp D detached *and* HP East preamp inserted into preamp A slot. Various monochromator angle settings.**

**4. Preamp D detached, HP East preamp in A slot, *and* sample probe angle changed from 8.5° to 21.5°. Monochromator at 360°.**

Figure 27: Dithered spectra obtained for each progressively improved detector configuration. Each step's spectra were surveyed after adjusting the monochromator to shift Au $4f_{\frac{7}{2}}$ binding energies as close to 84 eV as possible.

peak intensity and width

5. Set manipulator angle to different values and repeated steps (3) and (4) to observe effect of $\theta$ on detector response

Because the roughly "optimized" value I found for $\psi$ was very close to a previously used value of 21.5°, I set the value of $\psi$ to 21.5°. To summarize, juxtaposition of the dithered spectra obtained for each configuration is contained in Figure 27.

Once I had set the sample position and angle to the above orientations, $\varphi$ was varied slightly to ascertain a qualitative intensity, width, and apparent binding energy dependence; $\varphi = 360°$ seemed to provide the smallest FWHM and smallest shift from the expected binding energies. Though the binding energy is not a suitable criterion for component orientation optimization, it is adequate for a rough, preliminary setting. Continuing work on the HP West restoration project, however, should include

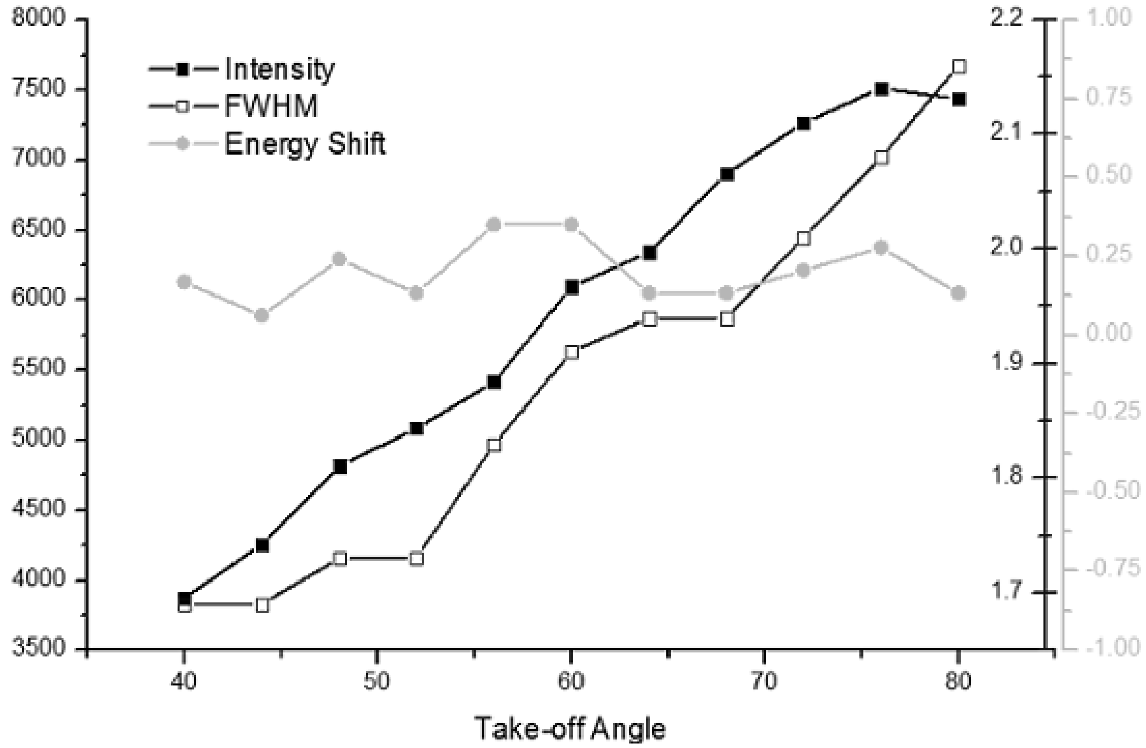

Figure 28: Spectral attributes at the rough "optimum" position for various $\theta$.

a further, more detailed optimization based on careful analyses of spectral data at many orientations and comparison to data presented by Baird and Fadley [5]. Some of my suggestions for this work are outlined in Section 7.1.

To test for an optimized monochromator, the take-off angle ($\theta$) was varied in 4° increments and dithered spectra were surveyed to look for shifts in apparent binding energy, peak widths, and peak intensities. Peak intensities increased as expected with increasing $\theta$ (see Section 2) and Au $4f_{\frac{5}{2}}$ binding energies varied very little from the expected 84.0 eV (see Figure 28). Altogether, the above process gave an approximate optimum orientation of:

$$\varphi = 360°, \psi = 21.5°, \Delta\theta = 8.5°$$

Though a sharp increase in resolution (decrease in width) at a specific value of $\theta$ was not observed, meaning dispersion-compensation had not been achieved, the consistency of apparent binding energies demonstrated by Figure 28 at the above component orientations was determined to be sufficient for the two more spectroscopy-oriented studies in this thesis.

Near the end of my work in adjusting the various component orientations and exploring detector configurations, I noticed while acquiring Au 4f spectra that occasionally, the position of the spectral peaks in the detector would shift dramatically near the mid-point of a survey. I scanned the most recent record book for any mention of similar or related phenomena and found, on page 65, a discussion of a very similar "jumping" problem that had been encountered and that the problem was found in the 6131C digital power supply by Britt Holbrook. Time constraints prevented my investigation of this problem, but it appears to only affect some spectra and not all, so my experiments were only marginally affected; the only action necessary to side-step the problem was to re-sample the affected spectra (or simply remove the anomalous data, in the case of the time-resolved spectra of Section 6.2). An example of an affected spectral scan is depicted in Figure 29. This should be carefully

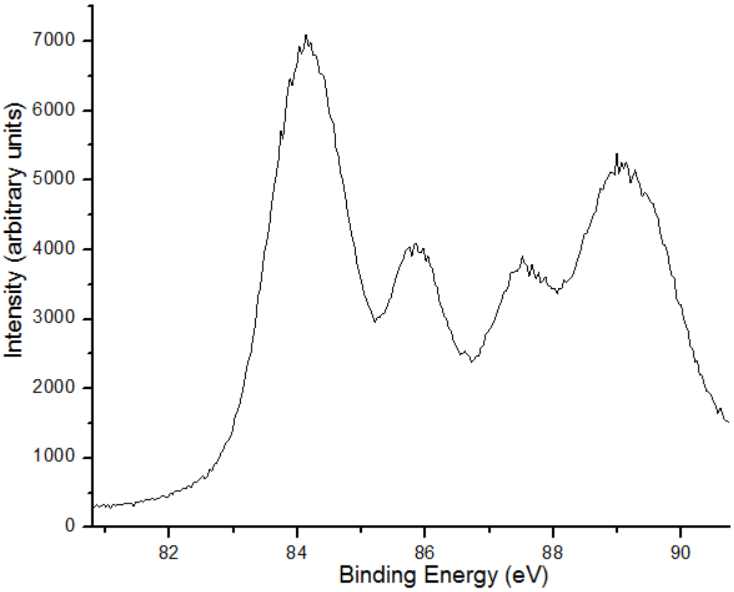

Figure 29: An example of HP 6131C dither voltage "jumping." The displayed scan was the first of the "clean" Au scans discussed in Section 6.2 and was not included in the study.

watched for in future work, and if it occurs more than occasionally, troubleshooting and repair will be needed.

# 6 Experiments

Once the preparation, repair, and calibration work had finally been completed, experimental investigations using HP West were able to begin. Fortunately, a small evaporator filament had already been installed in the sample prep chamber (see Figure 7), and even more fortunately, there was still plenty of gold left in it to be used to evaporate a fresh layer onto the sample while under UHV. A total of three simple experiments were carried out; the power-up inconsistency experiment was performed prior to rearranging the detector preamps, so the spectra appear at a much lower resolution, but the qualitative results should not be affected by an increased resolution.

The experiments undertaken were designed to be simple and brief because the main focus of my project was to return HP West to operating condition and also because once the machine had been restored very little time remained for conducting experiments. Because some work still remains to be done ensuring that the spectra HP West produces are fully optimal, in my last days with the machine more focus was placed on delineating those tasks (Section 7.1) for my successors in the complex restoration project.

## 6.1 Power-Up Inconsistency Test

When working long days in the Fadley Group Lab, I sometimes noticed that over the course of the day, peak intensities and binding energies seemed to shift dramatically when a given spectral window and component orientation were sampled for a second time. The suspicions of inconsistency that arose from these observations prompted me to analyze the variations in spectra at a fixed orientation over the course of the first two hours of operation. The HP 5950A operating and service manual [16] notes that variations in spectra are guaranteed to be insignificant after the first 2 hours of recommended warm-up.

Dithered Au 4f spectra were sampled with a 1-second dwell interval and 10 eV spectral window continuously for the 2 hour experimental intervals. Using a dithered scan "sweeps" the detector window across the region so that any and all detector effects are averaged over; this prevents any detector inconsistencies from affecting the data. Due to a detector electrical problem of unknown origin, the spectra sampled for this experiment all have greater widths and lower peak intensities than those of the other experiments. Nonetheless, the results extracted from the data in this instrument test should apply at any orientation and detector state provided the orientation remains the same throughout the entire experiment.

I initially forgot to deactivate the various power supplies controlling the lens voltages, chevron plate voltages, and dither control voltage (hereinafter referred to as HP supplies) when leaving the lab the night before I began my first power-on warm-up test; my original intention had been for all power supplies to be off and so I decided to include this extra variable and run three total tests (four including the warmed-up control test).

Figure 30 shows the spectra from each test configuration all plotted simultaneously on the same axes. The spread in intensities in each of the spectral plots is due to warm-up effects of each of the components tested. In the control test, where both the X-ray power and the HP supplies had been on for over 24 hours, the spectra are all clustered very close together, and the range of peak intensities is from about 1400-1600 counts. Each scenario was examined by scanning dithered spectra as described above consecutively over a two hour interval. The time required for each dithered

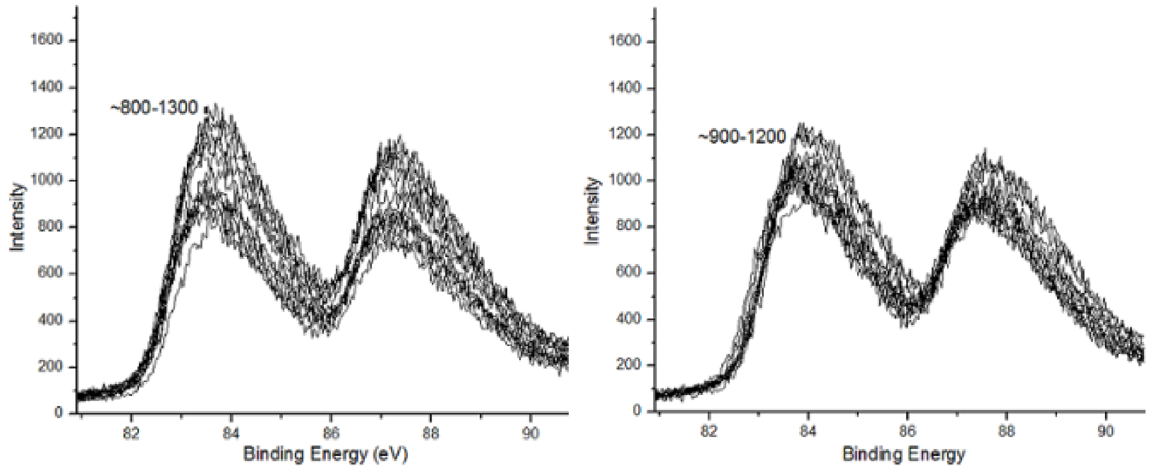

(a) Both X-ray power and HP supplies "cold."

(b) Only HP supplies "cold."

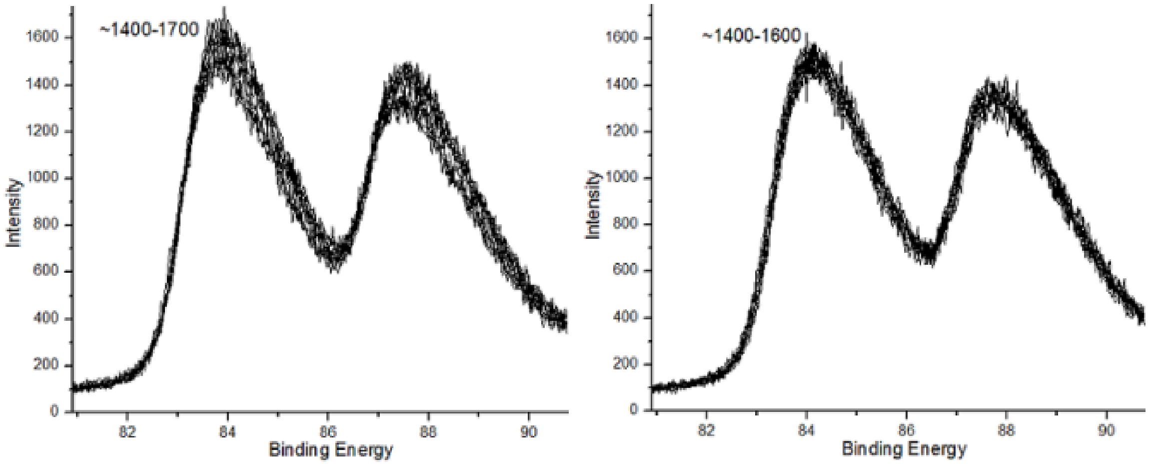

(c) Only X-ray power "cold."

(d) Both X-ray power and HP supplies "warm."

Figure 30: Power-up inconsistency test spectra. Lines appear blurred due to superposition of spectra taken over the 2-hour sampling interval; the more blurred the superposition, the less consistent are the spectra.

scan was about 8.5 minutes, which was assumed to be short enough that there would be no significant change in spectral response over that interval.

Figure 30 also demonstrates both the inconsistency of and lower intensity response of HP West when the HP supplies are still warming up. In the plots of Figure 30a and 30b, the intensities of the various overlapping plots increases as the time increases. Should the test have continued until the X-ray power and HP supplies were all at equilibrium, the peak intensity would very likely have risen into the 1400-1600 range as with Figures 30c and 30d. The spread in intensities in the worst-case scenario, over the period when both the X-ray power and HP supplies were warming up, indicates the absolute necessity of using only spectra surveyed after both the X-ray and HP supplies have been warmed up. The *range* of peak intensities of Figure 30a (800-1300) is much greater than that of the control and is centered at a much lower intensity. The effect of the X-ray power warm-up, while significant, is considerably less significant than the effect of the HP supplies' warm-up. Fortunately, the HP supplies, like the ion pumps and ion gauge, are designed to run for long periods of time without interruption [16].

In conclusion, it is recommended that the HP supplies be allotted a 24-hour warm-up window before extracting data for use in any quantitative experiment (at least 6 hours, but it is often convenient to simply activate such systems a day in advance). It is also recommended that the HP supplies be left running constantly when many spectra will be surveyed over the course of a long experiment (days or weeks). The X-ray power warm-up period does not appear to have any significant effect after the 2 hours recommended by HP have passed. Therefore, a 2-hour warm-up period for the X-ray power is also suggested when spectra will be involved in quantitative experiments.

## 6.2 Contaminated Sample Study

When Peter Greene of the Liu Group sputtered a fresh, 200 nm-thick layer of gold onto the sample I had been using, an extreme improvement in the spectra surveyed followed. Observing this huge shift (see Figure 31) encouraged an investigation of the differences in spectra at various levels of contamination.

To truly examine the effect of sample contamination on spectra, a gold sample needed to be prepared *in situ*, so that it remained under UHV conditions between preparation and spectral analysis. "Dirty" samples were available in the lab and a freshly sputtered gold sample had been prepared by Peter Greene; to my delight and extreme convenience, I discovered that there was not only an evaporator filament installed in the "cross probe" of the sample preparation chamber (see Figure 7), it also still had a small slug of gold resting in the conical filament.

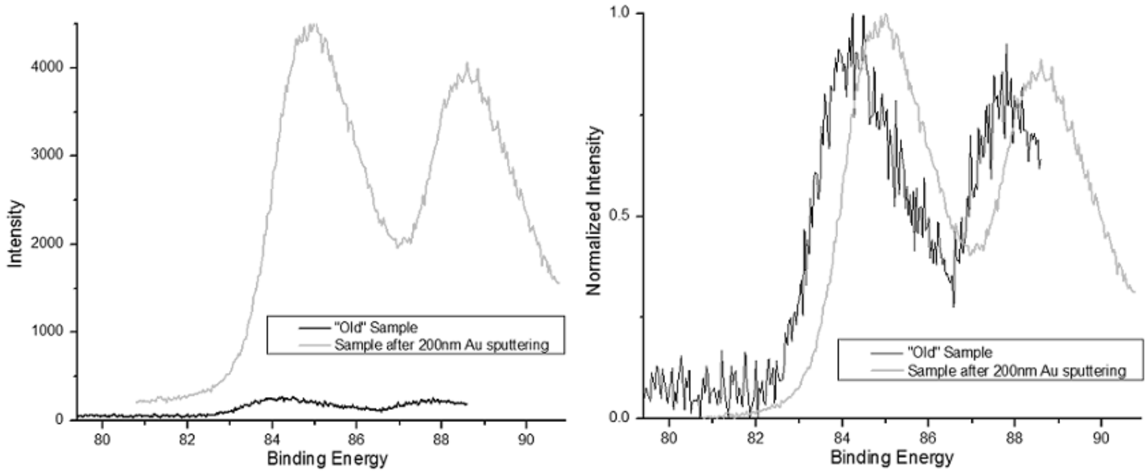

(a) Absolute intensity comparison between "dirty" sample and the same sample after 200 nm Au sputtered onto sample surface.

(b) Normalized intensity comparison of the data in Figure 31a. The large variations in the dirty spectrum appear because the noise amplitude is close to the same order of magnitude as the spectral peak intensities.

Figure 31: Sample comparison. Au sputtering carried out by P. Greene, courtesy of Dr. K. Liu.

A clean gold sample was prepared by facing the sample directly toward the filament, which rests about 6 mm from the face of the sample, and passing a current through the filament using a Variac power supply. The filament was measured to have a resistance of 1.8 Ω, and the Variac, drawing power from an outlet at 110V AC, was increased to a maximum of 5% of drawn power. The applied power was limited to 5% of the maximum because, although the filament was obscured from the viewing window by the sample and sample probe, the prep chamber became very brightly lit due to the heating of the filament (and its subsequent blackbody behavior). The high intensity of the light emitted from the filament indicated a high temperature and evaporation of the gold slug in the filament. The gold was allowed to evaporate for about 2 minutes; when the sample was turned to face the viewing window, the face of the sample and the rails of the sample manipulator had clearly been coated with a layer of gold.

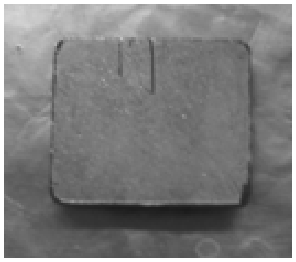

(a) Sample prepared by *in situ* Au evaporation.

(b) Dirty Au sample.

Figure 32: Sample comparison. The dirty sample appears nearly featureless because adsorbed contaminants reflect light isotropically.

Figure 32 shows a visual comparison of the freshly evaporated sample (after removal from the chamber) and a dirty sample from the collection in the lab. On the dirty sample the surface appears blurred due to the smoothing effect the deposits have on reflection of visible light by the surface due to roughness; the "clean" sample appears more detailed because slight surface imperfections reflect visible light in a noticeably different pattern than the smooth bulk surface. Figure 33 displays wide scan spectra for both the clean and dirty samples on the same axes. Important differences include the obvious presence of the O 1s peak, the enhanced C 1s peak, and the decreased Au peak intensities all observed in the dirty sample. To further elucidate the differences, the wide spectrum survey on the dirty Au sample alone is displayed in Figure 34.

Au 4f spectra and C 1s spectra were surveyed throughout the first 8 hours following the fresh Au evaporation. The dirty sample and sputtered sample were both surveyed in the same manner (over 8 hour periods) in order to obtain control measurements. Figure 35 displays the first and last Au 4f and C 1s spectra taken for each sample. The first and last spectra for both the dirty and sputtered samples are identical after accounting for spectrometer noise. The first and last C 1s spectra for the clean gold sample are also identical – this means that the carbonaceous overlayer was fully established within the first 10 minutes after the Au evaporation. The only clear difference between the sputtered sample and the clean sample spectra is the higher intensity of the carbon peaks, attributable to the sputtered sample's transit through atmosphere prior to spectral surveying. The difference in peak shape of the dirty sample's C 1s peaks is likely attributable to the presence of multiple chemical states of the atmospheric carbon and dust deposited on the dirty sample.

For each of the dirty and sputtered samples, both the first and last spectra were identical within the variation of experimental uncertainty. For the clean sample Au 4f spectra, however, a small but significant drop in intensity was observed. Unfortunately, the first and second of the *in situ* evaporated sample's spectra displayed anomalous peak shifts; the first spectrum sampled was observed to be shifted by "jumping" of the 6131C power supply mid-way through the survey (see Section 5.2.3, Figure 29) and the second spectrum appears to have been affected by the same problem (to a lesser extent). Included in Figure 35 is the third Au 4f spectrum sampled over the 8-hour sampling window. A drop in intensity is the only clear difference between the first (third) and last Au 4f spectra and no clear difference is observed

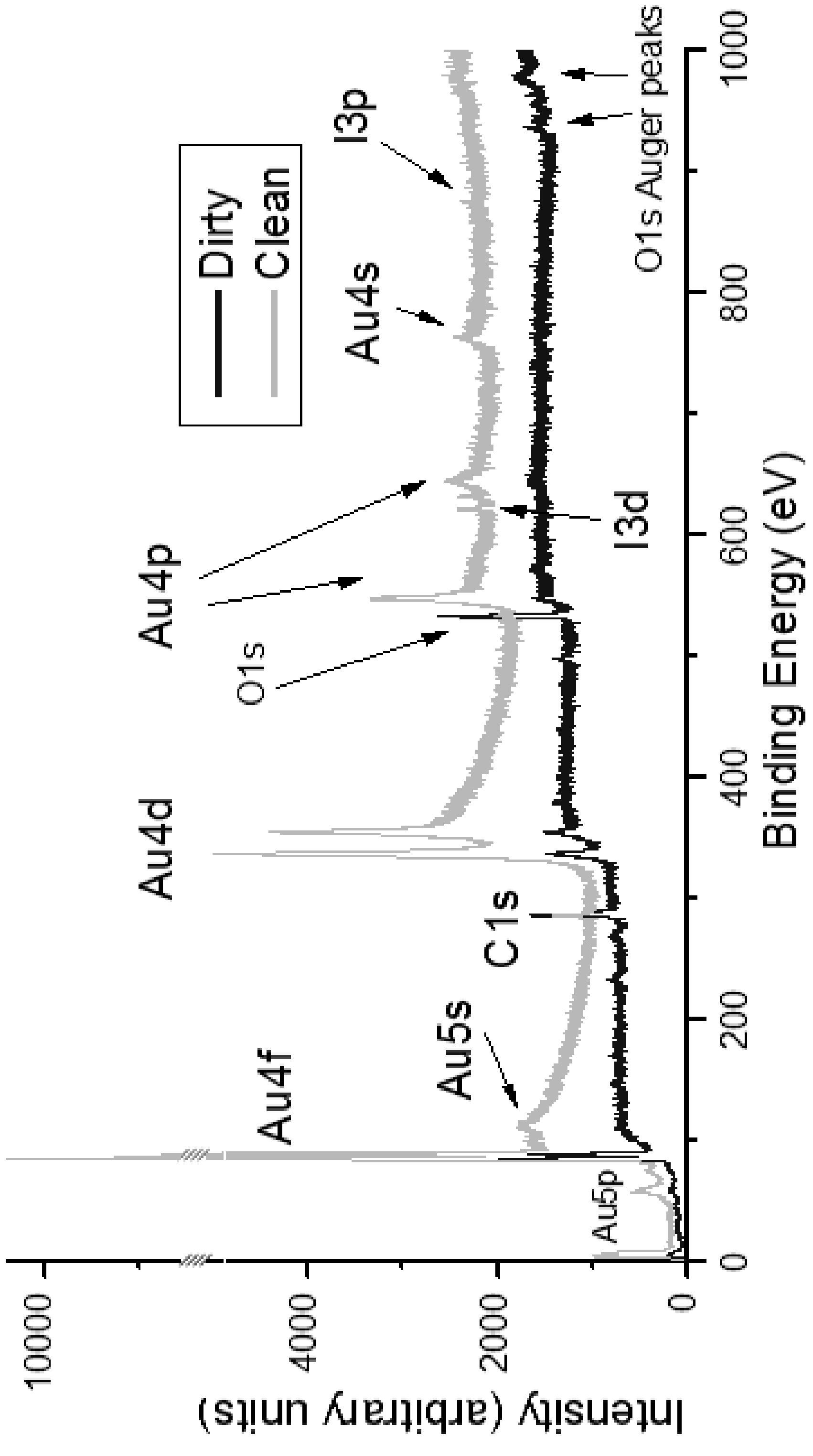

Figure 33: Wide spectrum surveys for a clean Au sample begun 16 hours after evaporation under UHV and for a dirty Au sample.

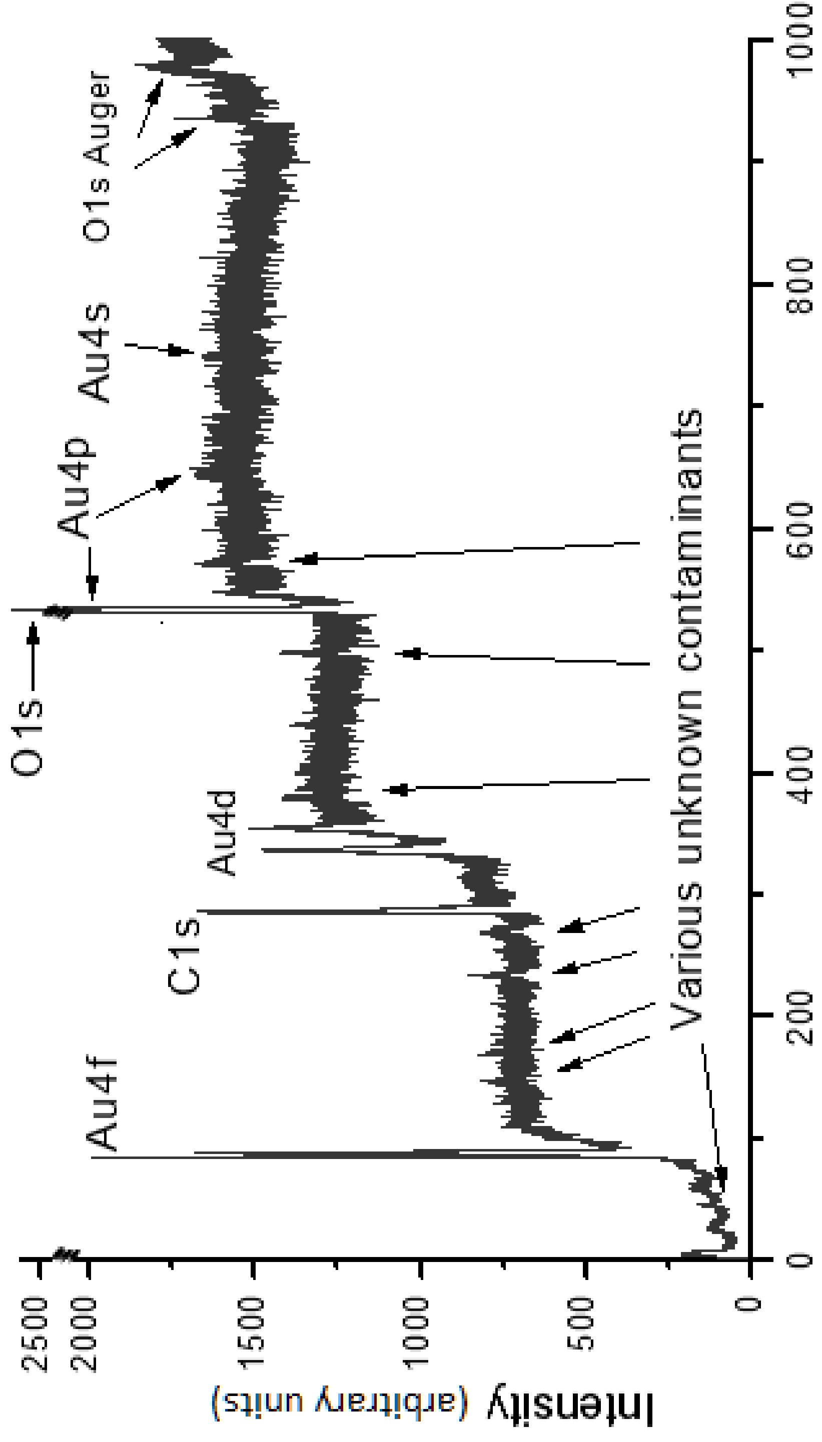

Figure 34: Wide spectrum survey for a dirty Au sample. Potential contaminants include Fe, La, As, W, and Se, based on sample examination history by HP West soon before dormancy and comparison of peak energies to a table of binding energies [16]. The appearance of the myriad contaminant peaks is potent evidence of the sensitivity of XPS measurments.

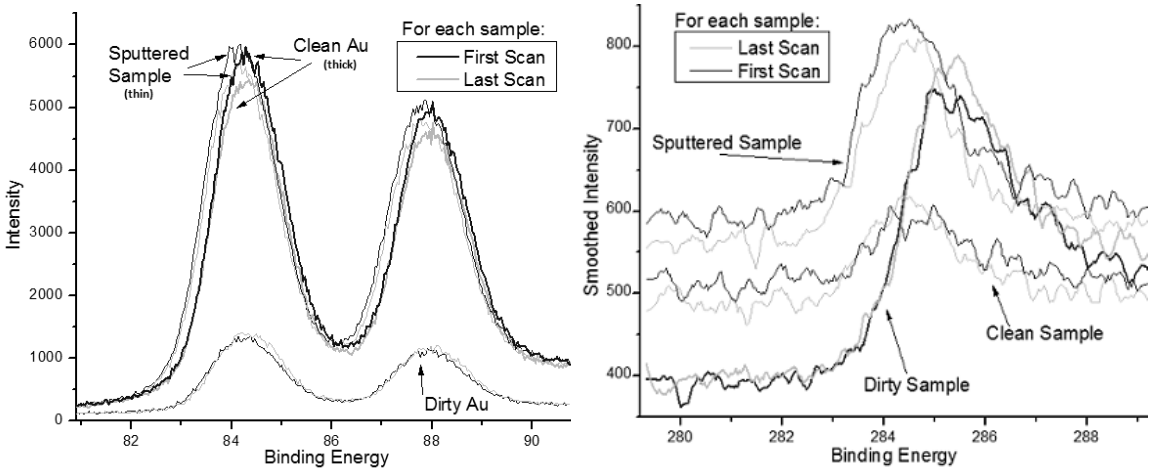

(a) First and last Au 4f scans over 8 hour interval.

(b) First and last C 1s scans over 8 hour interval. Note the significant shift in peak shape for the dirty sample.

Figure 35: Beginning and ending scans of 8-hour sampling intervals. The "first" scan of the in situ prepared Au sample is actually the third Au 4f spectrum surveyed; the first two displayed anomalous peaks and are suspected to have been shifted by the HP 6131C dither voltage "jumping" during sampling as discussed in Section 5.2.3.

between the last clean Au 4f spectrum and either of the 200 nm-sputtered spectra depicted.

Perusal of recent record books revealed that the evaporator has not been used in over 15 years; a wide spectrum survey taken after the sample had been in the chamber for about 24 hours revealed several unexpected spectral peaks. After comparing the observed peaks with a list of electron binding energies found in the HP West operation manual [16], the mystery contaminant was speculated to be iodine. The most prominent spectral lines observed, between 600 and 650 eV and about 10 eV apart, appeared to be a spin-orbit doublet. Only two elements in the region 600 - 650 eV fit that profile: radon and iodine. Because radon gas is rare as an atmospheric component [22], the contaminant was surmised to be iodine. A theoretical spectrum generated by the SESSA program [23] for pure gold with a thin surface layer of iodine

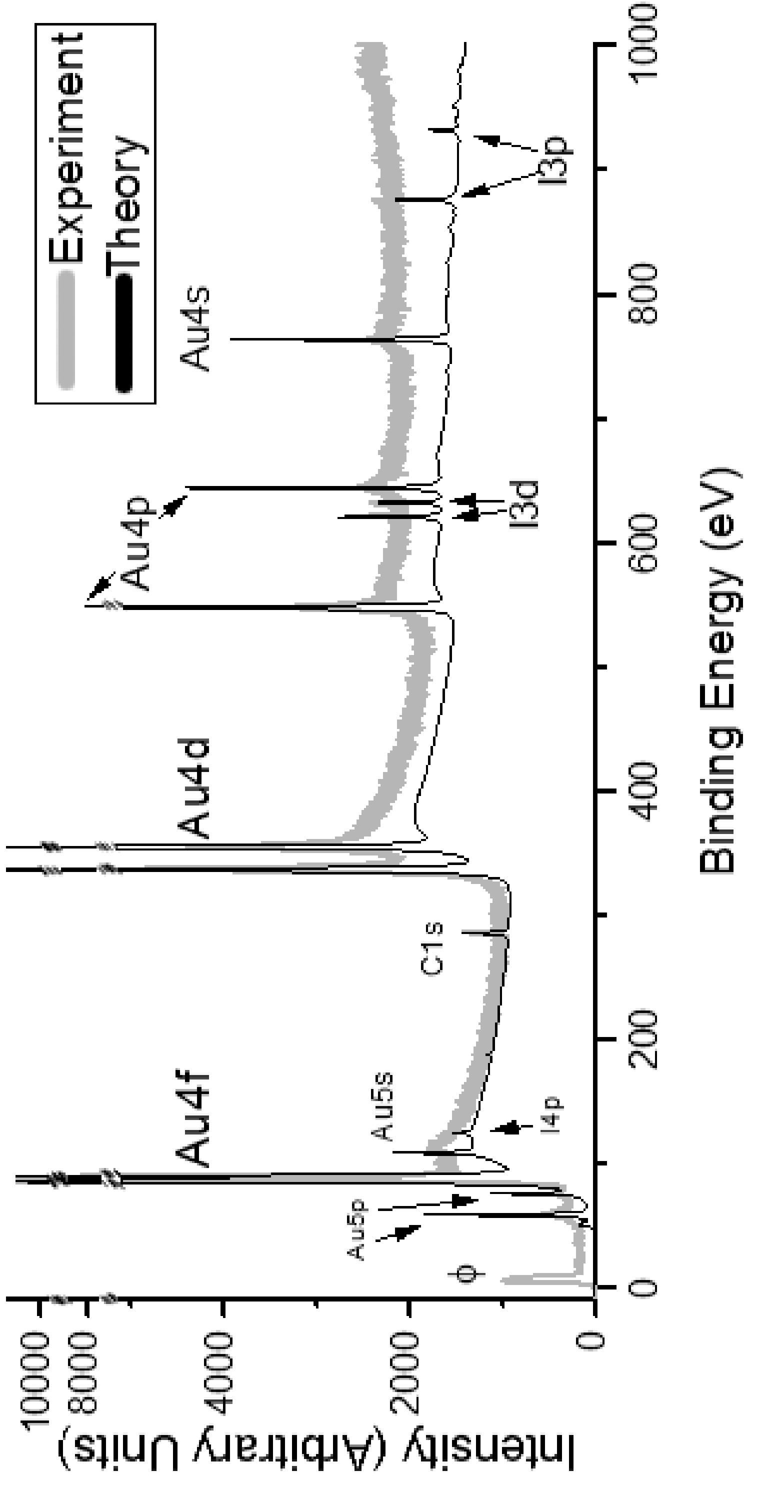

Figure 36: Wide survey spectral scan for the "clean" Au sample. A SESSA [23] simulation of the spectrum for clean Au with a 2Å I overlayer and 1Å C surface contaminant is plotted together with the experimental results.

and a sparse (less than one monolayer thick) layer of carbonaceous contaminant was compared to the experimental spectrum; the excellent correlation of the experimental peaks with this theoretical configuration is displayed by Figure 36.

The iodine contaminant is likely to have entered the chamber on a sample intended for spectral analysis; HP West has previously been commissioned for the analysis of samples for researchers in other departments. The record books show a wide variety of samples being analyzed and so it is not unlikely that a sample containing iodine was placed into the sample chamber and the UHV conditions therein sublimated some of the iodine in the sample. The iodine was not observed until the *in situ* evaporated gold was examined, and was clearly not present in the dirty sample's wide scan, which was taken after the evaporated gold spectrum was taken. The residual iodine present in the chamber may then have been adsorbed to the chamber inner surfaces, including the evaporation filament and the small hemispherical cup surrounding it. The heating of the filament may have caused sublimation of the iodine adsorbed on these surfaces and resulted in a deposition on the gold sample; the iodine on the sample would then be of a higher concentration than the other chamber surfaces because all of the iodine in the extra surface area of the evaporator would be directed onto the surface of the sample.

The cleanliness of the samples being used for XPS analysis is clearly an important quality to be considered before reasonable experimentation may be carried out. The results of this experiment demonstrate the necessity of incorporating only samples with a fresh deposition for the purposes of machine calibration. "Dirty" samples tend towards drastically suppressed intensities of bulk elements and a host of unwanted contaminants which certainly interfere with the measurements. These contaminants appear to both attenuate and shift energies of the electron intensity response.

## 6.3 Si Oxide Layer Study

Synthetic nanometer-scale multilayers have been shown [25] to provide a novel method for probing buried interfaces (between layers) by generating standing waves that then excite photoelectrons. At present, this is a major research direction for the Fadley Group. X-rays are Bragg-reflected off of a multilayer mirror to generate a standing wave by superposition with the incident X-rays. The standing waves created have a wavelength equal to the mirror bilayer thickness, regardless of photon energy, provided that the photon wavelength is short enough to Bragg-reflect from the multilayer. Typical bilayer thicknesses are in the 3-4 nm range. Growing a wedge-shaped bilayer atop the multilayer as a second step in sample fabrication also allows translation of the standing wave through the interface simply by translating the sample perpendicular to the X-ray propagation direction (see [3]). Analyzing the photoelectron intensity response as a function of sample position and angle may then reveal details about the bilayer, such as layer thicknesses, magnetic properties at the bilayer interfaces, and the extent of inter-layer surface mixing.

Multilayers made of silicon and molybdenum are also employed commonly in photolithography using extreme ultraviolet (EUV) light – a promising technique with great potential for use in the semiconductor industry. Photolithography selectively removes material from a layer deposited on a Si substrate crystal by exposing it to a beam of photons partially blocked by an optical mask. Si/Mo multilayers are used extensively in EUV lithography to reflect, focus, and transmit light for specific purposes [25]. Such mirrors are thus the key components for future EUV lithography, where they will be used to reduce feature sizes from a mask down by approximately five times on the surface to be lithographically exposed. These multilayers are chosen because, although all solid materials absorb photons at the relevant EUV energies (about 90 eV) and above, because of the periodicity of the multilayer, Bragg reflection results in high reflectivities [25]. A schematic diagram of the Si/Mo multilayer analyzed with HP West is displayed in Figure 37. For future reference, the multilayer studied had a Berkeley Center for X-ray Optics (CXRO) designation of CX080918B.

Oxide layers naturally form atop the exposed silicon surface of these multilayers. This natural oxide layer affects the optical properties of the multilayer. Theoretical adjustments must then be made to model the multilayer's optical performance accurately; without knowledge of the thickness of the oxide overlayer, calculations may not be completed with full accuracy, and that is where HP West becomes involved. Si 2p orbitals become hybridized in bonding with the oxygen at the surface and shift in energy [18][22]. The associated energy spectrum displays both peaks simultaneously; ARXPS may be utilized to enhance the surface of the sample (see Section 2, [6], [26]), in particular making use of the fact that lower electron takeoff angles relative to the surface will increase the Si 2p peak intensity of the $SiO_2$ peak relative to the elemental Si peak [18]. Quantitative analysis of this enhancement can then yield a precise determination of the oxide thickness.

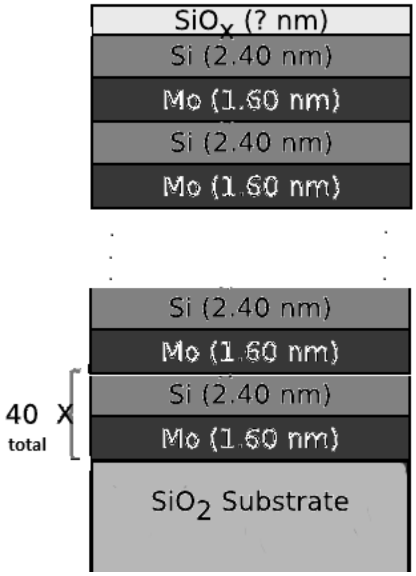

Figure 37: A schematic drawing of the Si/Mo multilayer crystal analyzed. The sample itself, mounted in the manipulator, is depicted in figure 6.

### 6.3.1 Experimental Data and Analysis

Once the experimental data had been taken – Si 2p spectra for varying angles of $\theta$ – several steps still remained before a quantitative analysis was possible. The normalized raw data (Figure 38b) suggested the expected dependence on $\theta$ of the

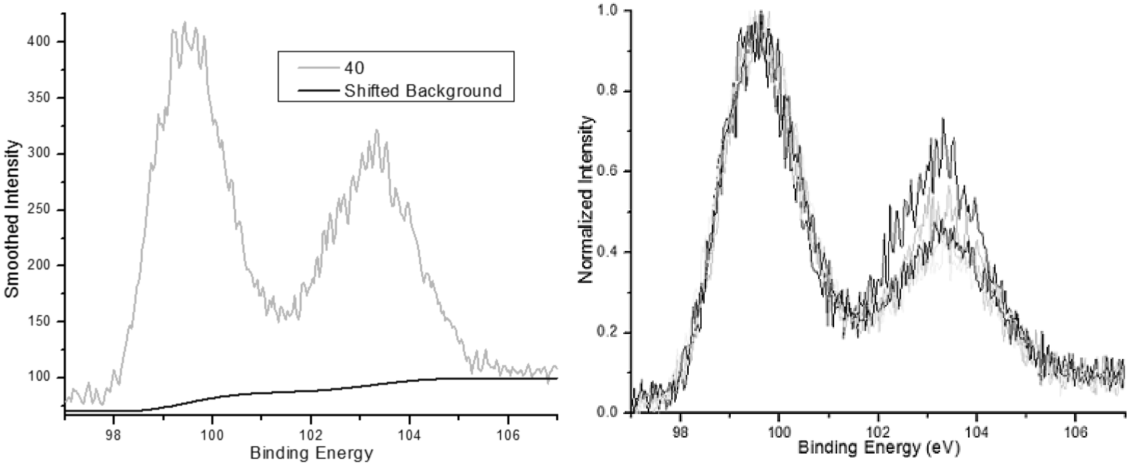

(a) Si 2p spectrum from the multilayer and the Shirley Background calculated. The background displayed here has been raised by a constant value for easy comparison.

(b) Normalized Si 2p spectra from the Si/Mo multilayer. The surface enhancement effect is displayed through the shifting peak intensity ratio.

Figure 38: Example of calculated Shirley Background; raw normalized Si 2p spectra.

relative intensity of the Si 2p (oxide) / Si 2p (element) peaks, so the data at least appeared reasonable – a necessary preliminary step. The extrema, $\theta = 40°$ and $\theta = 80°$, were chosen for the comparison involved in the experimental analysis; the largest variation in the peak area ratios would then be obtained, thereby yielding the best estimate on the accuracy and validity of the assumptions made in the analysis. In the interest of simplicity, the statistical and experimental error calculations for this experiment have been omitted.

To simplify the investigation of the oxide overlayer thickness, several assumptions were made regarding the sample:

1. In order to utilize Eq. (13) for the calculation of the overlayer thickness, the sample was treated as a semi-infinite Si substrate with an $SiO_2$ overlayer of finite thickness.

2. The transition region between top-layer Si the substrate and overlayer was as-

sumed to be effectively just $SiO_2$ (with an abrupt interface at a well-defined depth).

3. The adsorbed surface contaminants on the overlayer were assumed to attenuate both Si 2p and Si 2p (oxide) electrons equally.
4. The kinetic energies of the electrons from the substrate Si 2p and overlayer Si 2p were assumed to be so close that various instrumental factors of Eq. 11 could be cancelled in analyzing intensity ratios.

For a more complete (and accurate) analysis of the oxide overlayer thickness, some of these assumptions would need to be revised; the shortcomings of the model assumed are presented below. Aside from accounting for surface contaminants as described in [18], the simplified model is used in calculating the overlayer thickness here, but with later comparison to a more accurate calculation using the SESSA method.

The inaccuracies introduced by the above assumptions are as follows:

1. The Si substrate is far from infinite – the topmost Si layer is only 24Å thick and some of this will be "used up" in forming the oxide overlayer. Between the top layer of Si and the next Si in the multilayer there is a 16Å-thick layer of Mo which will attenuate the electrons from the lower Si more than if there was no Mo. This will decrease the intensity of substrate electrons $N_{Si}(\theta)$ from the intensity that would be expected from a semi-infinite Si sample; the effect will cause the results to be less accurate at higher $\theta$, when the sample surface is not enhanced.
2. The transition region between the topmost Si layer and the $SiO_2$ overlayer will be composed of a combination of $Si_2O_3$, SiO, and $Si_2O$ [18], which will all have binding energies between that of the elemental Si and the $SiO_2$ binding energies.

The transition layer thickness is typically small compared to the $SiO_2$ overlayer [18], however, so the effect of this on the intensities $N_{Si}$ and $N_{SiO_2}$ should be small.

3. The surface contaminants will contribute to an overestimation of the overlayer thickness [18]; to account for this overestimation, an adjusted value for the general ratio $\frac{N_{SiO_2}^{\infty}}{N_{Si}^{\infty}}$ found in [18] was used in Eq. (13).
4. Assuming equal Si 2p photoelectron kinetic energies introduces a small error (about 0.25%) which will have negligible effect on the overlayer thickness calculations.

### 6.3.2 Final Results of Oxide Layer Thickness Analysis

The only quantities thus required in Eq. (13) for calculating overlayer thicknesses, as experimentally determined from data acquired by HP West, were the peak intensity area ratios $\frac{N_l(\theta)}{N_k(\theta)}$. The method for calculating these ratios and using them to determine overlayer thicknesses follows. From the raw data, the background was first subtracted. The background was modeled using the Shirley Background method, which uses an iterative procedure to estimate the background from the peak areas, initial, and final background energies [19]. An example of the Shirley Background, shown along with the $\theta = 40°$ spectrum for which it was calculated, is shown in Figure 38a. Once the background had been subtracted, the 40° and 80° peaks were normalized to a maximum intensity of one and a Gaussian peak fit was applied; Figure 39 shows the peak fits for the peaks of the spectra for both angles. The ratio of the areas for each pair of peaks $\frac{N_{SiO_2}(\theta)}{N_{Si}(\theta)}$ then corresponds to the ratio $\frac{N_l(\theta)}{N_k(\theta)}$ which appears in Eqs. (11) and (13). The ratios calculated are:

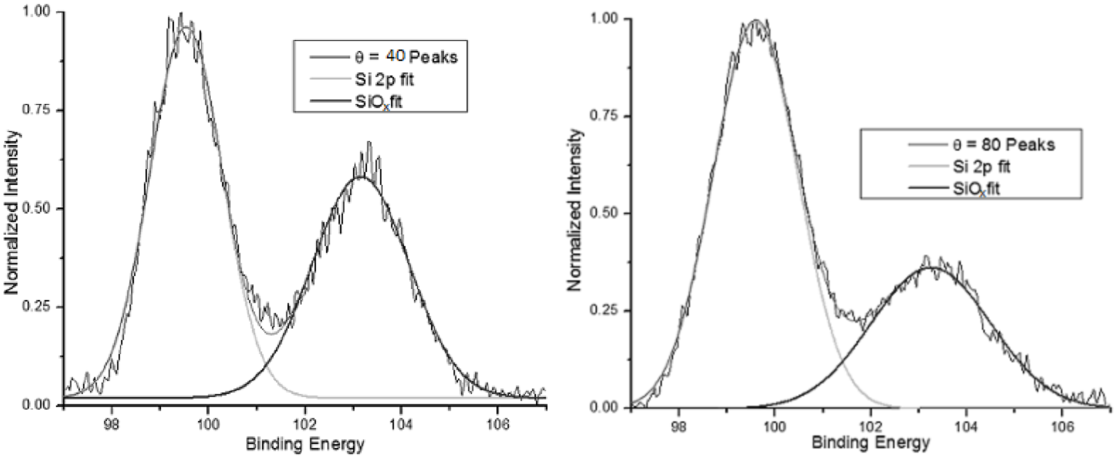

(a) Background-subtracted, smoothed, normalized Si 2p peaks and Gaussian peak fits for $\theta = 40°$.

(b) The same for $\theta = 80°$.

Figure 39: Gaussian peak fits for the Si 2p (oxide) and Si 2p (element) peaks. COD($R^2$) values for the fits were 0.983 and 0.994 for $\theta = 40°$ and $\theta = 80°$, respectively.

- 40° peaks: $\frac{Si2p(ox)}{Si2p} = \frac{N_l(40°)}{N_k(40°)} = \frac{1.408}{1.777} = 0.792$
- 80° peaks: $\frac{Si2p(ox)}{Si2p} = \frac{N_l(80°)}{N_k(80°)} = \frac{1.133}{2.206} = 0.514$

Because the electron kinetic energies $E_{Si}$ ($= E_l$) and $E_{SiO_2}$ ($= E_k$) were assumed to be equal, Eq. (13) may be solved for $t$:

$$t = \Lambda'_e(E) \sin\theta \ln \left( 1 + \frac{\left\{ \frac{N_{SiO_2}}{N_{Si}} \right\}}{\left\{ \frac{N^\infty_{SiO_2}}{N^\infty_{Si}} \right\}} \right) \tag{19}$$

where an experimentally determined ratio $\frac{N^\infty_{SiO_2}}{N^\infty_{Si}}$ is selected such that it will account for surface contaminants and allow a more accurate determination of $t$ [18]. The value for this ratio suggested by [18] is 0.88. The only other quantity yet to be inserted into Eq. (19) to determine $t$ is $\Lambda'_e$, which may be looked up. For excitation of Si 2p electrons with Al-K$\alpha$ X-rays, the best estimate of the electron inelastic mean free path from prior experiements is $\Lambda'_e \approx 3.4$ nm [18]. Inserting the experimentally determined $\frac{N_{SiO_2}}{N_{Si}}$ into Eq. (19) resulted in calculated oxide overlayer thicknesses of $t(40°) = 14.0\text{Å}$ and $t(80°) = 15.4\text{Å}$.

As an independent check on this value, a theoretical calculation of the overlayer thickness was carried out by Alex Gray in the Fadley Group with the SESSA program; background-subtracted peak area ratios $\left(\frac{N_{SiO_2}}{N_{Si}}\right)$ were compared to the experimental ratios for varying oxide layer thicknesses. The theoretical oxide layer thickness whose peak area ratio matched most closely with the experimental ratios was $t_{SESSA} = 15\text{Å}$. The agreement between the theoretically calculated $t_{SESSA}$ and the experimentally derived $t(40°)$ and $t(80°)$ is remarkable, especially considering the simplifications involved in modeling the multilayer. Choosing another experimentally determined average value for $\frac{N^{\infty}_{SiO_2}}{N^{\infty}_{Si}}$ $(= 0.76)$ which does not account for surface contaminants [18] yields overlayer thicknesses of $t(40°) = 15.6\text{Å}$ and $t(80°) = 17.3\text{Å}$, clearly less in agreement with the theoretical value calculated with SESSA, but still within the normal error range for such determinations.

Because the $t(40°)$ overlayer thickness is less affected by incorrectly assuming the multilayer to be a semi-infinite Si substrate than is the $t(80°)$ thickness (for reasons discussed in Section 6.3.1), I have arbitrarily chosen the $t(40°) = 14\text{Å}$ value to be the final result of my experiment. Unfortunately, time limitations prevented the analysis of a second Si/Mo multilayer similar to Figure 37 except with 50 periods of 3.2 nm bilayers with the same Si-to-Mo bilayer thickness ratio.

My measurements have thus provided a useful first determination of the oxide layer thicknesses on such Si/Mo mirrors, and this general type of oxide layer thickness measurement will be continued by others in the Fadley Group. Future data analysis will make use of the SESSA program to more accurately allow for the precise multilayer geometry, while at the same time also including information from the extensive prior study of parameters for such $SiO_2$ thickness determinations by Seah and Spencer [18].

# 7 The Future of HP West

HP West is an aging piece of equipment, but it still retains its value. In this era of strained academic budgets and selectivity in research funding, an older model such as this is likely to be passed over, as there are bigger, better, and sometimes more efficient devices that are capable of taking similar data and tend to be less problem-prone. However, to purchase such an instrument with upgraded versions of all that is present in HP West would cost about $1 million, and these funds are not yet available. Thus, although HP West may not be fit for doing *truly state-of-the-art XPS* research, it provides an excellent avenue for the newly initiated to build a platform of experience working with a well-known and well-documented piece of equipment. It also provides an interactive way to learn about solid state physics and surface physics with the actual materials just inches away. Finally, since there is no other available XPS machine on the Davis Campus, HP West should provide access for a number of research groups who would like to carry out XPS analyses of their samples, until such time as funding may become available to purchase a new, state-of-the-art system for the campus. Interest from the researchers in the Chemistry and Chemical Engineering departments had already been expressed at the time of writing.

Though my work with HP West ended with the machine in much better condition than when I began, much still remains to be done to fully optimize its operation; my work with the machine, well documented in the record book and in the preceding pages, will provide an excellent jumping-off point for the next students to follow and complete the project. Another potentially great use for HP West, once other students have taken the reigns, is in sample analysis for other UC Davis researchers (or even researchers from outside of Davis!), as noted above. HP West is still capable of providing excellent data characterizing samples in many ways, and once the machine has been optimized, "routine" analyses for other researchers will also add another interesting venue from which future students may learn.

## 7.1 Remaining Tasks

Because my time with HP West was limited, there are still many items associated with HP West that are not critical to operation, but may either restrict future operation or prevent complete optimization of the system. Several actions must still be taken:

- **Upgrade the operating system of the computer interface.** As noted earlier, HP West is currently running Windows 3.1 on an old PC and there are numerous problems associated with it. The interface devices are somewhat archaic, and although they still function adequately, establishing an interface with a newer computer is a worthwhile undertaking for many reasons. Limitations of the computer in use include: lack of hard drive space and memory available; the necessity of using a $3\frac{1}{2}$" floppy disk to transfer files from the HP West computer to the (Windows XP) lab computer, which is connected to the internet; slow program startup speed and inability to multitask – files may not be loaded onto a disk for transfer while a scan is in progress; other useful programs like SESSA (for theoretically simulating spectra) may not be run on it; and finally, a lack of internet connectivity for data transfer. Alex Kay, who coded the program used to acquire data from the spectrometer interface electronics designed by Britt Holbrook and built by Georgi Rumiansev, gives hope that the operating system upgrade will not be terribly complicated. Dr. Kay suggests that because the code was designed to be highly modular, updating his code, rather than programming an entirely new code, is the best approach. Additional programming expertise is also available from Robert Gunion at LBNL, who has modified another of the Kay software programs for use on a VG spectrometer in Berkeley.

- **Iron out detector problems.** The detector problems detailed at the end of Section 5.2.3 are probably the most pressing of all the remaining issues plaguing the system. The proper functioning of all four preamps installed on the outside of the detector box must be verified, and this will likely require the expertise of Britt Holbrook. There may be more to the detector problems than the preamps, as well; several such suspected issues are the lens voltages specified by various circuit diagrams in the HP West service manual [16]. Setting these voltages requires supervision by someone with experience working with high voltage equipment and specialized meters and leads to read those voltages. The 6131C "jumping" problem mentioned at the end of Section 5.2.3 and on page 65 of the most recent record book also demand attention, and the removal of this problem will also likely require assistance from Britt Holbrook.

- **Ion pumps may need recharging/cleaning.** Throughout my time working with HP West, all of the ion pumps (especially the main chamber pump) except for the monochromator chamber have seemed to slowly raise their base pressures. This observation, coupled with the fact that it has certainly been a very long time since they have been serviced, leads me to suggest a service package for all four pumps.

- **Reproduce old plots.** In both the record book and the troubleshooting manual for the detector [15], plots of electron intensity vs. X-ray power at a fixed

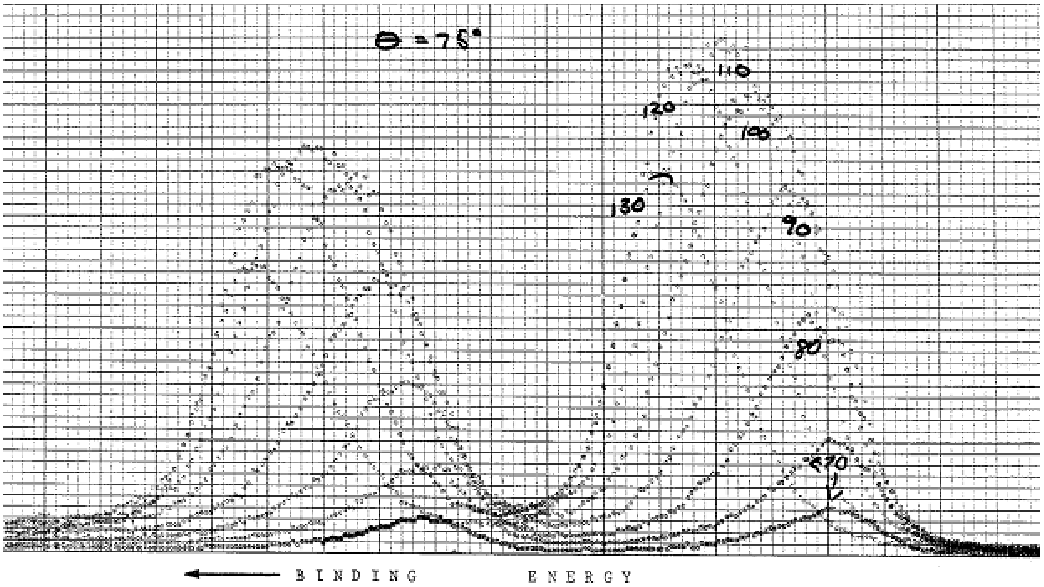

Figure 40: A plot of the spectral dependence of the monochromator angle $\varphi$. Extracted from Fadley Group record book.

orientation and of peak shape as a function of monochromator angle at fixed $\theta$ and $\psi$ are shown and described (see Figures 22 and 40). These tests will add a handy set of data to the full description of the current state of the machine, and possibly suggest directions for future optimization work.

- **Careful sweep over many $\theta, \varphi, \psi$.** Part of the reason why the surfaces of Figure 24 extrapolated from the spectral data are so complex is because of a lack of data points. A "sweep" such as that described in Section 5.2.2 will provide much useful data now that the detector has been configured to work better and the relationships between various angles are better understood. Sweeping not just the monochromator and the sample probe angles, but also the sample angle, will be much more time-consuming but will also prove much more useful – especially if the dispersion-compensation orientation is located.

- **Repair Ion Pump Control Unit Gauges.** The voltage setting of all pump control units except the 20L (differential seals) ion pump is non-operational and reads 0V; the main chamber pump control unit exhibits erratic behavior and occasionally the needle becomes stuck at certain positions (at about 1/3 and 2/3 of the gauge range); the power light for the 20L ion pump does not light; all of these issues need addressing because it is important for all gauges to be functional so that pump operation may be closely monitored. The 5956B power light also does not light; when addressing the aforementioned issues, this problem should also be rectified. An excellent troubleshooting table found in the back of each of the VacIon (ion pump) operating manuals [14] may be used in conjunction with the accompanying circuit diagrams for diagnosing and correcting the above problems.

## 7.2 Concluding Remarks

HP West is still a great machine and it rests in a great department at a great university. The restoration project has been a wildly beneficial undertaking for my own purposes and it will be a great tool for teaching new students about repair work on the type of machines used in experimental physics. The strong human resources available in and around the Physics Building at UC Davis will continue to be an excellent guide for those in the future who choose to concern themselves with HP West enough to resume where I have abruptly concluded. I sincerely hope that this document will provide a detailed reference for those who will follow and that the elusive dispersion-compensation angle is rediscovered.

# Acknowledgments

Many thanks to all those who have assisted me in reviving HP West. Peter Klavins, especially, as he has provided innumerable ideas, suggestions, opinions, and advice; without his help and experience I would never have finished my year-long project even close to on time. Much thanks to Alex Gray for teaching me how to use Origin, giving me information about the silicon oxide layer studies, and backing up my experiment with theoretical calculations. Thanks also to Peter Greene and the Liu Group for sputtering fresh gold onto a sample for me – it's a move that pushed me in the right direction at a critical point in the project. Thanks to Chris Papp and Benny Balke for showing me the ropes at LBNL and teaching me much of the physics relevant to XPS and necessary to work with HP West. I would also like to thank my father, who I was fortunate enough to work with and learn from how to truly assess problems and take action to fix them. Lastly, a very large thank you to Prof. Fadley for making this all possible: giving me the chance to earn the priceless experience I have gained working with the complex machinery in the lab, the important task of reviewing and proofreading this document, teaching me (directly and indirectly) how, where, who, and what to find help from when I need it, and encouraging me every step of the way.

# References

[1] H. R. Hertz, *Annalen der Physik*, vol. 267, no. 8, p. 983-1000.

[2] A. Einstein, *Annalen der Physik*, vol. 322, no. 6, p. 132-148.

[3] C. S. Fadley, "Atomic-Level Characterization of Materials with Core- and Valence-Level Photoemission: Basic Phenomena and Future Directions," Submitted to Surface and Interface Analysis as part of the Proceedings of the Sixth International Symposium on Atomic-Level Characterizations of New Materials and Devices, Kanazawa, Japan, 2007.

[4] K. Siegbahn et al., "Atomic, molecular and solid-state structure studied by means of electron spectroscopy" Nova Acta Regiae Soc. Sci. Ups. 20.1-282, (1967).

[5] R. J. Baird and C. S. Fadley, *J. Elec. Spec. and Rel. Phen.*, 11 (1977) 39-65.

[6] C. S. Fadley, "Basic Concepts of X-ray Photoelectron Spectroscopy," Chapter 1 of Vol II of C. R. Brundle and A. D. Baker, *Electron Spectroscopy, Theory, Techniques, and Applications*, Pergamon Press, 1978.

[7] K. Siegbahn et al., *Science*, 176 No. 7032, (1972) 245.

[8] V. Behrens, "11 Beryllium". in Beiss, P. Landolt-Börnstein – Group VIII Advanced Materials and Technologies: Powder Metallurgy Data. Refractory, Hard and Intermetallic Materials. 2A1. Berlin(2003): Springer. 1–11.

[9] C. Kittel, *Introduction to Solid State Physics* ($8^{th}$ edition). Wiley, John & Sons, Inc. (2004).

[10] G. Burns, *Solid State Physics.* Elsevier Science & Technology Books, (1985).

[11] T. Swain et al., "Vacuum Technology – an introductory laboratory course" ($2^{nd}$ edition). http://lpc1.clpccd.cc.ca.us/lpc/tswain/lab_notes.htm

[12] Varian/Vacuum Division VacSorb Pump Instructions, Varian Inc., Palo Alto, CA.

[13] Varian/Vacuum Division New Large-Cell VacIon Pumps Instruction Manual, Varian Inc., Palo Alto, CA.

[14] Varian/Vacuum Division VacIon Pump Control Unit Instructions, Varian Inc., Palo Alto, CA.

[15] HP SSL Model 239 ESCA Detector Instruction Manual, Hewlett Packard, Palo Alto, CA.

[16] HP 5950A Spectrometer System Operating Manual, Hewlett Packard, Palo Alto, CA.

[17] T. A. Moore, *Six Ideas that Shaped Physics: Unit T: Some Processes are Irreversible.* William C. Brown Publishing, (1999).

[18] M. P. Seah and S. J. Spencer, *Surf. Interface Anal.* (2002); 33: 640–652.

[19] CasaXPS, "Peak Fitting in XPS."
http://www.casaxps.com/help_manualmanual_updates/peak_fitting_in_xps.pdf

[20] B. L. Henke, "X-Ray Attenuation Length."
http://henke.lbl.gov/optical_constants/atten2.html

[21] D. J. Griffiths, *Introduction to Electrodynamics* ($3^{rd}$ edition). Benjamin Cummings (1999).

[22] R. H. Petrucci, W. S. Harwood, G. E. Herring, J. Madura, *General Chamistry: Principles and Modern Application* ($9^{th}$ edition). Prentice Hall, (2006).

[23] NIST Database for the Simulation of Electron Spectra for Surface Analysis (SESSA): Version 1.1. http://www.nist.gov/srd/nist100.htm

[24] S.-H. Yang et al 2002 J. Phys.: Condens. Matter 14 L407

[25] F. T. Chen, Proc. SPIE 5037, pp. 347-357 (2003)

[26] C. S. Fadley, Progress in Surface Science, Vol. 16, (1984) 275-388

[27] NIST Chemistry WebBook. http://webbook.nist.gov/

# Appendix A: HP West Pumpdown Procedure

Note 1: This procedure is for pumpdown from atmospheric pressure only. If any chamber has a starting pressure lower than 1 mTorr, consult Prof. Fadley before proceeding.

Note 2: Smaller pumps may require pressing "reset" button (if overload light has become lit) and larger pumps may sometimes trip off and require restart when outgassing as pumping begins. DO NOT *hold* the "reset" button on the smaller pumps.

Note 3: DO NOT activate the X-ray power supply until the pressure in the monochromator chamber is below $10^{-7}$ Torr.

1. Ensure all valves are closed and there are no chamber openings
2. Bake both cryosorption pumps overnight WITH THE STYROFOAM BUCKETS REMOVED
3. Allow cryopumps to cool to room temperature
4. Activate mechanical pump
5. Open ALL valves EXCEPT #10, #4, and #5
6. While wearing appropriate cryogenic safety gear: attach styrofoam buckets, add liquid nitrogen to cool cryopumps
7. Once pressure has reached 250 mTorr or lower and cryopumps are cooled to the point of low, stable boiling of the LN, close valve #8 and open valve #4 (F pump); check time

8. After about 15 minutes have passed, as soon as the pressure stops dropping and air can no longer be heard rushing into the "F" cryopump, close valve #4 and open valve #5
9. Allow "R" cryopump to operate for about 30 minutes
10. Switch all ion pumps into "start" mode and activate them, close valves #1, #6, and #7
11. Switch all ion pumps into "protect" mode once each reads a pressure below $10^{-6}$ Torr
12. Open valve #8 when differential seals pressure reads above 100 mTorr

# Appendix B: HP West General Operation

**Starting up HP West:**

1. Activate the computer; at the DOS prompt, type "win" and press enter
2. Open the "ESCA West Acquisition" program; follow the instructions to properly activate the interface box, 6131C power supply, lens voltages and chevron plate voltages – allow **24 hours** for warm-up or leave all supplies permanently on (excludes interface box)
3. Activate heat exchanger and cooling fans; switches are in the rear of the rack
4. Activate the X-ray power supply ONLY when the pressure in the monochromator chamber is below $10^{-7}$ Torr
5. When high voltage "ready" light comes on, begin ramping up energy one step in energy every 5 minutes up to 800W
6. Allow 2 hours for X-ray anode to warm up
7. While wearing nitrile gloves, carefully insert your sample ALL THE WAY into the keyway holder on the sample rod, with the sample spring underneath
8. Insert your sample until the handle is *just* past the "pause" indicator on the probe track and wait until the mechanical pump reaches its base pressure
9. Close valve #8 and insert the sample steadily all the way to "cross probe;" reset the differential seals ion pump, if necessary
10. Once the pressure in the sample prep chamber has reached $10^{-7}$ Torr, open valve #11 all the way until it stops

11. Slowly insert the sample all the way into the main chamber and slide the probe into the appropriate pins
12. Gently remove all counter-clockwise play with the translation handle and gently remove the handle
13. Open valve #8 once differential seals pressure gauge reads 100 mTorr or above (during operation, only valves #3, #8, and #11 remain open)
14. Slide out the manipulator pin and set the manipulator to the desired angle; ALWAYS turn counter-clockwise to set the angle, turning right to pass and left to return as needed
15. Define a survey region and/or begin your experiment

**Swapping samples during operation:**

1. Set manipulator to zero (always turn counter-clockwise to set manipulator angles!) and engage safety locking pin
2. Slowly retract the sample from the chamber until the handle reaches the "cross probe" indicator
3. Close valve #11 until it does not slide easily; use the torque wrench to apply a torque of 35 ft-lb to the bolt
4. Slowly retract the rod until the handle is about half-way between the "accessory ports" and "pause" indicators; retract the rod quickly but steadily through the differential seals

5. Wearing nitrile gloves, carefully remove sample from manipulator and place into container
6. Still wearing gloves, place the sample spring back into the manipulator (it usually falls out) and carefully insert your new sample ALL THE WAY into the manipulator
7. Insert your sample until the handle is *just* past the "pause" indicator on the probe track and wait until the mechanical pump reaches its base pressure
8. Close valve #8 and insert the sample steadily all the way to "cross probe;" reset the differential seals ion pump, if necessary
9. Once the pressure in the sample prep chamber has reached $10^{-7}$ Torr, open valve #11 all the way until it stops
10. Slowly insert the sample all the way into the main chamber and slide the probe into the appropriate pins
11. Gently remove all counter-clockwise play with the translation handle and gently remove the handle
12. Open valve #8 once differential seals pressure gauge reads 100 mTorr or above

**Shutting down HP West:**

1. Set X-ray power to "standby" and turn the power off
2. Turn off heat exchanger, fans, and interface box
3. Exit "ESCA West Acquisition" program and close Program Manager; at the DOS prompt, shut off the computer

4. Set manipulator to zero (always turn counter-clockwise to set manipulator angles!) and engage safety locking pin
5. Insert translation handle into manipulator catch

If you will be shutting down the system for an extended period:

6. Turn off the 6131C power supply and spectrometer power supplies
7. Slowly retract the sample from the chamber until the handle reaches the "cross probe" indicator
8. Close valve #11 until it does not slide easily; use the torque wrench to apply a torque of 35 ft-lb to the bolt

If you wish to raise the system to atmospheric pressure:

9. Deactivate all ion pumps and the ion gauge
10. Connect dry nitrogen supply to valve #10 (DO NOT begin nitrogen flow yet)
11. Close valve #8, deactivate mechanical pump
12. Slowly open valves #1, #6, and #7 in that order, wait at least 5 minutes for pressures to equilibrate
13. Begin nitrogen flow, as little flow as possible, and open valve #10
14. Once pressure gauge reads ~1 atm (avoid positive pressures), close valve #10, shut off nitrogen supply, and close *all* remaining valves

# Appendix C: List of Problems Encountered and Solutions Applied

| **Problem Encountered** | **Solution Applied** |
|---|---|
| Differential seals pressure gauge inoperable | Swap thermocouple, gauge |
| Ion pump refuses to start even after pressure is below $10^{-4}$ Torr | "Shake" pump body by striking with a soft (rubber) object to knock Ti flakes loose |
| Poor main chamber pressure after days of pumping | Open valve #3 to allow mechanical pump to maintain a low pressure barrier in plumbing manifold |
| Slow pumpdown (higher base pressures during pumpdown) | Use mechanical pump to pre-pump chamber;<br>Ensure overnight bakeout of cryopumps, venting after bakeout;<br>Start pumping with "F" pump and valve off after 15 minutes to facilitate "drag" pumping of inert gases before switching to "R" pump and giving ample time to reach "R" cryopump's base pressure |
| Ion gauge inoperable | Swap HP West gauge/control unit for unused unit |
| X-ray filament taking a long time to preheat (more than 1 minute) | Wait up to 30 minutes; Swap control unit |
| X-ray power indicator light off when button is depressed | Flip breaker on the rear of stack power supply (just above X-ray transformer fluid reservoir) |

| **Problem Encountered** | **Solution Applied** |
|---|---|
| X-ray power indicator light on, filament preheat indicator light off<br>**(interlock open)** | Activate heat exchanger;<br>Heat exchanger flow rate low: turn output valve in pump housing clockwise (toward closed) until flow rate rises above 2 gal/min;<br>Check for tripped-off ion pumps, reactivate them if necessary (ion pumps must be running or interlock will open)<br>Allow X-ray to preheat before changing power setting from "standby" |
| X-ray repeatedly trips off power supply breaker<br>X-ray intensity intermittent, unstable | Ramp up energy slowly (5 minute warm-up at each power setting), allow 2 hours warm-up time at 800W |
| Heat exchanger switch "on" but pump not running | Replace fuse, replace water filter inside pump housing;<br>Replace broken fuse holder, re-solder wires inside power box |
| Water temperature in heat exchanger reservoir high (over 37°C) | Activate fans;<br>Fill reservoir to max level with distilled water |
| Main chamber or monochromator pump tripping off repeatedly after chamber has been pumped down | Check cooling fan on rear of control unit, replace if seized, push with screwdriver if stuck |

| **Problem Encountered** | **Solution Applied** |
|---|---|
| Count rate low | Allow X-ray anode 2 hours warm-up time at 800W to stabilize;<br>Switch to cleaner sample, sputter/evaporate new layer onto sample;<br>Align monochromator and sample probe ($\varphi = 360°, \psi = 21.5°$);<br>Power down and vent chamber, scrub X-ray anode |
| Apparent binding energy is shifted from expected value | Align monochromator and sample probe;<br>Binding energy too low: increase $\varphi$<br>Binding energy too high: decrease $\varphi$ |
| Spectral line widths (FWHM) large (1.6 eV+), intensity peaks misshapen | Align monochromator, check detector electrical box setup;<br>Set lens voltages, chevron plate voltages to suggested values [15] |
| Little or no counts observed | Close "ESCA West Acquisition," turn off detector interface box, 6131C, and spectrometer power supplies, and restart "ESCA West Acquisition," following the instructions;<br>Check X-ray power supply for activity and setting at 800W, and look inside monochromator chamber for light from filament |
| Detector range shifts suddenly during dithered scan | "Shake" 6131C, deactivate, wait ∼5 seconds, reactivate |